UNIVERSITY OF CANTERBURY

DOCTORAL THESIS

Model-Based Hemodynamic Monitoring in Critical Care for Improved Diagnosis and Treatment

Author:
Shun Kamoi

Supervisor:
Dr Chris Pretty

A thesis submitted in fulfilment of the requirements for the degree of Doctor of Philosophy

in

Bioengineering,
Department of Mechanical Engineering

October 2016

"A way that can be described is not the eternal way"

Laozi

Abstract

Cardiac and circulatory dysfunction are leading causes of admission, cost, and mortality in the intensive care unit (ICU). However, choosing a suitable treatment is extremely difficult, as a wide range of complex and patient-specific dysfunction types are found. Furthermore, due to the limits and constraints on the currently obtainable data, a full, clear picture of patient state cannot be precisely delineated, which can result in misdiagnosis and incorrect treatment choices.

To overcome this problem, cardiovascular parameters essential for correct diagnosis and treatment must be accurately estimated from clinically available measured data. Specifically, the volume of blood ejected from the heart per beat, known as stroke volume (SV), needs to be estimated from easily accessible measurements, such as blood pressure, as it is an important hemodynamic parameter for assessment of cardiovascular performance. This goal can be accomplished by "adding value" to existing clinical data using physiological models of the cardiovascular system.

This research develops a novel aortic model and patient-specific hemodynamic parameter identification method for continuous and accurate estimation of SV using measurements commonly available in the ICU. Thus, SV can be acquired in a non-additionally invasive fashion. In addition, use of this SV measurement can enhance the diagnosis, treatment and therapeutic decision support of bedside clinicians.

The aortic model developed in this thesis uses continuous aortic pressure waveform and pulse wave velocity (PWV) as inputs to estimate SV. The parameters within the aortic model are aortic characteristic impedance, aortic compliance, and systemic resistance, and are identified

beat-to-beat. These parameters are used to compute blood flow and thus to estimate SV for every heartbeat.

The SV estimation method is validated with two series of pig experiments involving administration of dobutamine and inducing septic shock, where direct and invasive measurement of SV is obtained for a gold standard comparator. In addition, SV is significantly changed throughout the experiment by modifying preload using various levels of positive end-expiratory pressure, as well as fluid administration. The method developed is also compared against the PiCCO system from PULSION, a commercially available pressure-based SV estimation device that is currently considered the most accurate in the critical care.

The Bland-Altman results from the porcine study showed clinically acceptable accuracy within approximately ± 30% by the developed model. The PiCCO system also showed similar accuracy compared with the direct SV measurement. However, the PiCCO system required multiple calibrations during the pig study, while the developed method only required one. This result suggests that the developed model and methods are more accurate and clinically useful, particularly when hemodynamic instability is present.

Overall, the model developed in this research shows great potential for improving patient care in the ICU. The model offers key hemodynamic parameters for optimizing cardiovascular treatment. In particular, accurate titration of fluid, inotropes, and vasoactive drugs to patient-specific responses are now possible. The overall methods and model can be generalized to outpatient management.

The overall outcome provide new opportunities to reduce the cost of care, while improving quality. Adding value to existing measurements has not previously been proven in circulartory

management. Hence, this research provides a template for further advances, particularly in the highly monitored critical environment.

Acknowledgements

I would like to first thank my supervisor, Dr Chris Pretty, for his patience and guidance with my research. Thank you for giving me the flexibility to explore my interest and teaching me how to achieve academic goals. Also, thank you for coming down to minion office regularly, which made "research meetings" much more fun and interesting.

I would like to thank my co-supervisor, Prof Geoffrey Chase and Dr Thomas Desaive, for making my research possible, organizing experiments, and giving me the opportunities to travel the world. Thank you for your support and making my PhD a rich experience.

I would like to also thank Dr Yeong Shiong Chiew and Dr James Revie for letting me have long discussions to come up with new ideas and solutions for my research problems. Thank you for your understandings and constant support.

To everyone in my office: I cannot express all my thanks in words here. Without you guys, my PhD journey would have been like a sandwich without meat and butter, a boring one. Thank you to Guo, Jennifer, Musabbir, Daniel, Felicity, Kent, Joel, Shaun, Alexander, Tony, Sophie, Vincent, Tony, Claire, Sarah and many more.

Many thanks go to my friend, Josh Flores, Ben Braithwaite, Lance Bendall, and Dane McColl, for making my off-time very enjoyable. You guys allowed my mind to rest from work, so that I could stay fresh even when the road was bumpy.

Lastly, I would like to thank my girlfriend, Yiting Yu and my parents, for walking this journey with me.

Contents

List of Figures

List of Tables

Nomenclature

Roman Symbols

A	Area
C	Compliance
D	Distensibility
L	Length
P	Pressure
Q	Flow
R	Resistance
r	Radius
t	Time
x	Distance
V	Volume
Z	Impedance

Greek Symbols

ρ	Density
μ	Dynamic Viscosity

Subscripts

ao	Aorta
aoa	Aortic arch
abao	Abdominal aorta
cal	Calibrated
cvp	Central venous pressure
ed	End diastolic
es	End systolic

ex	Excess
res	Reservoir
vent	Ventricular
w	Wesseling

Acronyms

CO	Cardiac output
ECG	Electrocardiogram
EDPVR	End diastolic pressure volume relationship
EDV	End diastolic volume
ESP	End systolic point
ESPVR	End systolic pressure volume relationship
ESV	End systolic volume
FIR	Finite impulse response
HR	Heart rate
ICT	Isovolumetric contraction time
ICU	Intensive care unit
ME	Mechanical efficiency
PAC	Pulmonary arterial catheter
PEEP	Positive end expiratory pressure
PV	Pressure volume
PVA	Pressure volume area
PWV	Pulse wave velocity
RM	Recruitment manoeuvre
SV	Stroke volume
SW	Stroke work
VAC	Ventricular arterial coupling
VET	Ventricular ejection time

Chapter 1: Introduction and Motivation

1.1 Motivation

Cardiovascular disease, dysfunction, and cardiac surgery are major causes of intensive care unit (ICU) admissions, cost, and mortality in the western world (Mozaffarian et al., 2015). In New Zealand, these patients comprise more than 20% of all ICU admissions, accounting for approximately 2400 patients per year (ANZICS, 2015). The majority of these patients require therapeutic interventions to restore and maintain cardiovascular system function (Pearse and Rhodes, 2004). However, a number of different causes and dysfunctions may appear essentially the same in typical ICU measurements, which can lead to incorrect diagnosis and treatment (Perkins et al., 2003, Franklin and Mathew, 1994, Brun-Buisson, 2000).

Many measurements can be taken from an ICU patient, such as blood pressures, electrocardiogram, and heart rate. These common measurements show the effects of the body's response to the underlying problems, but do not identify the physiological changes responsible for these effects (Graham and Parke, 2005). For example, blood pressure can increase or decrease, and the cause can be in the heart, or in the circulation, or a combination of both (Lamia et al., 2005). With clinical measurements only revealing a part of the patient's cardiovascular state, accurate diagnosis and treatment is not guaranteed (Asfar et al., 2014, Dubin et al., 2009, LeDoux et al., 2000). In addition, incorrect treatment can cover further negative effects and further mask the underlying problems, which could lead to further harm (Hayes et al., 1994).

To provide correct diagnosis and optimal treatment for patients with cardiovascular complications, blood pressure measurements along with physiological parameters directly related to cardiac and circulatory functions must be monitored (Marik et al., 2010). The key cardiac and circulatory parameters to monitor are the volume of blood ejected from the heart per beat, known as Stroke Volume (SV), and vascular properties affecting SV and peripheral circulation, such as vascular stiffness and resistance to blood flow (Antonelli et al., 2007). The combination of information from these physiological parameters provides a full and more complete picture of a patient's cardiovascular state, and thus allows clinicians to differentiate dysfunction types (Vincent and De Backer, 2013). Moreover, typical cardiovascular and circulatory managements/treatments involving inotropes and vasopressors directly modify these physiological parameters (Overgaard and Dzavik, 2008). Hence, optimal treatment can be enabled by accurate evaluation of relevant patient-specific response to therapy, forming direct "dose-response" relationships not currently available.

Measurement of SV provides rich information on the heart performance and also enables estimation of the level of oxygen delivered around the body (Tibby and Murdoch, 2003). SV also reveals the blood flow through the main arteries, and vascular properties can easily be determined through knowledge of blood pressure measurement combined with SV (Dart and Kingwell, 2001). Therefore, obtaining the value of SV in real-time and in response to care is crucial for improving ICU patient care.

While measurement of SV is essential for accurate diagnosis and optimal treatment in cardiac and circulatory failure, direct measurement requires inserting invasive sensors directly into the heart, which is clearly not clinically feasible. In general, the use, number, and positioning of catheters containing sensors are determined by the perceived risk to benefit ratio (Bellomo and

Uchino, 2003). For these reasons, measurement of SV is often limited and only available for patients requiring significant treatment (Eisenberg et al., 1984, Antonelli et al., 2007).

Currently, several methods for indirect estimation of SV are available (Marik, 2013). Accurate methods involving cardiac imaging, such as MRI and echocardiography can be conducted, but are very expensive (Oren-Grinberg et al., 2013) and often only provide static, intermittent SV values. These methods are also not feasible during rapid hemodynamic changes, which is the critical time they are most needed to inform and guide care, and often the case for cardiovascular complications.

There are other methods and commercial devices available for continuous SV measurement (Marik, 2013). However, studies show most of these methods are unreliable during hemodynamic instability (Pugsley and Lerner, 2010), meaning these monitors cannot be used effectively when the SV data is most needed and useful (Bein et al., 2007). These significant limitations with current SV monitoring and estimation indicate the need for a cost-effective, accurate, and reliable continuous SV estimation method.

This research aims to develop a novel continuous SV estimation method from typical ICU measurements. A specific goal is accurate SV estimation when hemodynamic properties are significantly altered. Such a method would enable SV monitoring for patients with cardiovascular dysfunctions without the need for additionally invasive measurements, and would thus be clinically practical and cost effective. Most importantly, estimated SV can greatly improve quality of cardiovascular treatment and patient care.

1.2 Cardiovascular Physiology

This chapter first introduces the important aspects of cardiovascular physiology necessary for this research. It then describes the four main types of cardiovascular dysfunctions. The purpose is to provide a basis for the clinical importance of SV measurement in critical care and context for the precision and performance required.

1.2.1 Cardiovascular System Overview

The cardiovascular system is responsible for pumping blood around the body. The system consists of two key areas: the heart, which pumps the blood, and the circulation, which channels the blood to every part of the body. The blood represents approximately 7% of the body mass (Alberts, 2012), and is responsible for delivery and removal of nutrients, gases, hormones, and metabolic end product, which help to provide homeostasis and basic functions of human cells and organs. An overview of the anatomy of the cardiovascular system is shown in Figure 1.1.

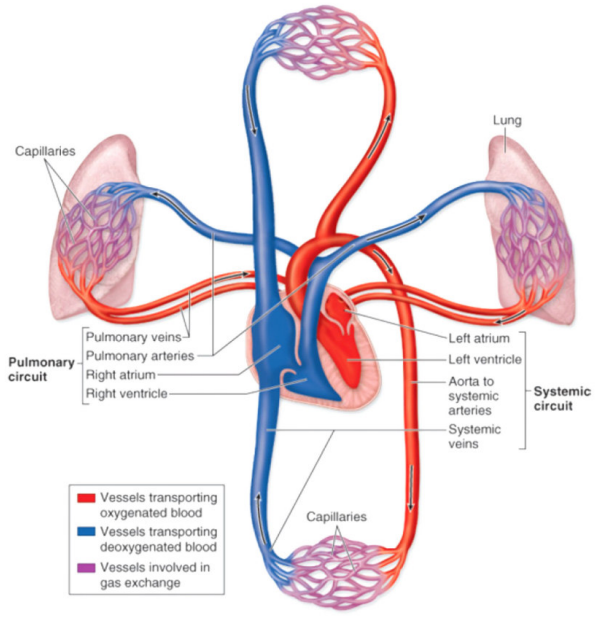

Figure 1.1 – Overview of the anatomy of the cardiovascular system (McKinley and O'Loughlin, 2007).

1.2.2 The Heart

The heart is composed of two synchronised pumps, each comprising two chambers. The left ventricle pumps oxygenated blood to the body's periphery via the systemic circulation. The right ventricle pumps blood to the lung to be re-oxygenated via the pulmonary circulation. Each ventricle has a preceding atrium chamber. The purpose of the atria is to store the blood returning to the heart while the ventricle is active, and to pump the stored blood into the ventricle when it is relaxing.

The heart has four valves, control blood flow. The right atrium receives deoxygenated blood from the body and delivers it to the right ventricle through the tricuspid valve. This blood is then pumped to the pulmonary circulation through the pulmonary valve, preventing back flow while right ventricle relaxes. Oxygenated blood from the lungs is received by the left atrium and delivers it to the left ventricle through the mitral valve. This blood is then pumped to the systemic circulation through the aortic valve. A diagram of the heart showing all chambers and valves is illustrated on Figure 1.2.

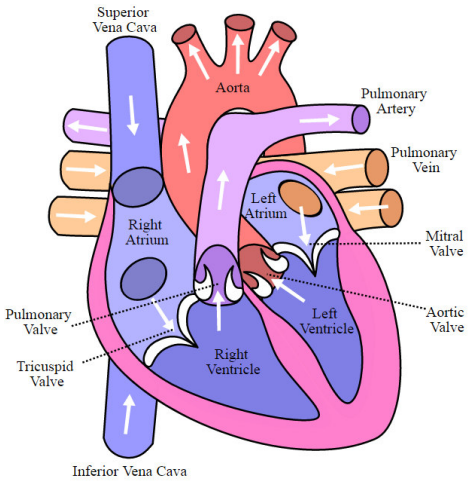

Figure 1.2 – Anatomical features of the heart and blood vessels connected to the heart. (Adapted under the Creative Commons Attribution-Share Alike 3.0 Unported License).

Figure 1.2 shows the valve positions when the ventricles are contracting, and this phase of the cardiac cycle is called *systole*. During systole, the tricuspid and mitral valves are closed to prevent back flow, and the pulmonary and aortic valves are both open to eject blood to the pulmonary and systemic circulation, respectively. All valve states are reversed when ventricles are relaxing and receiving blood, and this phase is called *diastole*.

1.2.3 The Circulation

The circulatory system consists of two main circuits. The pulmonary loop passes blood through the lungs to be oxygenated, and the systemic loop that supplies oxygenated blood to the organs of the body. Both circuits have three major parts: the arterial system, the capillary system and the venous system.

1.2.3.1 Arterial system

The arterial system comprises the blood vessels that transport blood away from the heart to the capillary system. The diameter of the arteries becomes successively smaller as they get further from the heart and branch to supply the peripheral tissues and organs. The arterial system has three main vessel types: 1) elastic arteries, 2) muscular arteries, and 3) arterioles with the elastic arteries being closest to the heart and arterials being furthest.

The elastic arteries have low elasticity and can easily be stretched from changes in pressure. Due to the low elasticity of these vessels, some of the blood ejected from the ventricle is stored during systole and released during diastole. This buffering action of elastic arteries helps to provide more continuous flow in the peripheral arteries.

There are two major elastic arteries connected to the heart, the aorta and the pulmonary artery. The aorta receives oxygenated blood ejected from the left ventricle and supplies the systemic

circulation. The pulmonary artery receives deoxygenated blood from the right ventricle and supplies the pulmonary circulation to re-oxygenate the blood.

The elastic arteries branch to muscular arteries, where the vessel walls are thicker and these vessels thus have higher elasticity. The gradual change in the arterial stiffness from the heart to the periphery enables efficient dissipation of energy introduced from the heart, leading to efficient and relatively constant blood flow and pressure in the vital organs. The muscular arteries further branch to the arterioles, where they connect to the capillary system.

1.2.3.2 Capillary System

The capillaries are the smallest blood vessels and the walls are only one endothelial cell layer thick. The diameters of capillaries range from 5 to 10 μm, which in some places is smaller than a single red blood cell of approximately 8 μm. These micro-vessels allow the exchange of gases, nutrients, and other products between the blood and the tissues. Capillary vessels are distributed all around the body to reach every tissue cell to meet its demand.

1.2.3.3 Venous System

The venous system comprises the blood vessels that return blood back to the heart from the capillaries. The blood from the capillaries enters the venous system, starting with venules. After the blood has travelled through the venules, it then moves into the veins, where the walls get thicker and the diameter increases. The blood pressure in the venous system is much lower than in the arterial system. Due to lower blood pressure in the veins, there are several valves in these vessels to prevent the back flow of blood. The venous system has much lower wall elasticity than arterial system and contain the largest proportion of blood, approximately 64% of total blood volume (Tortora and Derrickson, 2008).

1.2.4 Mechanical Properties of the Heart

Cardiac performance can be analysed through pressure-volume (PV) information in the ventricle. The PV relationship for a single cardiac cycle drawn on the pressure (y-axis), and volume (x-axis) diagram is called a PV loop. From the PV loop, many properties of the heart can be derived. An example of PV loop is shown in Figure 1.3. The general characteristics of the PV loop is the same for both left and right ventricles.

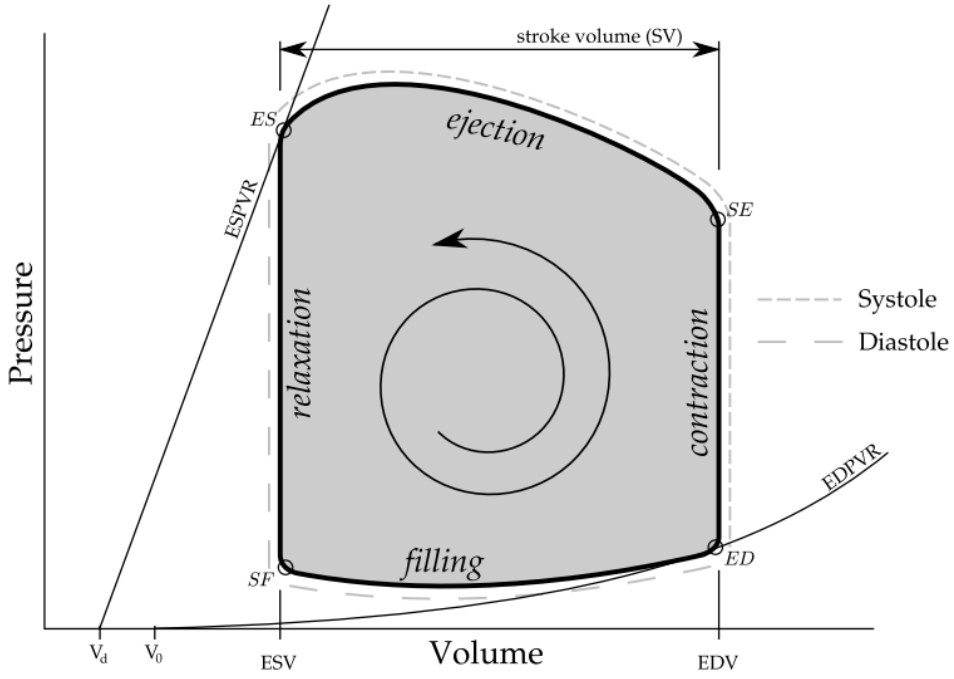

Figure 1.3 – Example of ideal ventricular pressure-volume loop showing the four phases of the cardiac cycle (Stevenson, 2013). ES: end systole, SF: start filling, ED: end diastole, SE: start ejection, ESPVR: end systolic pressure volume relation, EDPVR: end diastolic pressure volume relation, ESV: end systolic volume, EDV: end diastolic volume.

Three important metrics can be calculated from the PV-loop: SV; the end-systolic PV relation (ESPVR); and the end-diastolic PV relation (EDPVR), these metrics are all shown in Figure 1.3. The SV is simply the difference in the volume before and after heart contraction. Hence, it is the end-diastolic volume (EDV) minus the end-systolic volume (ESV). The ESPVR and

EDPVR lines represent the ability of the heart muscle to contract and stretch for a given blood volume. These relationships also determine the approximate shape of the PV-loop from a given EDV and ESV. In addition, the area enclosed by PV-loop represents the external work done to the artery by the heart, known as *stroke work*.

1.2.4.1 Cardiac Cycle

The cardiac cycle consists of four phases that cycle anti-clockwise on the PV-loop, as shown in Figure 1.3. At the start of systole, the ventricular muscle contracts with a very small volume change, resulting in sharp increase in ventricular pressure. This phase is called isovolumetric contraction. When the ventricular pressure exceeds the pulmonary artery/aortic pressure, the corresponding valves open and the ejection phase begins. The blood in the ventricle ejects into the artery until the pressure in the ventricle decreases below the arterial pressure due to ventricular relaxation and flow ceases. This pressure decrease and loss of flow causes the aortic/pulmonary valves to close, and the isovolumetric relaxation phase starts. When the ventricular pressure becomes lower than the pressure in the atrium, the tricuspid/mitral valves open and blood from the venous system starts filling the ventricle. After the ventricles are filled to EDV, the cardiac cycle starts again with ventricular contraction.

1.2.4.2 Frank-Starling Mechanism

Frank-Starling mechanism describes the nonlinear relationship between the volume of blood filling the ventricle (EDV) and resulting force of contraction by the ventricular muscle (Frank, 1895). Increased filling causes greater expansion of the ventricular muscle, and further stretched myocardium fibres can contract more forcefully to eject blood. This mechanism allows SV to be synchronised with the venous return, thus providing efficient control of the cardiovascular system without needing external regulation. Frank-Starling curve showing relationship between EDV and SV is shown in Figure 1.4.

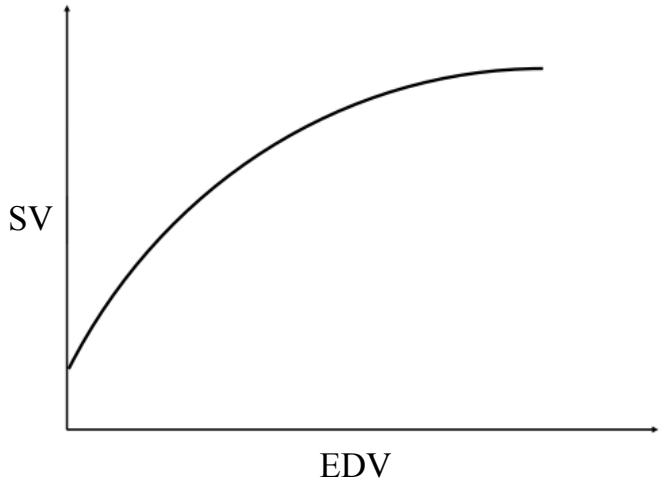

Figure 1.4 – Ideal Frank-Starling curve showing nonlinear relationship between end diastolic volume (EDV) and stroke volume (SV).

1.2.4.3 Preload

Preload is defined as all of the factors that contribute to passive ventricular wall stress at the end of diastole (Norton, 2001). It is thus a measure of the circulations ability to fill the ventricle. The most direct contributing factors include, the end-diastolic ventricular radius, the end-diastolic filling pressure, and the heart muscle wall thickness. Ideally, all these metrics should be measured to determine accurate preload status of the heart. However, it is not practical or feasible to make frequent measurement of cardiac geometry in vivo. In clinical settings, the value of EDV and/or end-diastolic pressure are often used as surrogates to represent preload (Nahouraii and Rowell, 2010).

Changes in preload have a crucial effect on SV. Increase in preload causes greater filling of the ventricle, and thus, EDV increases. This causes greater force of contraction by Frank-Starling mechanisms. The outcome is increased EDV and SV with wider PV loop. Figure 1.5 shows the effect of increased preload on the PV loop.

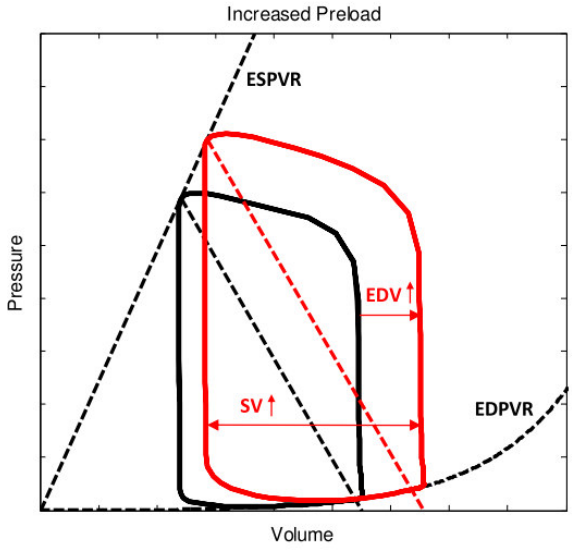

Figure 1.5 – Effect of increased preload and end-diastolic volume on the pressure volume loop. The black line shows the control state and the red line shows the increased state (Revie, 2013).

Clinically, EDV cannot be increased directly, and alternatively, factors influencing EDV are changed. Changing these factors generally occurs by modifying the vascular properties and/or total blood volume in the circulation. For example, the total amount of blood volume returning to the heart can be increased by increasing the venous wall stiffness. The veins contain the largest proportion of blood volume in the circulation and act as a blood reservoir. When venous wall stiffness is increased, the reserved blood is reduced, pushing a greater percentage of blood around the circulatory system, increasing blood pressure and flow. A similar condition can be induced by increasing the total amount of circulating blood as stiffness is dependent on the blood volume. Thus, EDV can also be changed from treatments such as fluid administration and vasoactive drugs.

1.2.4.4 Afterload

Afterload can be defined as all of the factors that contribute to ventricular wall stress during the ejection period (Norton, 2001). The main factors affecting afterload are the aortic properties such as its stiffness, and resistance to flow. These properties shape the aortic pressure waveform, which is the pressure load the ventricle must overcome to eject blood into the aorta. Hence, mean aortic pressure is a simple measure of ventricular afterload. However, strictly speaking, aortic pressure is determined by the interaction of both the arterial system and of the ventricular effort of the heart. Thus, the total aortic pressure value does not uniquely index or capture just arterial system properties (Burkoff, 2002).

An increase in afterload reduces the amount of blood the heart can pump into the artery. This reduction results in increased ESV for the same EDV, as shown in Figure 1.6. The effect of afterload on SV is less significant than a change in preload, as there is no direct influence on the heart contractility from Frank-Starling law. For this reason, preload has a greater impact on SV than afterload.

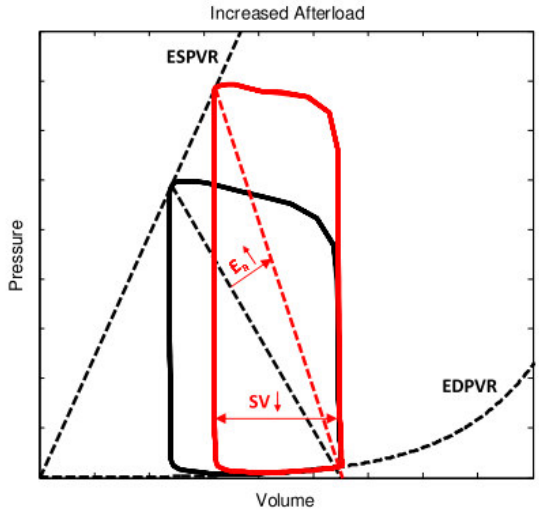

Figure 1.6 – Effect of increased afterload on the pressure volume loop. The black line shows the control state and the red line shows the increased state (Revie, 2013).

1.2.4.5 Heart Rate

Heart rate is the number of cardiac cycles that occur within one minute. SV multiplied by heart rate is called cardiac output (CO), which estimates the average blood flow around the circulation per minute, and often used in clinical settings to approximate level of oxygen delivery around the body. Heart rate is controlled by the autonomic nervous system. Sympathetic stimulation, for example via inotropes, increases both the heart rate and the force of the heart contraction. In contrast, parasympathetic stimulation decreases heart rate without greatly decreasing the strength of contraction (Hall, 2011).

The baroreflex is one of the negative feedback mechanisms responsible for the nervous stimulation of the heart (Cheryl, 1999), thus controlling heart rate. Sensory neurons called baroreceptors are located in the vascular wall to monitor pressure levels in arteries and the veins. Baroreceptor are excited by stretch of the blood vessel. Thus, changes in pressure within the vessel activates baroreceptors, which triggers the central nervous system responsible for the heart's autonomic reflexes. Increases in blood pressure results in sympathetic activation, and parasympathetic inhabitation. Conversely, when blood pressure decreases, the opposite nervous stimulation occurs. Finally, drug therapies can add to sympathetic or parasympathetic stimulation to modify pressures in circulation and cardiac management.

1.2.5 Mechanical Properties of the Blood Vessels

Properties of the circulatory system play an important role in maintaining an efficient cardiovascular system, and therefore transport of gases, nutrient and waste. In particular, vascular stiffness and resistance to blood flow have significant influence on the preload and the afterload, and thus performance of the heart. The vascular properties can be assessed from blood pressure and flow information within the blood vessels, using a well-known physical law combined with simplified representation of vasculature.

1.2.5.1 Vascular Resistance

The Hagen-Poiseuille equation describes a linear relationship between pressure drop and flow in a cylindrical pipe of constant cross section, and is analogous to Ohms law for electric circuit. The slope of the relationship is determined by the size of the pipe and the dynamic viscosity of the fluid, which captures the resistance to flow. The equation is written:

$$\Delta P = RQ \tag{1.1}$$

$$R = \frac{8\mu L}{\pi r^4} \tag{1.2}$$

Where P, R, Q, μ, L, and r are pressure, resistance, flow, dynamic viscosity, length of pipe, and pipe radius, respectively.

Using Equation (1.1) with the blood flow rate and blood pressure across the circulation, an estimate of vascular resistance can be computed. The main factor affecting the level of resistance is the blood vessel radius, as can be seen in Equation (1.2). Vessel radius is controlled by a range of homeostasis mechanisms that exist within the cardiovascular system (Ackermann, 2004). By controlling vascular resistance, blood flow to the vital organs can be regulated, so that adequate tissue perfusion that is neither too high nor too low is maintained.

With varying vascular resistance and blood flow, the amount of blood returning to the heart is influenced. An increase in vascular resistance could reflect low flow in the circulatory system, and thus reduced preload. Alternatively, an increase in vascular resistance could induce high pressure gradients across the capillary system with constant flow, and thus increased afterload. As Equation (1.1) requires two known variables to identify the third variable, knowledge of

one variable alone, such as a measured pressure value, is not enough to identify its unique condition.

Another type of vascular resistance beside capillary/systemic resistance is aortic characteristic impedance. This parameter describes resistance of aorta from pressure and flow generated by the ventricular ejection (Murgo et al., 1980). The relationship between aortic pressure, flow, and aortic characteristic impedance is the same as Equation (1.1). However, aortic wall cannot be assumed rigid with constant cross-sectional area as aortic wall has low elasticity unlike peripheral arteries. For this reason, Hagen-Poiseuille equation is not suited, and thus, resistive phenomenon of aorta is defined using water hammer equation, where conservation of momentum is considered for flow through elastic tube (Khir et al., 2001).

1.2.5.2 Vascular Stiffness

Clinically, the most commonly used index for describing vascular wall stiffness is compliance. The value of compliance is calculated as the ratio of change in volume from a given change in pressure, and its value is the reciprocal of elastance. Compliance is defined:

$$C = \frac{\Delta V}{\Delta P} \tag{1.3}$$

The value of vascular compliance represents the ability of a blood vessel to recoil toward its original dimension from an increased distending force, such as pulse pressure from the heart. Physiologically, the vessel radius is controlled by contraction of vascular smooth muscles, which directly alter its compliance. The blood vessels are narrowed when vascular compliance is reduced and this process is called vasoconstriction. The opposite process of increased vascular compliance with widening blood vessels is called vasodilation. The value of vascular

compliance, thus significantly influences vascular resistance, which subsequently has a significant impact on afterload and preload.

1.2.6 Summary

In a normal healthy cardiovascular system, preload, afterload, heart rate, vascular resistance, and vascular compliance are all continuously changing/modulating under the controls of both passive and active mechanisms to maintain adequate blood flow and to meet demand from tissues and organs in the body. Any significant change in these cardiac and circulatory parameters decreases the efficiency of the cardiovascular system, and could thus lead to life-threatening medical situations. In such cases, blood pressure information alone is inadequate to uniquely identify the metrics responsible for the abnormality.

To examine cardiac and circulatory performance, both pressure and volume information are required to uniquely ascertain this relationship (Bellomo and Uchino, 2003), which can then be converted into clinically useful physiological values. Mechanical properties of the heart are determined from PV loops of the ventricles, which are affected by the preload and the afterload. The loading conditions of the heart are thus affected by the vascular properties, which can be determined through pressure-volume relationships within the blood vessels. In addition, SV which is the amount of volume transferred from the heart to the circulation contains rich information, as SV provides volume information of both systems and its interactions.

1.3 Cardiovascular Dysfunctions

Cardiovascular dysfunction is a common condition in critical care, affecting approximately 30% of patients in the ICU (Sakr et al., 2006). All cardiovascular dysfunction results in inadequate cellular oxygen utilization, due to insufficient oxygen delivery by the

cardiovascular system. The end results are severe cellular dysoxia and multiple organ failure, leading to death if not treated appropriately (Cecconi et al., 2014).

There are many cardiovascular dysfunction types, but the causes can be categorized into four main pathophysiological mechanisms: 1) distributive; 2) cardiogenic; 3) hypovolemia; and 4) obstructive (Weil and Henning, 1979). Each mechanism reflects an abnormality in a different part/function of the cardiovascular system. The following sections detail each dysfunction.

1.3.1 Distributive

Distributive dysfunction is the most common form of cardiovascular dysfunction in the ICU and accounts for approximately two-third of patients with cardiovascular dysfunction. In particular, sepsis and septic shock, which is a form of distributive dysfunction, makes up most of these patients (Vincent and De Backer, 2013). Septic shock is a major problem in ICU today with reported case-fatality rates in the range of 40-50%, and reaching as high as 80% (Jawad et al., 2012).

Distributive dysfunction can be characterised as a dysfunction in the capillary system and its regulatory functions. This dysfunction is most commonly caused by bacterial infection introducing toxins into the circulation (Elbers and Ince, 2006). High levels of toxins in the blood activates the inflammatory response, which in turn affects regulation of vascular properties, leading to abnormalities in the micro circulation (Werdan, 2001).

The loss of vascular function due to distributive dysfunction causes a decrease in vascular stiffness and an increase in capillary leak, leading to low systemic vascular resistance and afterload as well as reducing exchange with the tissues (Ince, 2005). These effects decrease the ability of the systemic circulatory system to exchange nutrients and oxygen, and return blood

back to the heart. In untreated cases, reduced venous return and preload to the right ventricle causes a reduction in SV, when the body actually requires greater SV. The hemodynamic profile is generally modified by increasing circulatory blood volume with fluid resuscitation, where the CO is normalised or elevated due to low systemic resistance (Dellinger, 2003). This elevated CO is a unique feature of distributive dysfunction as the other three dysfunctions are all associated with low CO (Cavazzoni and Dellinger, 2006).

1.3.2 Cardiogenic

Cardiogenic dysfunction is defined as a state of reduced cardiac performance in the presence of adequate intravascular volume (Nieminen and Harjola, 2005). This dysfunction is the second largest cause of cardiovascular dysfunction in the ICU (Vincent and De Backer, 2013). A multinational observational study of patients hospitalized for an acute coronary syndrome showed in-hospital case-fatality rate of approximately 60% for patients who developed cardiogenic shock (Awad et al., 2012).

The cause of cardiogenic dysfunction can be due to mechanical complications, such as ventricular septal rupture and valve regurgitation, myocardial ischemia from insufficient coronary perfusion, and secondary effects from other types of cardiovascular dysfunctions (Reynolds and Hochman, 2008). When cardiac function is depressed from cardiogenic dysfunction, myocardium contractility is compromised and SV is reduced. This reduction causes less blood delivery to the coronary artery and body's periphery, leading to cellular hypo-perfusion. The ischemia induced to the myocardium from reduced coronary blood flow can further decrease the cardiac function. The end result is progressive myocardial dysfunction, leading to a positive feedback loop and a downward spiral of cause and effect (Hollenberg et al., 1999).

1.3.3 Hypovolemia

Hypovolemia is a state of decreased intravascular blood volume. This condition is often found in trauma patients suffering severe haemorrhages (Kelley, 2005). The loss of blood volume in the circulatory system decreases preload and SV. In cases where the blood loss is up to approximately 30%, baroreflexes can restore the blood pressure back to normal levels by vasoconstriction (Cheatham et al., 2008), masking this dysfunction and its diagnosis. However, the cardiovascular system is significantly compromised in severe cases and tissue perfusion in the vital organs is decreased.

1.3.4 Obstructive

Obstructive cardiovascular dysfunction is the least common of the four types of cardiovascular dysfunction found in the ICU (Vincent and De Backer, 2013). It is a cardiovascular system failure due to physical obstruction of blood flow into or out of the heart. The causes can be found in the pulmonary circulation, such as tension pneumothorax and pulmonary embolism, or in the systemic arterial system, such as in severe aortic stenosis (Morgan and Wheeler, 2013).

Obstruction in the circulatory system leads to reduction in preload and an increase in afterload. The effects of these hemodynamic changes lead to reduced SV for both pulmonary and systemic cases as described in Section 1.2.4.3 and 1.2.4.4. The loss of blood flow from obstruction combined with decreased cardiac function results in inadequate oxygen delivery to the body, organ failure, and death if not treated.

1.3.5 Summary

Although each cardiovascular dysfunction originates from different parts of the cardiovascular system, the common consequence of all dysfunction types is the reduction in ability of the heart to pump a sufficient amount of blood to the tissues. Distributive dysfunction reduces SV via

less preload due to low systemic resistance and hypotension. Cardiogenic dysfunction depresses cardiac contractility, and thus the ability of the heart to eject blood out of the ventricle is decreased. The loss of blood volume/flow in hypovolemia and circulatory obstruction lessens SV from reduced preload and blood received by the heart. While each dysfunction type are discussed separately, comorbidities are common with patient with cardiovascular dysfunctions, and thus, induce greater loss of heart performance.

Proper cardiac function relies on proper function of the circulatory system, and vice versa. Due to their interdependence, SV is affected directly or indirectly in all cases, which is the key parameter in determining the level of oxygen delivery around the body. For this reason, SV monitoring could play a key role in cardiovascular system management, resuscitation, and optimization.

1.4 Clinical Significance of Stroke Volume

Arterial pressure measurement is commonly used in patients suffering from cardiovascular dysfunction in the ICU. However, pressure changes can be driven by alteration in cardiac or circulatory functions, and when volume measurement, such as SV is not available, accurate diagnosis and treatment cannot be performed. ICU clinicians have access to other hemodynamic variables, such as central venous pressure and blood oxygen/carbon dioxide saturation levels. However, the addition of SV measurements would provide a much clearer picture of patient condition from large amounts of often contradictory numerical data.

When both pressure and volume measurements are available, key physiological parameters, such as systemic resistance with the Poiseuille equation, and vascular stiffness from pressure-volume ratio, can be obtained. These identified values directly relate to the mechanisms of each of the cardiovascular dysfunctions. Thus, precise diagnosis of dysfunction types become much

easier. In addition, response to therapeutic intervention can be effectively monitored as treatments involve reversing/normalizing these parameters.

The goal of cardiovascular treatment is to maintain adequate oxygen delivery and tissue perfusion (Pearse and Rhodes, 2004). To achieve this goal, patients commonly receive one or a combination of three main treatments: 1) fluid therapy; 2) inotropic agents; and 3) vasoactive agents (Vadakel and Rizzolo, 2013). Fluid is administered in an attempt to increase SV through increasing intravascular volume and preload (Phillips and Brierley, 2015). Inotropic and vasoactive agents are used to increase cardiac and circulatory performance through sympathetic and parasympathetic activation/inhibition (Ellender and Skinner, 2008). Excess amount of fluid/doses can be harmful when desired outcome is not achieved (Phillips and Brierley, 2015, Overgaard and Dzavik, 2008), and thus titration is key to successful treatment.

The combined information from pressure and SV enabling assessment of vascular resistance and stiffness can correctly guide treatments by measuring its direct response. Monitored SV can be used to titrate fluid and inotrope therapy in real-time. In addition, estimated vascular stiffness using the value of SV with measured pressure can be used to guide treatment using vasoactive agents.

1.5 Goals for This Research

The aim of this thesis is to investigate, develop, and validate methods for continuous and accurate beat-to-beat estimation of SV using non-additionally invasive and/or typical ICU measurements. Accurate SV data would provide a means to unmask the hidden dynamics and interactions in the pressure measurements, enabling clearer diagnosis of dysfunction and a much better understanding of "cause and effect". The outcomes of this research would provide

ICU clinicians a stronger foundation for cardiovascular treatment, thus enhanced patient outcomes.

In this research, SV estimation models are developed and examined with porcine experimental data, where hemodynamic parameters were modified using inotropes, and induced septic shock and fluids. Animal experiments allows direct, invasive measurement of SV by inserting a sensor into the heart, which enables the SV estimated by a model to be validated against a direct measurement. Significant hemodynamic variability induced in the experiment is used to assess model robustness and accuracy in the transient dynamic situations of clinical importance.

1.6 Preface

The remaining thesis chapters cover this topic as follows:

Chapter 2 gives background information of the current methods and techniques available for estimating SV.

Chapter 3 investigates the relationship between SV and PWV, a clinical surrogate of vascular elasticity, to evaluate the potential for monitoring SV using beat-to-beat changes in PWV.

Chapter 4 presents three-element aortic model for interpreting aortic pressure contours. SV is estimated using calibrated/constant model parameters, and its accuracy is analysed.

Chapter 5 extends the aortic model in chapter 4 by combining aortic pressure and PWV measurements. SV estimation error introduced from constant model parameter is decreased using dynamic model parameters calculated using water-hammer equation.

Chapter 6 compares accuracy of SV estimation method developed in chapter 5 with pressure contour method developed by Wesseling et al. (1993) and PiCCO system from PULSION.

Chapter 7 analyses the relationship between contractility, mechanical efficiency of the heart and the output model parameter values of extended aortic model in chapter 5, to expand the clinical usefulness of developed model.

Chapter 8 investigates the method of estimating PWV using ECG and a single aortic pressure measurement to improve clinical practicality of the model developed in chapter 5.

Chapter 9 and 10 summarise the conclusions drawn from this thesis, and examine potential avenues for future work.

Chapter 2: Current Hemodynamic Monitors for Stroke Volume

This chapter gives a brief overview of the current methods available for estimating SV. It is intended to provide the background information needed to understand the advantages and limitations of each method.

2.1 Aortic Flow Probes

An aortic flow probe measures blood flow rate within the aorta, which can be integrated over the systolic period to estimate beat-to-beat SV. The ultrasound flow probe utilizes a property of sound waves propagating through fluid in motion. Sound waves travel faster in the direction of flow and slower against the flow. Using this principle, the time difference between the ultrasound emitter and the receiver placed upstream and downstream can be used to determine flow (Dean et al., 1996). A picture of the aortic flow probe (Transonic Scisense Inc., Ontario, Canada) used in the pig experiments described later in this work is shown in Figure 2.1.

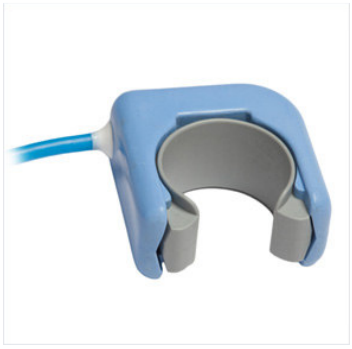

Figure 2.1 – Aortic flow probe by Transonic Scisense. The device is wrapped around the aortic vessel to measure blood flow rate (Transonic, 2015).

Flow measurement from the aortic flow probe is considered very accurate. The method has been validated in vivo using data from pig experiments, where aortic flow was controlled and varied by bypassing the pulmonary circulation with roller pump (Dean et al., 1996). The result showed that this technique is capable of capturing aortic flow with an accuracy of ±2%.

Although aortic flow probes have the ability to produce accurate results in ideal conditions, quality of the measured signal can be reduced depending on the variation in the attenuation of the ultrasound signal and how the equipment is placed (Eren, 1998). For example, the transit time measured by the flow probe could vary when the angle of incidence of the ultrasound beam is changed. Thus, the absolute flow value measured by the device could over/under-estimate the actual flow rate.

The major limitation of measuring SV using an aortic flow probe is that it cannot easily be used in the ICU environment, as it is extremely invasive procedure. The flow probe is placed around the blood vessels, and thus requires direct access to the aorta. Currently, the use of aortic flow probes is mainly limited to experimental and conceptual work (Yang et al., 2013, Phillips et al., 2012).

2.2 Admittance Catheters

Admittance catheters uses the relationship between conductance changes within the ventricle from applied electric field and changes in ventricular blood volume for estimating SV. Admittance catheters commonly comprise excitation electrodes, voltage recording electrodes, and a pressure sensor for obtaining pressure volume information within the ventricle. The catheter is placed directly into the ventricle, and measures the changes in voltage at the recording electrodes from electric field produced by the excitation electrode. The voltage change occurs due to the changes in conductivity induced from fluctuating blood volume within

the ventricle, and also the shape of the cardiac muscle during a heartbeat. The influence from the myocardium in the measured admittance signal is removed using Wei's equation (Wei et al., 2005), and the filtered signal containing only the changes due to conductivity of the blood is converted into a continuous volume measurement, thus SV can be calculated as EDV minus ESV. Mathematical details of the principles used for the admittance catheter can be found in the literature (Porterfield et al., 2009). A diagram of admittance catheter (Transonic Scisense Inc., Ontario, Canada) is shown in Figure 2.2.

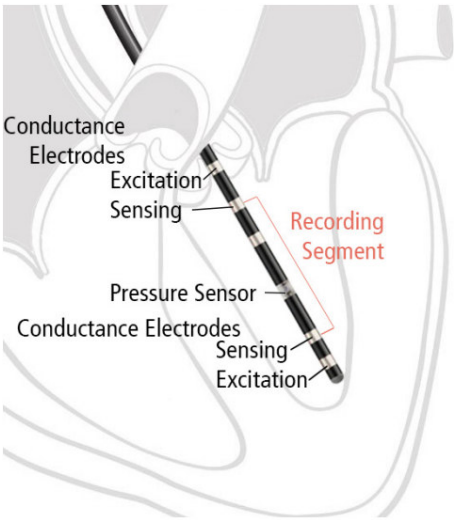

Figure 2.2 – Diagram showing an admittance catheter (Transonic Scisense Inc., Ontario, Canada), placed inside the left ventricle. The catheter comprises excitation electrodes, voltage recording electrodes and a pressure sensor (Transonic, 2013).

The result from a study comparing SV derived from a admittance catheter and three dimensional echocardiography showed precision of approximately ±30% between the two methods (Kutty et al., 2013). Since there is no "gold-standard" measurement for SV (Pugsley and Lerner, 2010), it is difficult to determine the true accuracy of either method. However, both techniques measure volume "directly" with little post-processing of the obtained signal

required. Thus, minimal approximations are made for the derivation of SV, and its reliability is justified by the physics of the method (Taylor, 1966, Porterfield et al., 2009).

The limitations of utilizing admittance catheters in the ICU are similar to those of the aortic flow probe. Placing a catheter within the heart chamber is highly invasive and could decrease the function of the heart by penetrating the ventricular-arterial valve, causing negative influence on blood flow within the ventricle (Evans et al., 2009). It could also increase the chance of blood stream infection (Cousins and O'Donnell, 2004). With the resulting high perceived risk to benefit ratio, the use of admittance catheters in the ICU is not clinically feasible.

2.3 Indicator Dilution Methods

The indicator dilution method estimates blood flow through the heart by measuring at an arterial site, a known quantity of substance or change in properties introduced into the venous system (Grodins, 1962). The "indicator" introduced into the circulation is diluted by the blood, and its level of dilution depends on the blood volume encountered. By measuring how fast the diluted indicator passes through the measurement site, blood flow can be estimated. This relationship between velocity of indicator, level of dilution, and blood flow is known as Stewart-Hamilton equation (Kinsman et al., 1929) and written:

$$Q = \frac{I}{\int c\, dt} \tag{2.1}$$

Where Q, I, and c are blood flow, total quantity of indicator, and indicator concentration, respectively.

The principle given in Equation (2.1) assumes mass conservation, implying the total amount of fluid entering the system must eventually leave the system. Thus, resulting dilution represents the amount of blood volume diluted the indicator, and not the volume permeated/lost into the system. It also assumes no recirculation. Specifically, it is assumed the indicator concentration change only occurs due to dilution in the blood volume and is not influenced by any other external input to the system (Valentinuzzi et al., 1969). These conditions are difficult to achieve in cardiovascular system, where the blood does recirculate, and is constantly leaving/entering blood vessels and tissues.

For example, continuous estimation of blood flow is mathematically possible by extracting the recirculated portion of the indicator (Zierler, 1962). However, the uncertainty involved with the amount of tissue perfusion creates a significant limitation. Thus, indicator dilution is most accurate when an impulse of the indicator is given, and generally limited to providing intermittent CO values (Schmid et al., 1999).

The limitations of the indicator dilution methods arise from the assumptions made in Stewart-Hamilton equation. However, this approach is less invasive compared with aortic flow probes or admittance catheters, as measurements can be made in the circulation and not directly from the heart. Currently, the most common indicator dilution method used in the ICU environment is thermodilution (Ganz et al., 1971).

The thermodilution method uses blood temperature as an indicator for estimating flow. Cold saline of known temperature and quantity is administered in the vein and the "dilution" of blood temperature is measured in the artery. By applying the values of specific heat and weight of the blood to Stewart-Hamilton equation, temperature change/thermodilution from saline can be converted to volume of blood. There are currently two main techniques available for

measuring CO using the thermodilution method, the pulmonary arterial catheter (PAC) and transpulmonary thermodilution (Sakka et al., 2012).

A PAC is introduced into the cardiovascular system via the venous system, then threaded through the right atrium, the right ventricle, and subsequently into the pulmonary artery. The PAC is equipped with a thermistor enabling the temperature of the pulmonary arterial blood to be measured. Cold saline is administered into the venous system and the resulting blood temperature in the pulmonary artery measures CO of the right heart, which must match that of the left heart to prevent blood accumulation in the pulmonary system. A typical path of PAC in the cardiovascular system is shown in Figure 2.3.

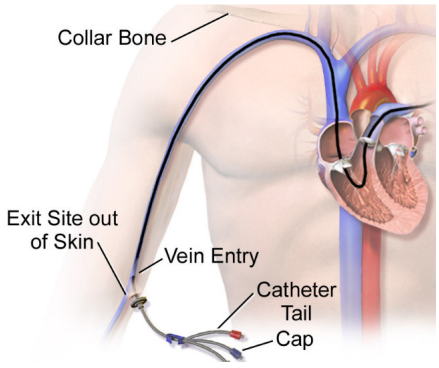

Figure 2.3 – An illustration of pulmonary arterial catheter inserted into cardiovascular system from the vein, through the right heart, and into the pulmonary artery. (Adapted under the Creative Commons Attribution-Share Alike 4.0 International License).

A PAC measures the degree of thermodilution without the indicator going through the capillary system. Therefore, mass is conserved and this approach satisfies the conditions necessary for use of Stewart-Hamilton equation. For this reason, the PAC is regarded as the most accurate indicator dilution method, and many of the modern SV monitoring devices use intermittent estimates from a PAC to validate their system (Pugsley and Lerner, 2010). However, PAC

based methods have precision error of greater than ±30% when compared against estimates from aortic flow probes (Yang et al., 2013). Hence, accuracy is significantly limited.

The PAC also requires penetration of the right heart and may increase catheter related complications (Evans et al., 2009). To overcome this limitation, transpulmonary thermodilution was developed, where the indicator temperature is measured in a systemic artery instead of the pulmonary artery (Sakka et al., 2012). Two separate catheters are required for this method, one in the vein for fluid injection, and another in the artery for indicator detection. However, no equipment goes through the heart.

Transpulmonary thermodilution is less invasive than using a PAC. However, the thermal indicator passes through the capillary system in the lungs and also travels longer distance to the measurement site. These influences on the thermal indicator add error to the estimation of flow, and produce slightly less accurate estimates of CO than using PAC (Sakka et al., 1999).

Finally, both methods are intermittent. However, there is no guarantee the measures are taken when the patient is dynamic and changing, a limitation of any intermittent measure. Hence, along with calibration requirements, these approaches are less suitable for the level of monitoring required.

2.4 Pressure Contour Analysis

Pressure contour analysis utilizes measured arterial pressure, combined with pressure-volume conversion algorithms to estimate blood flow. This method enables continuous estimate of SV as continuous arterial pressure measurements are often accessible in the ICU. Currently, there are several commercial devices available, each using their own unique algorithms (Montenij et al., 2011, Romano and Pistolesi, 2002, Gödje et al., 2002). However, due to lack of published

details in these proprietary devices, accurately assessing the model advantages and limitations of each model is difficult (de Wilde et al., 2008).

The foundation of all the algorithms used is based on the relationship between pressure, SV, compliance, and vascular resistance (Montenij et al., 2011). As discussed in Section 1.2.5, if compliance and/or vascular resistance of the artery can be identified, arterial flow and volume change can be calculated from the pressure, and thus, SV computed. The main difference between each algorithm can be found in the identification method for these vascular properties.

There are three main types of identification methods used in these pressure contour analysis based commercial devices: 1) using intermittent CO values with indicator dilution (e.g. PiCCO system, PULSION); 2) from patient demographic and physical characteristic (e.g. FloTrac system, Edwards Lifesciences); and 3) using only the shape of the pressure waveform (e.g. MostCare system, Vyetech Health). Commercial devices such as PiCCO and FloTrac using the first and second methods combine the third method to track/determine dynamic changes in vascular properties. The indicator dilution values and/or patient characteristics are used for initial/discrete calibration of the system.

The accuracy of commercial devices is validated against methods that are considered more accurate, such as the indicator dilution. In general, calibrated systems provide more accurate estimates than uncalibrated systems (Vincent et al., 2011). However, previous validation studies show that pressure contour algorithms become less reliable when there is changes in vasomotor tone (Yamashita et al., 2008, Yamashita et al., 2007, Monnet et al., 2010, Cecconi and Rhodes, 2010). This is a significant limitation of current pressure contour methods as the tone changes are inevitable in patients with dynamically evolving cardiovascular dysfunction

requiring circulatory treatment, especially once some circulatory resuscitation treatments seek to directly modify vasomotor tone.

2.5 Minimal to Non Invasive Methods

There are two well-known methods for minimal/non-invasively estimating SV, which are echocardiography and oesophageal Doppler. In contrast to the methods described in previous sections, these methods does not require breaking through body's membrane by the equipment. Echocardiography can be performed on the surface of the body and oesophageal Doppler only requires insertion of transducer probe down the oesophagus.

2.5.1 Echocardiography

Echocardiography uses the Doppler principle to determine flow velocity and cross-sectional area of aorta (Anavekar and Oh, 2009), thus integrating product of these two variables over systole produces an estimate of SV. The precision of Doppler echocardiography against thermodilution reported in a systematic review paper (Wetterslev et al., 2016) showed a mean error of ±32%.

The main advantage of echocardiography is that it is non-invasive and adds no further risks to the patient. However, this technique requires specialised device/personnel, and impractical to obtain continuous SV. Thus, echocardiography only provides intermittent SV and important transient data is missing when assessing/managing patient conditions.

2.5.2 Oesophageal Doppler

The oesophageal Doppler method uses same principle as echocardiography, except the Doppler probe is inserted into the oesophagus pointing towards the thoracic aorta. This method

overcomes the limitations of echocardiography by taking continuous estimate of SV without the operator by leaving the probe in place. However, this technique has a steep learning curve, and the accuracy of SV can be operator dependent (Marik, 2013). The probes are inserted blindly and the resulting waveform is highly dependent on its depth and its rotation (Lefrant et al., 1998). Studies found better accuracy is achieved when the operator was not blinded to the results of the CO obtained with a PAC (Valtier et al., 1998), suggesting correct positioning of the probe requires some reference measurements.

2.6 Summary

At present, there is no gold-standard measure for SV, despite several methods available with varying accuracies and invasiveness. SV estimates from aortic flow probes, admittance catheters, and PAC are considered most accurate as measurements are made closest/directly from the heart with well-accepted laws of physics, leading to minimal measurement error. However, these methods are impractical in the ICU environment due to their highly invasive nature. PAC provides the least invasive method out of the three, and its benefit may outweigh the risks involved, but only provides intermittent SV values.

In contrast, transpulmonary indicator dilution and pressure contour methods provide a less invasive, more clinically feasible means to estimate SV. Despite increased convenience by these methods, expected accuracies are lower as more assumptions need to be made on the principles used to identify SV. In addition, assessment of currently available pressure contour commercial devices is extremely difficult due to limited details available on the algorithms used, and their limitations cannot be easily investigated.

Minimal to non-invasive methods of estimating SV are possible with echocardiography and oesophageal Doppler. However, these methods require specialised personnel to operate and

can be cumbersome. Furthermore, echocardiography only provides intermittent SV values and estimates from oesophageal Doppler are ambiguous due to its results being highly operator dependent.

Currently, highly invasive methods offer continuous and more accurate estimate of SV. On the other hand, the accuracy is decreased and/or measurements of SV are intermittent as the method becomes less invasive. Thus, development of continuous, accurate, and non-additionally invasive method for estimating SV has significant value.

Chapter 3: Correlation between Stroke Volume and Pulse Wave Velocity

This chapter investigates the relationship between SV and pulse wave velocity (PWV) to evaluate clinical applicability of estimating SV using the value of PWV. Non-invasive PWV measurements are relatively easy to obtain in a critical care environment, and thus, the relationship could potentially provide a practical solution for monitoring SV in a non-invasive or minimally invasive fashion. The strength of this relationship is tested in various hemodynamic states to examine expected accuracy and reliability of SV estimation from PWV.

3.1 Introduction

PWV is the velocity of the pulse wave propagating through the arterial system and an indicator of arterial stiffness (Mackenzie et al., 2002). In particular, a high PWV indicates low arterial compliance as waves travel faster in a stiffer medium. In contrast, a low PWV implies high arterial compliance.

Several studies have established associations between high PWV and the incidence of cardiovascular disease (Blacher et al., 1999, Cecelja and Chowienczyk, 2012). For these reasons, PWV is generally used to assess cardiovascular risk of an individual (Ben-Shlomo et al., 2014). Currently, the gold standard method for measuring PWV is highly invasive, involving two pressure measurements at the carotid artery and the femoral artery (Laurent et al., 2006). However, non-invasive methods are also available (Yamashina et al., 2002, Horvath

et al., 2010) and the ease of obtaining these PWV measurements has led to many clinical applications using this parameter (Hirata et al., 2006).

In the ICU, titrating hemodynamic support therapies, such as fluid replacement and inotrope/vasoactive drugs is challenging (Michard and Teboul, 2002, Bangash et al., 2012). In particular, studies show approximately half of all fluid interventions are effective with the rest potentially harmful from the extra fluid introduced (Phillips and Brierley, 2015). This poor, effectively random outcome is mainly from the interventions being made without information on SV. Without monitoring changes in patient-specific SV, the efficacy of hemodynamic support therapy cannot be correctly identified, particularly in highly dynamic and transient scenarios.

Consequently, excessive fluid introduced to the patient may cause tissue oedema, and organ damage, and has been demonstrated to increase mortality during septic shock (Vincent et al., 2006, Boyd et al., 2011). Although information on SV is important in making correct decisions, SV is difficult to measure even in the ICU and usually requires additionally invasive measurements (Gomez and Palazzo, 1998) and/or expensive specialised equipment (Mehta and Arora, 2014).

This chapter analyses mathematical relationships between SV and PWV to investigate whether PWV could be used as an alternative index for capturing SV dynamics. Since PWV measurements are much easier to obtain than direct SV measurements, the relationship could provide minimally invasive and cost effective solutions for monitoring patient SV changes, and optimising hemodynamic treatment. In addition, the SV values obtained can be used to access key cardiovascular parameters through physiological models, providing further useful information that is not currently clinically accessible.

3.1.1 Background

Moens and Korteweg first derived the equation relating the elastic properties of the artery to the velocity of pulse wave in 1878 (Tijsseling and Anderson, 2012).

$$PWV = \sqrt{\frac{Eh}{2r\rho}} \tag{3.1}$$

Where E, h, r, and ρ are elastic modulus, thickness of arterial wall, radius of the artery, and blood density, respectively.

Bramwell and Hill (Bramwell and Hill, 1922) reformulated Equation (3.1) to be more clinically applicable by relating PWV to "distensibility", which is the rate of volume increase with pressure increase. This modification was achieved by introducing the relationship that small increases in pressure, P, will cause small increases in the radius of the artery, r, where, $\delta r = \delta P r^2/Eh$, resulting in:

$$PWV = \sqrt{\frac{1}{\rho D}} \tag{3.2}$$

$$D = \frac{\delta V}{V \delta P} \tag{3.3}$$

Where V is the blood volume within the section of artery at the end of diastole and D is the distensibility of the arterial wall.

At present, the distensibility of the arterial wall is interpreted by assuming constant blood density and changes in the wave velocity result entirely from the elastic nature of the arterial wall. This latter assumption holds true only if the velocity of the blood carrying the pulse wave

does not vary with varying patient conditions, which it almost certainly does (SINGER et al., 1991).

Clinically measured PWV must be treated as the addition of a velocity of wave along the artery with no blood flow, and the velocity of the blood that carries the wave. Thus, a change in measured PWV does not necessarily come only from the elastic properties of the artery. For example, the magnitude of SV itself could influence the velocity of the blood without causing changes in the arterial distensibility. Thus, measured PWV is a function of distensibility and velocity effects:

$$PWV_{measured} = PWV_{distensibility} + PWV_{velocity} \tag{3.4}$$

Although, it has been reported that PWV values can be different between individuals (Collaboration, 2010), it can be assumed that intra-subject variability of arterial wall distensibility is a lesser component of changes in PWV. If this assumption holds, the changes in PWV should reflect the changes in the flow condition inside the artery generated by SV. Thus, this chapter investigates strength of the relationship between SV and measured PWV in various hemodynamic conditions, to investigate its validity.

3.2 Method

3.2.1 Porcine Trials and Measurements

This study uses data from experiments performed on pigs at the Centre Hospitalier Universitaire de Liege, Belgium. All experimental procedure, protocols and the use of data in this study were reviewed and approved by the Ethics Committee of the University of Liege Medical Faculty.

Experiments were performed on 8 healthy, pure pietrain pigs weighing between (20 – 29)kg. The pigs were premedicated with ketamine (20mg/kg) and diazepam (1mg/kg). Anesthesia was induced and maintained by a continuous infusion of sufentanil (0.5µg/kg/hour) and sodium pentobarbital (3mg/kg). The pigs were intubated via tracheotomy and ventilated using a Draeger Evita2 ventilator (Draeger, Lubeck, Germany).

Left ventricular pressures and volumes were directly measured using 7F micromanometer-tipped admittance catheters (Transonic Scisense Inc., Ontario, Canada) inserted into the ventricles through the right carotid artery. Pressure waveform measurements were captured at the aortic arch and abdominal aorta with 7F pressure catheters (Transonic Scisense Inc., Ontario, Canada). Catheters for pressure waveform measurement were inserted into the aortic arch through the left carotid artery and into the abdominal aorta through the femoral artery, respectively. In addition, aortic root flow was measured using an ultrasound flow probe (Transonic Scisense Inc., Ontario, Canada) for Pigs 7 and 8. All cardiovascular and respiratory data were sampled at 250 Hz.

3.2.2 Hemodynamic Modification

During the experiments, each pig underwent several step-wise positive end Expiratory pressure (PEEP) recruitment manoeuvres (RM). Increases in PEEP reduce systemic venous return to the right heart and increase pulmonary resistance. As a consequence, left ventricular preload decreases, causing a reduction in SV (Luecke and Pelosi, 2005). RM induced SV variations are similar to those made by volume expansion; as both of them modify SV as a result of changes in preload.

Each RM involved increasing PEEP with 5 cmH_2O steps to a maximum of (20-25) cmH_2O then reducing PEEP back to the original level in a step-wise manner for Pigs 1-6, and sudden

drop from maximum PEEP to original PEEP for Pigs 7 and 8. An example of the relationship between SV and PEEP from one of the RM period are shown in Figure 3.1, where SV was measured directly by the left ventricle volume catheter.

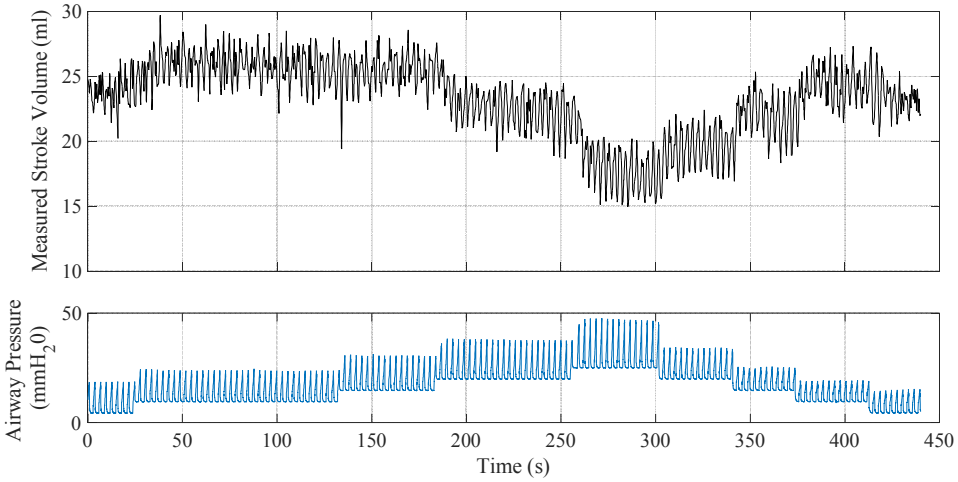

Figure 3.1 – Example of relationship between directly measured SV and PEEP from an experiment. Top Panel: Measured SV from left ventricular admittance signal. Bottom Panel: Measured airway pressure from mechanical ventilator.

The experiment also included multiple administrations of fluid boluses throughout the experiment. However, SV changes made by fluid boluses were insignificant and did not produce preload changes desired, likely due to the pigs being otherwise healthy. On the other hand, the RMs produced significant changes in preload with noticeable effect on SV. For this reason, this analysis uses data from RM period only, covering a wider range of preload changes than those expected from volume expansion.

The experiment also involved administering continuous dobutamine infusions to modulate contractility for Pigs 1 to 6. Dobutamine increases contractility of the heart and acts as a vasodilator (Ruffolo Jr, 1987), providing additional data for this study in modified hemodynamic conditions. Dobutamine was administered at a rate of (2.5, 5 or 10) µg/kg/min.

For Pigs 7 and 8, a single infusion of endotoxin (lipopolysaccharide from E. Coli, 0.5 mg/kg injected over 30 minutes) was administered to induce septic shock. Endotoxin causes capillary leak and significantly reduces the systemic resistance and afterload condition of the heart (Werdan, 2001). The effect provides further data to assess the relationship between PWV and SV in different hemodynamic conditions.

In summary, the data set for this analysis includes two RM periods: 1) baseline period where pigs received no intervention (dobutamine/Endotoxin); and 2) a period where the pig's condition was changed using dobutamine (Pigs 1-6) or endotoxin induced sepsis (Pigs 7-8). There was no baseline period for Pig 1 as dobutamine was administered at the beginning of the experiment due to a change in experimental protocol after the first experiment.

3.2.3 Pulse Wave Velocity Measurements

Pulse wave velocity can be measured by identifying the time taken for a pressure wave to travel a known distance within the artery, defined:

$$PWV = \frac{\Delta x}{\Delta t} \tag{3.5}$$

Where Δx is the distance travelled by the pressure wave and Δt is the time taken for pressure wave to travel the distance (transit time).

In this analysis, the PWV was obtained using experimentally measured aortic arch pressure and abdominal aortic pressure waveforms. The distance between the two catheters were measured on the body's surface by approximating the catheter locations. This method requiring estimation of distance may introduce small errors in the absolute value of PWV. However, as the catheters did not move within a given pig during the experiment, PWV trends were

estimated to be unaffected. The measured distance between catheter locations were approximately 40cm in all pigs and this value was used as Δx.

Transit time was determined by locating the 'foot' of the systolic rise on both aortic arch and descending aortic pressure waveform (Millasseau et al., 2005). In this analysis, the 'foot' of the pressure was identified as the intersection of the tangent line along the maximum systolic pressure gradient and the horizontal line along the minimum pressure, as shown in Figure 3.2.

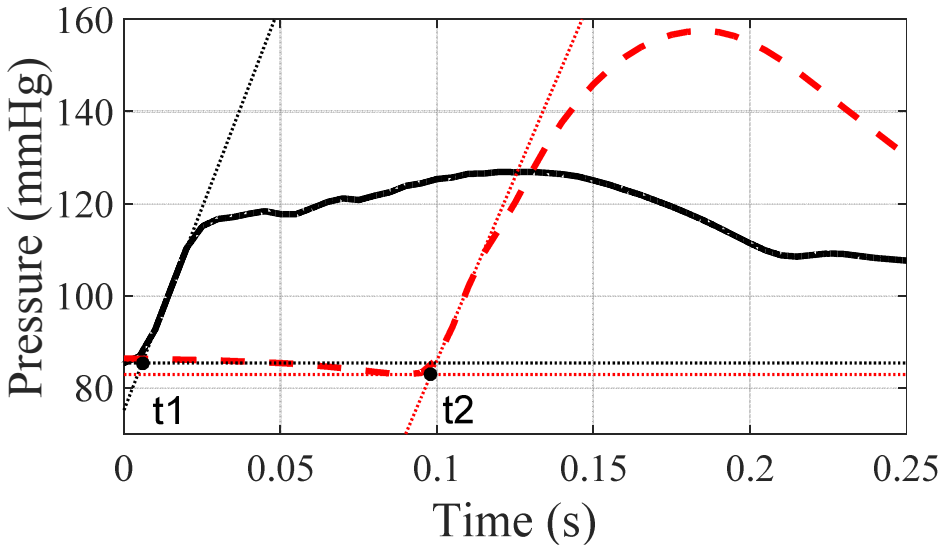

Figure 3.2 – Example of measured aortic arch pressure (solid black line) and abdominal aortic pressure (dashed red line) waveforms. Dotted thin lines represent maximum systolic gradient and minimum pressure line for aortic (dotted black) and descending aortic pressures (dotted red). Solid black dots represent identified 'foot' of the pressure waveforms at time t1 and t2 respectively.

3.2.4 Signal Processing

The raw volumetric and flow signals recorded by the admittance and ultrasound flow probe were filtered to remove the measurement noise. These signals contained high frequency components that are physiologically unrealistic. An example of the raw volumetric/flow measurement and its corresponding frequency spectrum are shown in Figure 3.3.

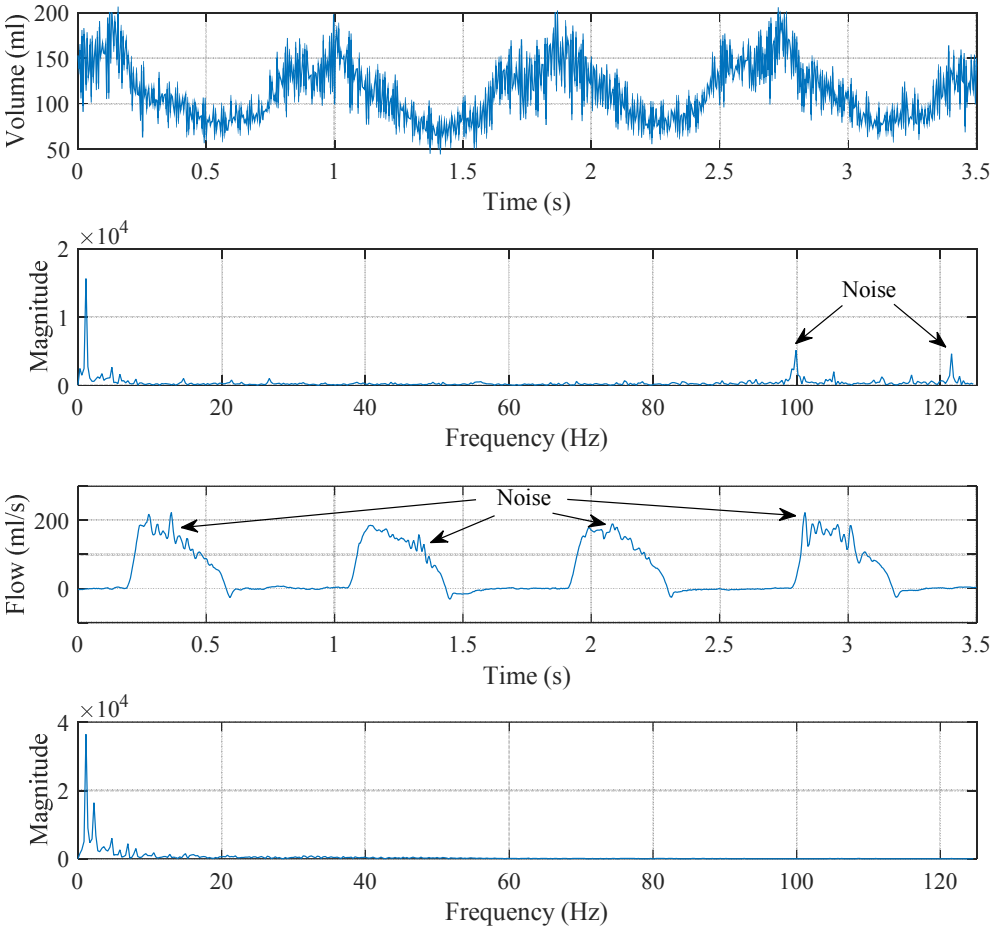

Figure 3.3 – Top Panel: Raw volume signal recorded by admittance catheter. Second Panel: Frequency spectrum of the volume signal. Third Panel: Raw flow signal recorded by electromagnetic flow probe. Bottom Panel: Frequency spectrum of the flow signal. Noise can be seen in both of the signal as pointed out in second and third panel.

Noise was removed by applying finite impulse response (FIR) filter. A 50th order low pass filter with cutoff frequency at 10 Hz, which is approximately 5 - 10 times the heart rate, were used based on the assumption that any changes in the signal beyond this frequency are unphysiological. Signals were filtered on MATLAB using the command 'fir1' (hamming window). The frequency response of the filter and filtered signals are shown in Figures 3.4 and 3.5, respectively.

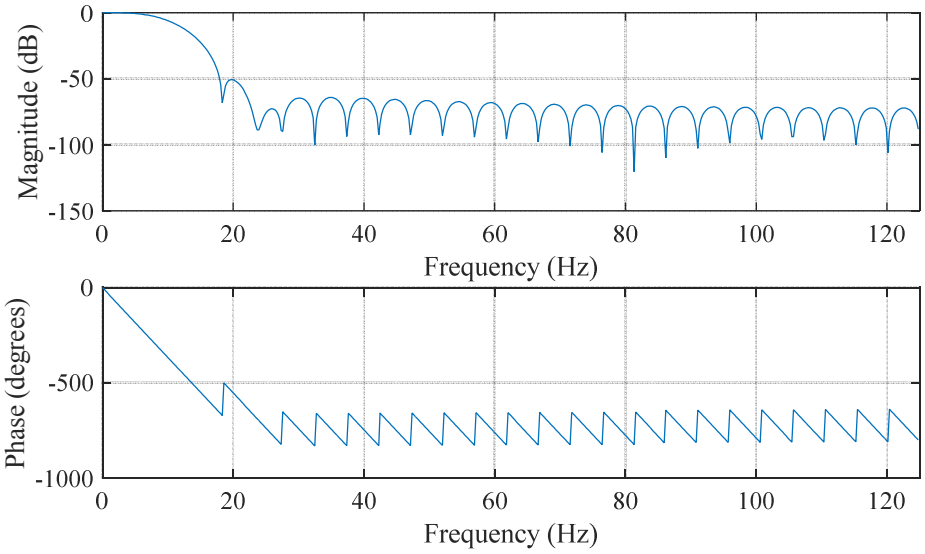

Figure 3.4 – Frequency response of the FIR filter used for admittance and ultrasound flow probe signals.

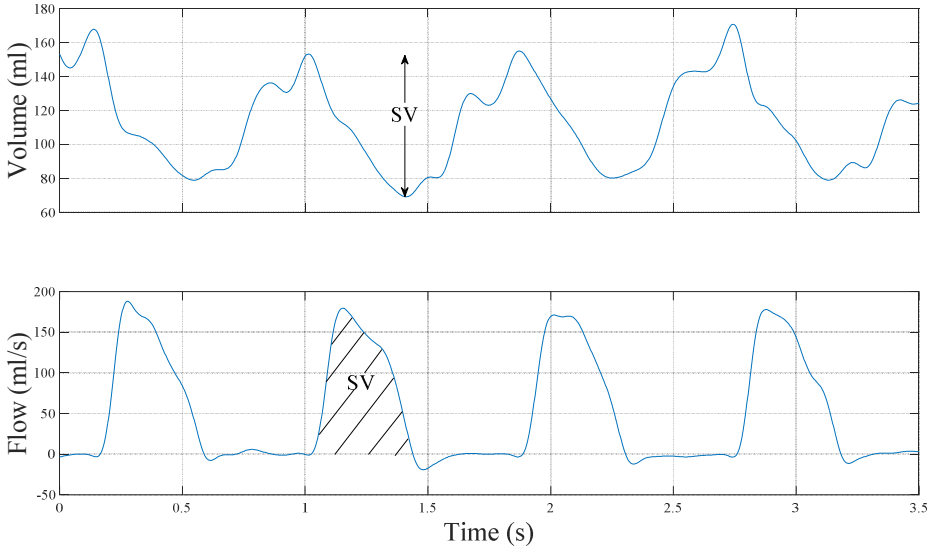

Figure 3.5 – An example of FIR filtered signal (blue line). Top Panel: Filtered volume signal from admittance catheter. Bottom panel: Filtered flow signal from ultrasound aortic flow probe. Stroke volume calculated from the signals are shown in each signal.

In the data pre-processing stage, measurements having obvious error due to equipment or catheter disturbance/failure were removed. Measured aortic arch pressure, abdominal aortic

pressure, and left ventricular volume waveform data were split into individual heart beats for the analysis of beat-to-beat changes in PWV and SV. For each beat, PWV was calculated using Equation (3.5) with aortic and abdominal aortic pressure waveforms. SV was calculated as the difference between maximum and minimum left ventricular volumes from admittance signals for Pigs 1 - 6. For Pig 7 and 8 the SV was measured using the integral of aortic flow rate per beat, as shown in Figure 3.5.

3.3 Results

3.3.1 Investigated Physiological Range

Table 3.1 shows the range of aortic arch pressure (P_{aoa}), abdominal aortic pressure (P_{abao}), heart rate (HR), SV, and PWV investigated in this study. It can be seen that wide ranges of induced hemodynamic changes are analysed, which should provide a robust estimate of the validity of any relation between SV and PWV. Dobutamine increased HR significantly in all pigs and had a different impact on SV depending on the subject, as expected. Aortic arch and abdominal aortic pressure varied as might be expected with dobutamine infusion and administration of endotoxin. Overall, a wide, clinically and physiologically relevant range was obtained.

There was large inter-subject variability in all physiological variables, even at baseline RM period, where no interventions were made. The average aortic pressures in Pig 2 were approximately four times larger than Pig 6 and 8. The value of PWV for Pigs 3 and 5 was approximately two times larger Pig 6.

Table 3.1 - Investigated range of physiological parameters P_{aoa}, P_{abao}, SV and PWV across Recruitment Manoeuvre (RM) period for each pig. Data are presented as the median [5 – 95th percentiles].

Baseline RM					
Subject	**P_{aoa} (mmHg)**	**P_{abao} (mmHg)**	**HR (min^{-1})**	**SV (ml)**	**PWV (ms^{-1})**
Pig 1	-	-	-	-	-
Pig 2	155 [145 – 161]	168 [151 – 180]	63 [61 – 65]	32.9 [30.9 – 34.6]	5.8 [5.4 – 6.1]
Pig 3	119 [111 – 123]	118 [109 – 123]	80 [76 – 81]	18.3 [17.0 – 19.9]	7.0 [6.7 – 7.3]
Pig 4	118 [69 – 154]	115 [67 – 150]	93 [80 – 99]	30.1 [27.3 – 34.5]	5.6 [5.0 – 6.3]
Pig 5	116 [104 – 125]	120 [110 – 129]	77 [70 – 82]	31.2 [26.3 – 37.7]	8.9 [8.5 – 9.2]
Pig 6	44 [38 – 49]	48 [42 – 52]	73 [71 – 74]	27.0 [22.4 – 33.3]	3.8 [3.5 – 4.0]
Pig 7	62 [51 – 72]	73 [60 – 82]	77[76 – 79]	56.3 [47.0 – 67.6]	5.1 [4.8 – 5.4]
Pig 8	47 [38 – 50]	43 [35 – 46]	74[72 – 75]	23.3 [18.6 – 28.0]	5.1 [4.6 – 5.3]
Dobutamine RM					
Subject	**P_{aoa} (mmHg)**	**P_{abao} (mmHg)**	**HR (min^{-1})**	**SV (ml)**	**PWV (ms^{-1})**
Pig 1	79 [72 – 105]	81 [73 – 106]	136 [120 – 143]	38.0 [33.5 – 46.9]	4.7 [4.3 – 5.3]
Pig 2	153 [124 – 170]	166 [129 – 199]	104 [90 – 108]	28.3 [24.4 – 34.3]	6.2 [5.9 – 7.0]
Pig 3	61 [44 – 91]	60 [45 – 89]	145 [136 – 146]	19.1 [13.6 – 26.4]	5.9 [5.1 – 6.6]
Pig 4	66 [55 – 98]	67 [55 – 99]	193 [190 – 197]	17.4 [12.7 – 24.9]	5.3 [4.8 – 5.9]
Pig 5	104 [90 – 91]	108 [94 – 119]	100 [90 – 110]	25.3 [23.1 – 27.5]	8.9 [8.5 – 9.3]
Pig 6	68 [50 – 91]	70 [53 – 94]	144 [141 – 151]	24.0 [18.4 – 27.0]	5.4 [4.8 – 6.1]
Endotoxin RM					
Pig 7	58 [49– 64]	67 [58 – 73]	71 [69 – 73]	59.2 [50.1 – 71.9]	4.8 [4.7 – 5.0]
Pig 8	45 [44– 46]	42 [41 – 43]	66 [65 – 67]	26.9 [25.1 – 29.2]	4.8 [4.6 – 5.0]

3.3.2 Correlation of Absolute Values

Correlation plots between absolute values of measured SV and PWV for each pig are presented in Figure 3.6. The analysis involved approximately 600 to 2000 heartbeats per pig and a total of more than 9500 heartbeats. The calculated correlation coefficients in each RM period and for each pig are shown in Table 3.2.

The correlation coefficient between SV and PWV showed higher values in the dobutamine RM period than the baseline RM period in most pigs. This might be due to the effect of increasing the inotropic state of the heart and preload responsiveness inducing higher SV changes from PEEP changes. This additional discrepancy in the data caused by the effect of dobutamine have allowed the increase in correlation coefficient.

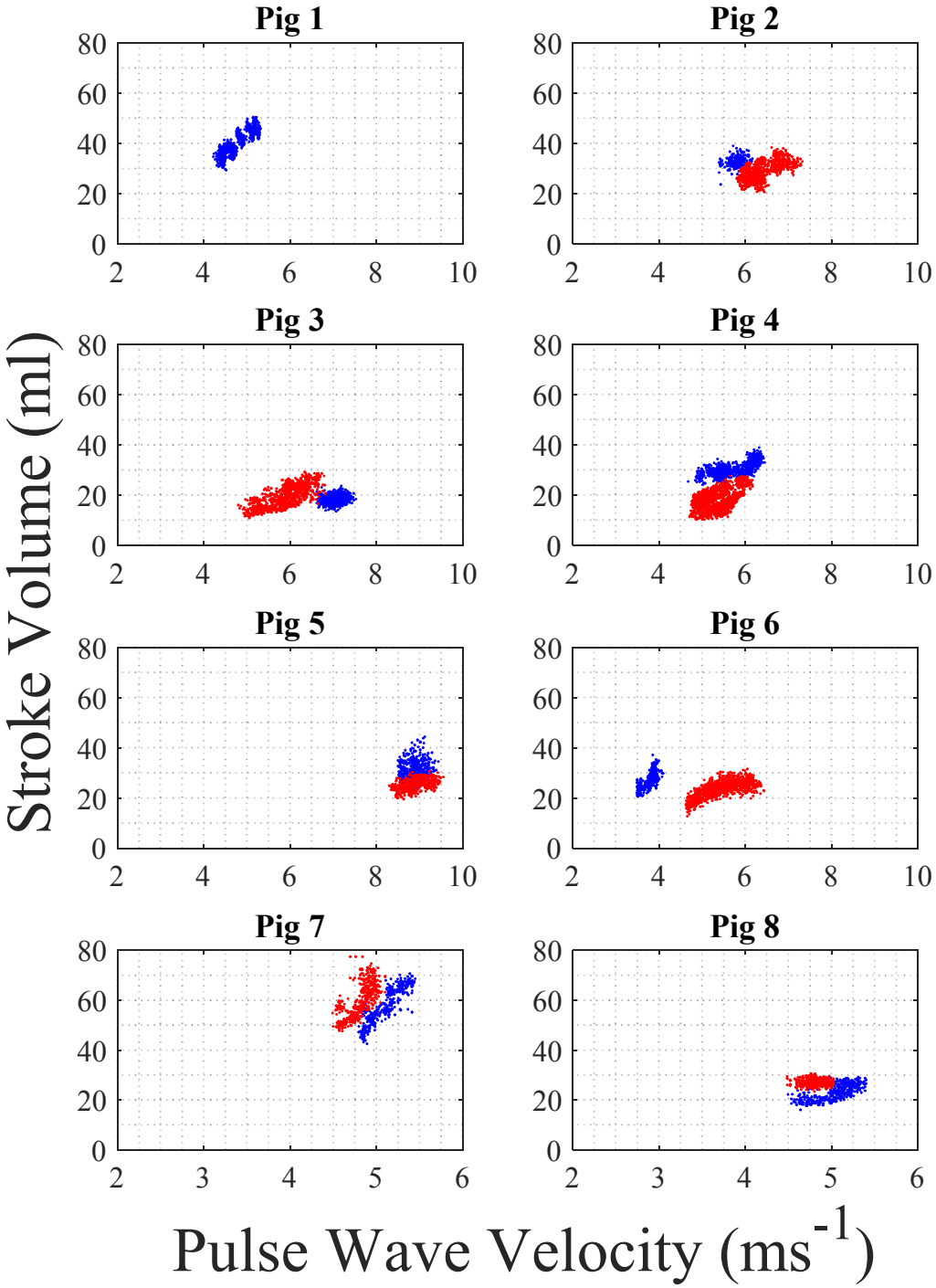

Figure 3.6 – Correlation plots between absolute value of SV and PWV for each pig. Baseline RM period are shown with blue dots and dobutamine/sepsis RM period are shown with red dots.

Table 3.2 – Correlation coefficient (R) between PWV and SV in each RM period and in individual pig.

SV-PWV (correlation coefficient)			
Subject	Baseline RM	Dobutamine/Endotoxin RM	Overall
Pig 1	-	0.86	0.86
Pig 2	0.24	0.63	0.23
Pig 3	0.15	0.73	0.19
Pig 4	0.70	0.43	0.58
Pig 5	0.25	0.46	0.18
Pig 6	0.67	0.70	-0.11
Pig 7	0.87	0.69	0.47
Pig 8	0.12	0.32	0.02

3.3.3 Correlation of PEEP Dependent Trend Values

It can be seen from Figure 3.6 and Table 3.2 that the overall relationships between absolute values of SV and PWV were poor across the hemodynamic modifications induced by administration of dobutamine/sepsis. However, relatively high correlation coefficient values were achieved between SV and PWV when SV varied only due to RM.

The next analysis looks at the relationship between trend values of SV changes and trend values of PWV induced by PEEP. To determine the trend relationships, data from each RM were separately analysed by subtracting the mean value of SV and PWV from the absolute SV and PWV values for the RM period, yielding 'SV – mean (SV)' and 'PWV – mean (PWV)'. This calculation removes the hemodynamic effect from dobutamine/endotoxin, and allows analysis of the SV and PWV relationship for SV changes due only to PEEP variations (preload). The correlation plots for each individual pig and all pigs combined are presented in Figures 3.7 and Figure 3.8, respectively. Pearson correlation coefficients (R) for each individual pig and the gradient value of the regression line are shown in Table 3.3.

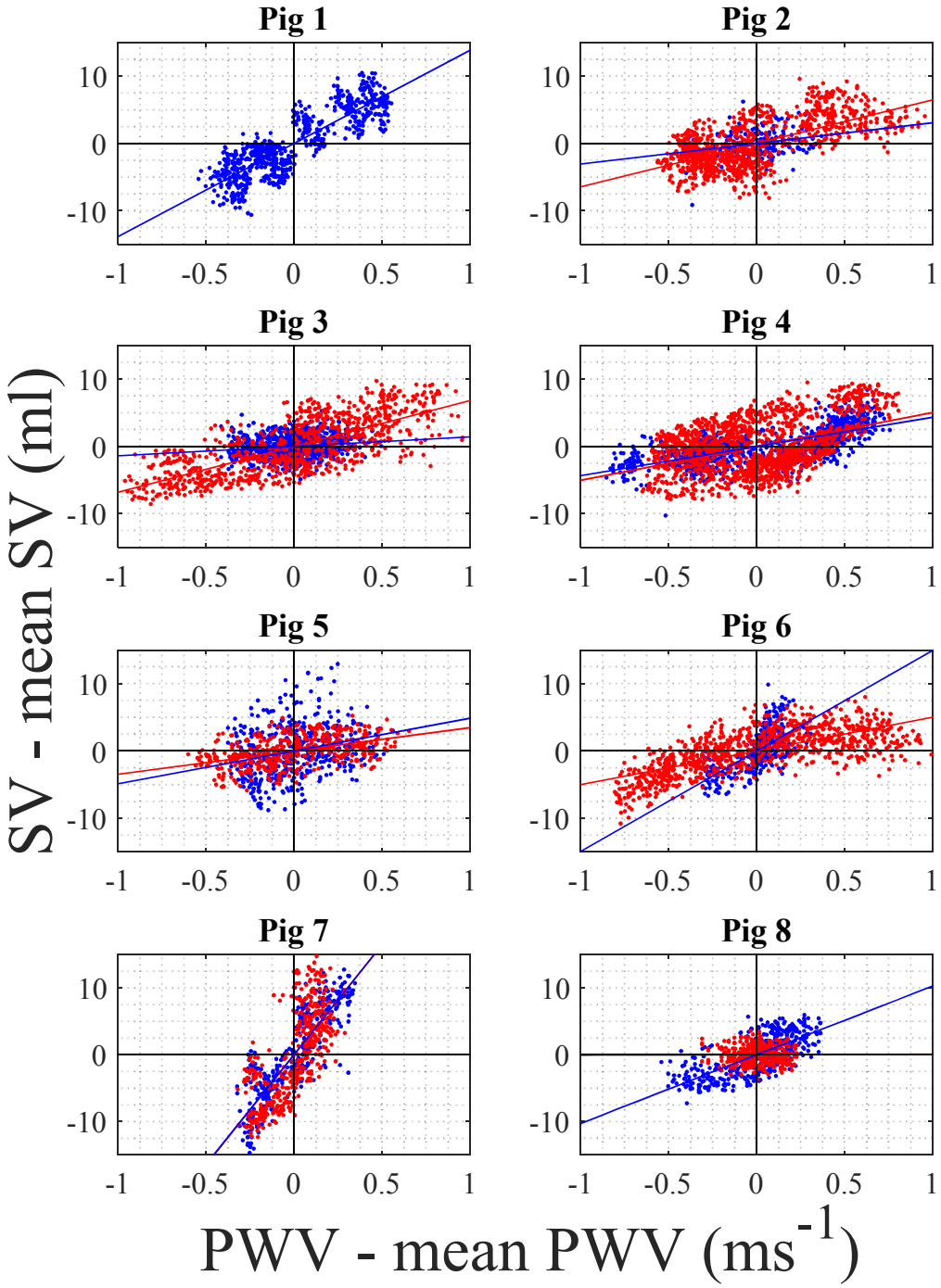

Figure 3.7 - Correlation plots between trend value 'SV – mean SV' and 'PWV – mean PWV' for each pig. Baseline RM period are shown with blue dots and dobutamine/sepsis RM period are shown with red dots. Regression line for each RM periods are also shown with corresponding colour. (Note: gradient of sepsis regression line for Pig 7 was same as baseline and very close to zero for Pig8, hence the line is not so visible).

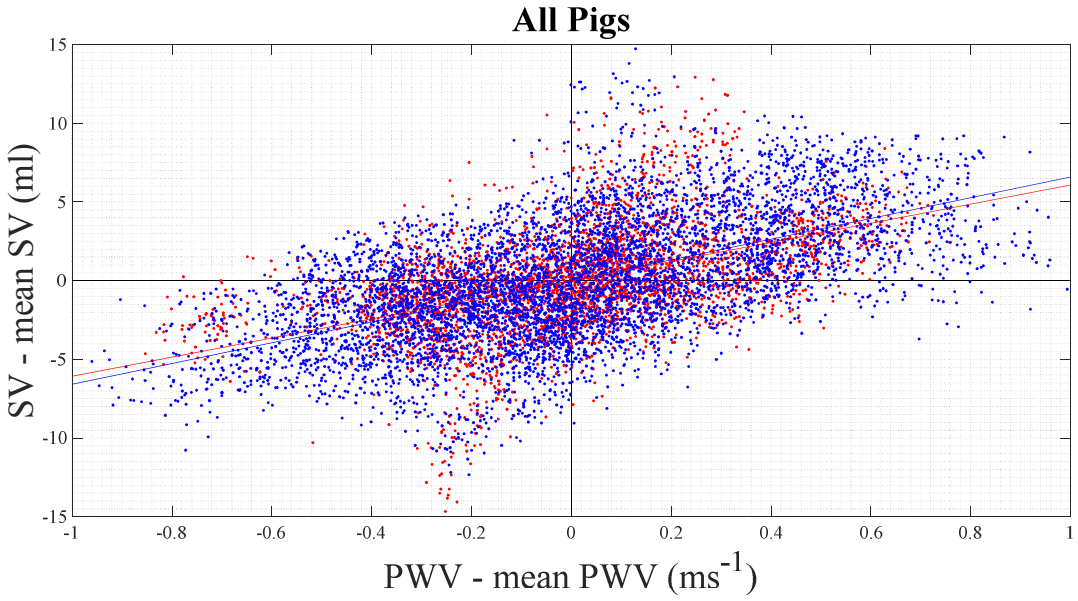

Figure 3.8 – Correlation plots and regression line across all pigs for trend values 'SV – mean SV' and 'PWV – mean PWV'. Baseline RM and dobutamine/endotoxin RM are shown with blue and red colour respectively.

Table 3.3 – Correlation coefficient (R) between PWV and SV for 'SV – mean SV' and 'PWV – mean PWV' in individual pig. Correlation coefficient represents data including both baseline and dobutamine/endotoxin RM.

SV-PWV (trend relationship)			
Subject	Baseline RM regression gradient	Dobutamine/Endotoxin RM regression gradient	Correlation coefficient (R)
Pig 1	-	13.85	0.86
Pig 2	3.06	6.45	0.61
Pig 3	1.40	6.82	0.66
Pig 4	4.33	5.03	0.51
Pig 5	4.87	3.46	0.31
Pig 6	14.93	5.00	0.66
Pig 7	32.84	33.03	0.77
Pig 8	10.28	0.07	0.57
All Pigs	6.08	6.59	0.56

3.4 Discussion

3.4.1 Relationship between PWV and SV

The results from Figure 3.6 shows the effect of changes in PWV from dobutamine and endotoxin. Dobutamine increases the contractility of the heart, HR, and reduces the arterial stiffness (Ruffolo Jr, 1987). Endotoxin significantly reduces the systemic resistance via capillary leak and vasodilation (Merx and Weber, 2007). Figure 3.6 displays these effects as the relationship between the absolute value of SV and PWV are altered with the intervention, seen in the difference between the blue dots and the red dots. Both dobutamine and endotoxin modify both distensibility and flow velocity, affecting PWV through changes in the arterial wall properties and systemic resistance. More specifically, with changes in distensibility independent of changes in flow conditions due to dobutamine and endotoxin, sum of these two factors could give constant measured PWV even when SV is changed or vice versa. Under these significant influences on hemodynamic conditions, the relationships between the absolute value of SV and PWV were weaker than expected.

Figure 3.7 analyses the relationship between 'SV-mean SV' and 'PWV – mean PWV' to assess normalized changes in SV and PWV, where SV were predominantly varied by alteration of preload conditions from PEEP variation (Pinsky, 1984) in the RM. Mean values of SV and PWV were subtracted from the absolute value of SV and PWV in each RM period to remove the effect of dobutamine/endotoxin. The figure shows a clear positive relationship between SV and PWV, not evident in Figure 3.6.

Table 3.3 shows good agreement between 'SV – mean SV' and 'PWV – mean PWV' with correlation coefficients above R=0.5 for all pigs, except for Pig 5. With only the variation in preload, changes in PWV from flow velocity and distensibility are thought to be both in the

same direction. Reduction in SV from increased PEEP decreased flow velocity, and with the reduction in amount of volume entering the artery, distensibility is also decreased. In such condition, where changes in flow condition is the main cause of changes in distensibility, and thus PWV, PWV correlated well with the changes in SV.

Figure 3.8 shows correlation plots for 'SV – mean SV' and 'PWV – mean PWV' for all pigs combined, and the correlation coefficient was R = 0.56. Although significant variation exists about the regressed line, the relationship suggests that the PWV could be used to determine trends of SV if hemodynamic conditions were changed only due to preload, such as fluid replacement (Monnet and Teboul, 2013). The wide variation of slopes in Table 3.3 and Figure 3.7 show why the variability in Figure 3.8 can be large. While relationships are stronger for each individual pig, it is clear that the relationship can be very different between pigs. This result provides the possibility of reducing the need for additionally invasive measures or expensive devices to help optimise fluid administration rates.

3.4.2 The Relationship in Assessment of Preload Responsiveness

It is common in cases of cardiovascular failure to assess patient preload responsiveness (Michard and Teboul, 2002). Clinical studies show that only 50% of patients with cardiovascular failure are fluid responsive and will benefit from volume expansion (Marik et al., 2009). In the case where a patient is not fluid responsive and volume expansion does not increase SV, the continuation of fluid therapy may result in worsening patient's condition (Roch et al., 2011). Thus, an improvement to the method for estimating preload responsiveness would provide significant benefits to care and patient outcome.

The assessment of preload responsiveness involves changing preload while monitoring SV (Mohsenin, 2015). The former can be achieved relatively easily by performing a fluid challenge,

passive leg raising, or changing airway pressure (Marik et al., 2010). However, evaluating the impact on SV from altered preload condition is very difficult due to lack of available information on SV. Currently, there are several methods available for monitoring SV, varying from non-invasive procedures such as echocardiography to highly invasive methods such as thermodilution (Alhashemi et al., 2011). However, all these methods require additionally invasive measurements and/or expensive equipment (Lavdaniti, 2008). Thus, the positive relationship and trend correlations found from this analysis can be used to identify SV trends from PWV, improving the accuracy of fluid responsiveness assessment in a minimally invasive and cost effective manner.

3.4.3 Limitations

3.4.3.1 Identifying Absolute Values of SV from the Relationship

The inter-subject variability of arterial wall properties and varying impact on vascular properties from dobutamine and endotoxin prevents use of the relationship between SV and PWV to estimate the exact impact on SV. Figure 3.7 and Table 3.3 show consistent positive relationships between SV and PWV. However, the slope of the relationship between each subject before and after the interventions can be very different. This difference in the slope prevents estimation of the degree of impact on SV, specifically the amount of change in ml, if there are significant hemodynamic modifications.

In addition, in the dobutamine/endotoxin modified RM period for Pig 6 and Pig 7, the relationships are shown to be nonlinear, making identification of the absolute value of SV from PWV even more difficult. This nonlinearity might be due to nonlinearity of the arterial wall property producing smaller or larger distensibility changes from the volumetric input into the artery from aorta (Langewouters et al., 1984). Another explanation is the nonlinearity of the Frank-Starling mechanism (Fukuda et al., 2009) producing different contractility level for a

given amount of SV. Different contractility would change the velocity of the blood as well as changing SV, and thus, producing nonlinear changes in the PWV.

3.4.3.2 Analysed Data and Equipment

A limitation of this study is that experiments were done on healthy pigs and pigs did not have valve regurgitation, aneurysm, and/or any arterial defect. Blood flow conditions in such cases are more complex than those examined in this study and may not follow the positive SV and PWV relationships identified in this analysis. Further validation and analysis must be done covering a wider range of cardiovascular systems and hemodynamic conditions to ensure the accuracy, strength and applicability of SV-PWV relationships found in this chapter.

Another limitation of this study is that signals from the admittance catheter can be sensitive depending on the location within the ventricle (Wei et al., 2014). This sensitivity could produce errors in the measurement of absolute value of SV and may provide slightly higher or lower SV values from the true SV. However, for a single pig, the admittance catheter locations were fixed and the SV trend values were accurately captured, except for Pig 4 where the admittance catheter was recalibrated, relocated, and replaced during the experiment. However, the overall SV-PWV trend relationship identified in this chapter is still valid. In addition, SV for Pigs 7 and 8 were measured from aortic flow probes and the relationships showed similar results providing additional validation of the admittance data from Pigs 1-6, and thus for the relationships found.

3.5 Summary

The relationship between SV and PWV can be drawn only when PWV increase or decrease reflect the changes in flow condition inside the artery generated by SV. Inter-subject variability

of arterial properties will produce different PWV values for the same amount of SV, and thus, the value of PWV alone is unreliable for capturing the absolute value of SV. In addition, the changes in afterload condition induced by dobutamine/endotoxin administration produces PWV changes from the arterial wall, as well as flow components. Hence, when both effects are present, the relationship between the values of SV and PWV are weaker, and thus less useful.

Despite its limitations, the relationships found can be used to estimate the overall trend of SV from measured PWV, when SV changes mainly due to changes in preload. The relationship could be used to support clinical decisions such as fluid replacement, where the main hemodynamic changes arise from preload changes. The value of PWV can be obtained from pressure measurements, and thus has the potential, in these titrations, to provide a non-additionally invasive and cost effective solution for monitoring patient SV. The relationship identified in this chapter thus has the ability to improve current cardiac and circulatory treatment, especially in fluid responsiveness assessment. In addition, the relationship could be integrated to existing physiological/cardiovascular models to improve the accuracy of the SV estimation method.

Chapter 4: Stroke Volume Estimation using Aortic Pressure Waveform

This chapter presents a method for continuously estimating SV from the aortic pressure measurements using a three element Windkessel model combined with the reservoir-excess hypothesis proposed by Wang et al. (2003). Continuous Beat-to-beat SV is estimated using patient-specific Windkessel model parameters calibrated from initial measurement of SV. The accuracy of the method is analysed and benefits/limitations of this approach are discussed.

4.1 Introduction

Methods for estimating flow from arterial properties have been extensively studied to assist clinical diagnosis and treatment (Shi et al., 2011). More realistic and complex models consisting of many physiological parameters (Steinman, 2002) can simulate precise flow conditions within the artery. However, identification of the model parameters for these complex models is much more difficult, and is usually not practical with the common measurements available in the ICU.

In contrast, simpler models require less information to identify model parameters. However, they can produce inaccurate results due to the assumptions being made and fewer number of model parameters available to capture the dynamics in the measured data (Westerhof et al., 2009). For a model to be useful and practical in the ICU, the complexity of the model must be

adjusted according to the available clinical measurements, as well as able to capture the clinically relevant observed dynamics

Aortic pressure measurements are clinically available in the ICU and converting aortic pressure to aortic flow allows absolute values of SV to be determined. The continuous waveform signal of the pressure measurements enables beat-to-beat estimation of SV, and thus, offers an advantage over conventional, discrete estimates of CO from indicator-dilution methods (Cousins and O'Donnell, 2004) or echocardiography (Slifka and Whitton, 2000). Identifying SV continuously provides more detailed SV dynamics, particularly in transient cases showing the effect of evolving patient condition and/or response to clinical interventions.

One of the most frequently used models in relating arterial pressure to flow is the three element Windkessel model introduced by Westerhof et al. (2000). The model consists of characteristic impedance, systemic resistance, and compliance of the artery. In many current applications, the model parameters are calibrated using discrete estimates of CO combined with area under the systolic pressure curve (Rivers et al., 2001) or from physical/demographic information (Marik, 2013). These methods calculate characteristic impedance, which is then used to continuously estimate the total amount of flow within the artery.

Despite the model having three elements, commercial devices often use characteristic impedance as the calibration parameter (Butlin, 2008, Metafratzi et al., 2002), and systemic resistance and compliance are then the model output. This approach is used because all three elements contribute to the shape and magnitude of the systolic pressure curve (Parker et al., 2012), and unless the magnitude of the pressure components corresponding to each parameter are known, the model parameters cannot be calibrated correctly. With the analogy of three element Windkessel model alone, separating the pressure due to each model parameter

component requires extra information on vascular properties in addition to pressure, and as a result, the method becomes less practical in the ICU.

The aortic model combining a three element Windkessel model and the reservoir-excess hypothesis proposed by Wang et al. (2003) provides the ability to decompose the aortic pressure waveform into two components: 1) reservoir pressure representing the energy stored/released by the compliance; and 2) excess pressure representing the excess amount of work provided by the ventricle to accelerate blood. This decomposition is done using the information obtained from the diastolic pressure decay curve, and does not require extra information in addition to the measured pressure waveform. Thus, the combined model is suitable for clinical use and allows parameters, such as resistance and compliance, to be calibrated for the beat-to-beat estimation of SV.

This chapter analyses this combined aortic model to estimate SV from the aortic pressure waveform by calibrating and fixing different Windkessel parameters. First, the aortic model and the method involved in separating the aortic pressure waveform into reservoir and excess pressure are presented. Second, the equations relating SV, the reservoir/excess pressure component, and the Windkessel model parameters are described. Finally, the accuracy of SV estimated using different calibration parameters is investigated and compared to the traditional characteristic impedance method. Bland-Altman plots are presented for each case to assess accuracy, error, and bias, and the results are discussed.

4.2 Method

4.2.1 Aortic Model

The reservoir-excess pressure theory was used to analyse measured aortic pressure. The theory interprets the measured pressure as the sum of two pressure components, reservoir pressure, P_{res}, and excess pressure, P_{ex}, as shown in Equation 4.1.

$$P_{ao}(t) = P_{res}(t) + P_{ex}(t) \tag{4.1}$$

Reservoir pressure represents the pressure components generated from compliance of the artery, and by this definition, the time dependent reservoir pressure, $P_{res}(t)$, can be expressed as a function of volumetric compliance, C_v ($= dV/dP_{res}$), and changes in aortic compartment volume, (dV/dt), yielding:

$$\frac{dP_{res}(t)}{dt} = \frac{dP_{res}(t)}{dV}\frac{dV}{dt} = \frac{1}{C_V}\left(Q_{in}(t) - Q_{out}(t)\right) \tag{4.2}$$

Where $Q_{in}(t)$ and $Q_{out}(t)$ are flow entering the aortic compartment from the left ventricle and flow leaving the aortic compartment, respectively.

Wang *et al* also validated proportionality between each pressure component, flow dynamics in the aorta, and Windkessel model parameters (Tyberg et al., 2014, Wang et al., 2003):

$$P_{res}(t) - P_{cvp} = RQ_{out}(t) \tag{4.3}$$

$$P_{ex}(t) = Z_{ao}Q_{in}(t) \tag{4.4}$$

Where R, Z_{ao} and P_{cvp} are systemic resistance, aortic characteristic impedance and central venous pressure, respectively.

In this analysis, P_{cvp} was assumed 8mmHg for all pigs representing a typical population value (Westerhof et al., 2015b). In addition, central venous pressures were measured in pigs administered endotoxin to induce sepsis and the average measured pressure were approximately 8mmHg. Substituting these relationships into Equation (4.2), the differential equation relating P_{res}, P_{ex}, and the three element Windkessel model parameters, R, Z_{ao}, C_v, can be written:

$$\frac{dP_{res}(t)}{dt} = \frac{P_{ex}(t)}{Z_{ao}C_V} - \frac{P_{res}(t) - P_{cvp}}{RC_V} \tag{4.5}$$

Applying the initial condition $P_{res}(0) = P_{ao}(0)$ at the beginning of a heartbeat, Equation (4.5) can be solved for $P_{res}(t)$ over one cardiac cycle (Kamoi et al., 2014):

$$P_{res}(t) = e^{-(\alpha+\beta)t}\left(\int_0^t e^{(\alpha+\beta)t'}\left(\alpha P_{ao}(t') + \beta P_{cvp}\right)dt' + P_{ao}(0)\right) \tag{4.6}$$

Where $\alpha = 1/Z_{ao}C_v$ and $\beta = 1/RC_v$.

The electrical circuit analogy of the aortic model used in this study is shown in Figure 4.1.

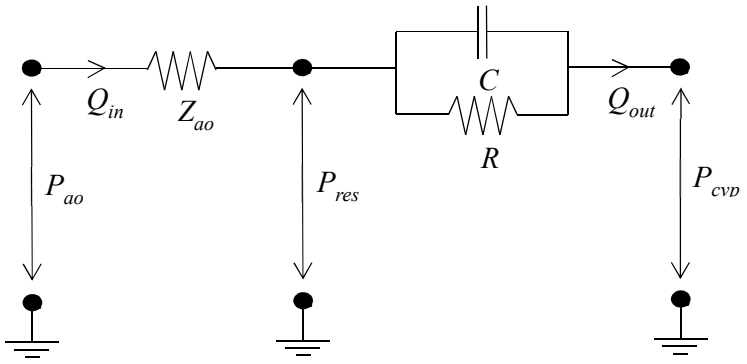

Figure 4.1 – Electrical analogy of the aortic model used in this study. The currents represents the blood flow through the artery (Q_{in} and Q_{out}). The node voltage represents different pressure components (P_{ao}, P_{res}, and P_{cvp}). The electrical components represents the Windkessel elements (R, Z_{ao}, and C_v). In this case, the ground/reference voltage represents atmospheric pressure.

4.2.2 Reservoir-Excess Separation

The separation method involves analysing the pressure decay in the diastolic period of the aortic pressure waveform. In diastole, the pressure decay is assumed to result only from the release of energy stored by aortic compliance during systole. Thus, the measured aortic pressure waveform in diastole represents the reservoir pressure. This condition is defined:

$$P_{res}(t_d<t<t_f) = P_{ao}(t_d<t<t_f) \tag{4.7}$$

Where t_d and t_f are the aortic valve closure time and total time for one cardiac cycle, respectively. Applying this diastolic condition to Equation (4.5) and solving the ODE for diastole, a simplified equation for P_{res} in diastole can be written:

$$P_{res}(t_d \le t \le t_f) = (P_{ao}(t_d) - P_{cvp})e^{-\frac{(t-t_d)}{RCv}} + P_{cvp} \tag{4.8}$$

In this form, the only unknown parameter in the equation is $1/RC_v$, which is β in Equation (4.6). Performing regression between the measured aortic pressure decay and pressure decay calculated using Equation (4.8), the parameter value for $1/RC_v$ can be identified. Once the parameter value $1/RC_v$ (or β) has been identified for a given heartbeat, this value is substituted into Equation (4.6) to solve P_{res} for the entire heartbeat.

For the identification of $1/Z_{ao}C_v$, another physiological condition was applied. At end systole (t_d), ventricular hydraulic force equals aortic reservoir force pushing against the ventricle. This equilibrium of force initiates aortic valve closure. Hence, maximum reservoir pressure will not exceed measured pressure at t_d. This condition is defined:

$$Max(P_{res}) \le P_{ao}(t_d) \tag{4.9}$$

Using constraints in Equation (4.8) and (4.9) with the identified parameter, $1/RC_v$, the parameter value $1/Z_{ao}C_v$ can be identified by regression between Equation (4.6) and measured diastolic decay. An example of the resulting separated pressures, P_{res} and P_{ex}, obtained from a measured aortic pressure waveform using this method is shown in Figure 4.2.

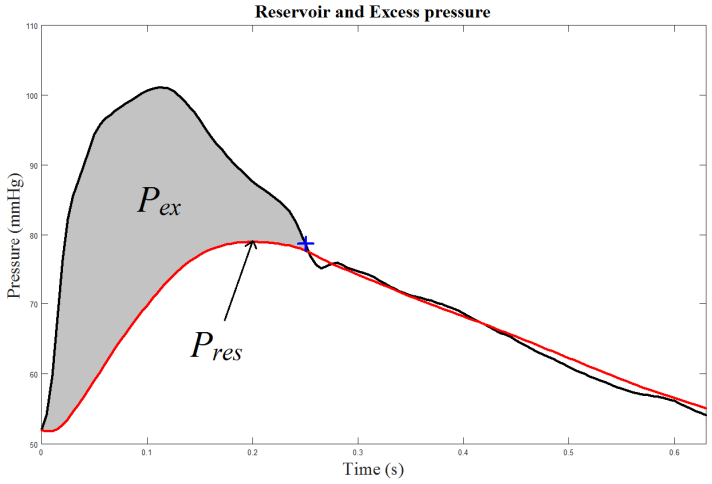

Figure 4.2 – Example of separated aortic pressure waveform. Calculated reservoir pressure P_{res} (red line), excess pressure P_{ex} (shaded grey area), and measured P_{ao} (black line). End systolic point, or duration systole, t_d, is indicated by blue plus mark.

4.2.3 Detection of End Systolic Point

Identification of the end systolic point (ESP) illustrated in Figure 4.2, is required for reservoir-excess separation. In this analysis, the ESP was identified as the maximum negative gradient point on the aortic pressure waveform (Abel, 1981). However, this condition alone was not enough to reliably detect ESP for typically measured aortic pressure waveforms, which can have multiple inflection points, and thus, multiple minima in the *dP/dt* waveform. An example is shown in Figure 4.3, which has two possible ESPs that can be found with the typical approach.

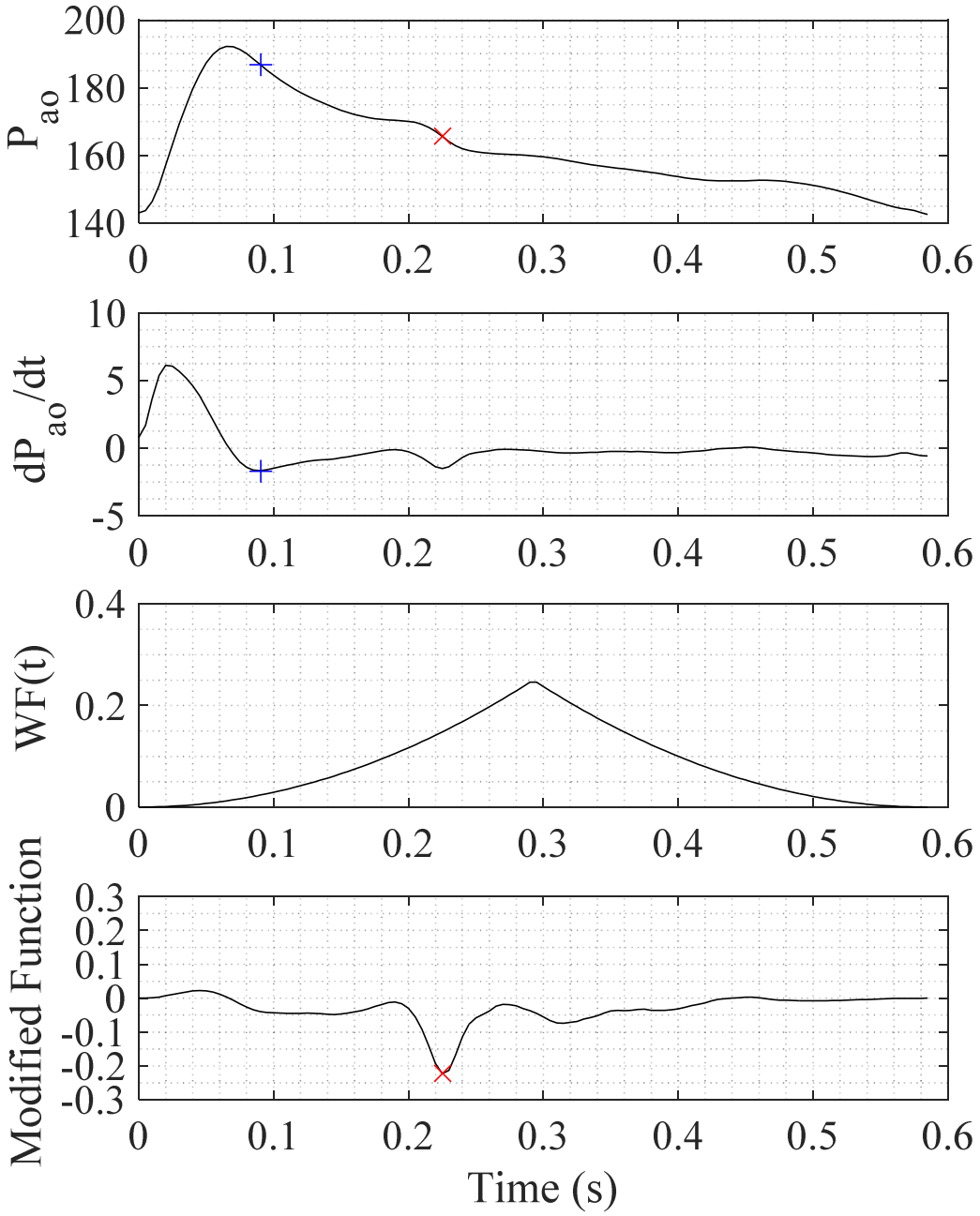

Figure 4.3 – Detected minimum gradient point (blue +) and detected end systolic point using the modified function (red x) on a single beat pressure waveform. Top Panel: measured pressure waveform having multiple descending inflection points. Second Panel: pressure gradient $dP_{measured} / dt$ and detected global minimum, shown as blue cross. Third Panel: Weight function WF(t) applied to $dP_{measured} / dt$. Bottom Panel: Modified function showing product of $dP_{measured} / dt$ and WF(t), where the red cross shows the identified location of the end systolic point.

Figure 4.3 shows local and global minimum gradient points. In this specific case, the correct location of the ESP would be the second maximum negative gradient point in the pressure curve, and not the global minimum of *dP/dt* point. To avoid false detection of the ESP, a generic weight function (WF) was applied to the gradient of the pressure curve, as shown in the third panel of Figure 4.3, and defined:

$$WF(t) = \left(0.5 - \left|0.5 - \frac{HR * t}{60}\right|\right)^2 \tag{4.10}$$

$$ESP = min\left(\frac{dP_{measured}}{dt} WF(t)\right) \tag{4.11}$$

Where HR is the heart rate, and *t* is time in seconds.

This WF applies a greater weighting to points near the midpoint of the cardiac cycle and thus, enhances minima in the expected ESP location. This procedure is illustrated in lower two panels of Figure 4.3. The identified ESP using the method as illustrated in Figure 4.3 is used for parameter identification of $1/RC_v$ and $1/Z_{ao}C_v$.

4.2.4 Stroke Volume Estimation

To estimate aortic flow from the separated pressure components, P_{res} and P_{ex}, one of the Windkessel model parameter must be calibrated or fixed using a discrete measurement of SV or estimated from physical characteristics. In this analysis, the first 10 beats of experimentally measured left-ventricular SV values for each pig were used to calculate a pig-specific value of R, C_v, and Z_{ao}. The calculated parameter values for each beat were then averaged. The calculation of these parameter values for each of the Windkessel model elements are defined:

$$R_{cal} = \left(\sum_{i=1}^{10} \frac{1}{SV_i} \int_{t_0}^{t_f} (P_{res}(t) - P_{cvp}) dt \right) \Big/ 10 \tag{4.12}$$

$$C_{v,cal} = \left(\sum_{i=1}^{10} \frac{SV_i \, RC_{identified}}{\int_{t_0}^{t_f} (P_{res}(t) - P_{cvp}) dt} \right) / 10 \tag{4.13}$$

$$Z_{ao,cal} = \left(\sum_{i=1}^{10} \frac{1}{SV_i} \int_{t_0}^{t_f} P_{ex}(t) dt \right) \Big/ 10 \tag{4.14}$$

The subscript *cal* refers to calibrated parameter. Equations (4.12) and (4.14) can be obtained by rearranging Equation (4.3) and (4.4), respectively, and taking the integral of the flow, which is SV. Equation (4.13) can be obtained by combining Equation (4.12) with the identified parameter $1/RC_v$ from Equation (4.8).

Using these calibrated parameters, three different estimations of SV can be calculated per heartbeat, each representing estimated SV using one of the calibration parameters above. The equations for each SV are calculated:

$$SV_R = \frac{1}{R_{\text{cal}}} \int_{t_0}^{t_f} (P_{res}(t) - P_{cvp}) dt \tag{4.15}$$

$$SV_{C_v} = \frac{C_{v,cal}}{RC_{identified}} \int_{t_0}^{t_f} (P_{res}(t) - P_{cvp}) dt \tag{4.16}$$

$$SV_{Z_{ao}} = \frac{1}{Z_{\text{ao, cal}}} \int_{t_0}^{t_f} P_{ex}(t) dt \tag{4.17}$$

The analysis examines the accuracy of each of SV estimates, and thus investigates if some of the calibration parameters perform better than the others depending on the cardiovascular conditions and/or clinical interventions. More specifically, is there a better or best choice of which of the three calibration parameters of equations (4.12) – (4.14) to use in general for given clinical scenarios.

4.2.5 Traditional Characteristic Impedance Method

The traditional method calibrates characteristic impedance using the entire (unseparated) area under the pressure curve (Butlin, 2008). The equation for parameter calibration with this method:

$$Z_{ao(trad),cal} = \left(\sum_{i=1}^{10} \frac{1}{SV_i} \int_{t_0}^{t_f} P_{ao}(t)dt \right) \Big/ 10 \tag{4.18}$$

In this traditional method, the entire pressure component is assumed to represent the ventricular flow instead of only the excess component. The difference in interpretation of the systolic aortic pressure is still inconclusive (Murgo et al., 1980, Hughes et al., 2012). However, the theory of Wang *et al* allows estimation of changes in pressure components from aortic compliance, and provides the possibility of improving the estimation of SV. In this study, Wang *et al* work is assumed to be correct and compares the accuracy to the SV estimation with entire systolic pressure as a flow component.

Given the calculated pig-specific impedance value using Equation (4.18), the traditional method estimates SV:

$$SV_{Z_{ao\,(trad\,)}} = \frac{1}{Z_{\text{ao(trad), cal}}} \int_{t_0}^{t_f} P_{ao}(t)dt \tag{4.19}$$

4.2.6 Data Analysis

In this analysis, porcine experimental data from Chapter 3 were used, as detailed in Section 3.2.1 and 3.2.2. However, Pig 1 and Pig 4 were excluded from the analysis because Pig 1 did not have baseline measurements and Pig 4 had multiple catheter disturbances/failures during the experiment. For all other pigs, continuous experimental data was used to estimate SV, and analyse its accuracy to the admittance catheter direct measurements.

For the dobutamine pigs, the experiment involved administration of five rapid saline boluses of 180ml up to a total of 900ml, except for Pig 6 where a total of 720ml of saline solution was given. After fluid admistration, the pigs received a continuous infusion of dobutamine at a rate of either 2.5 or 5μg/kg/min. In Pigs 5 and 6, further administration of a 180ml rapid bolus was given while continuing the dobutamine infusion.

For the induced sepsis pigs, the experiment involved slow infusion of 400ml saline solution, then a single infusion of endotoxin (lipopolysaccharide from E. Coli, 0.5 mg/kg) injected over 30 minutes. For Pig 7, a further administration of 400ml saline solution were given and for Pig 8, 400ml saline solution was given twice to total 800ml.

For all of pigs, RM were performed between each intervention. The summary of interventions made for each pig is given in Table 4.1. The overall experiment ensures a wide range of hemodynamic conditions, and thus a wide range of SVs might be expected.

As described in Section 3.2.1, two aortic pressure measurements were made in the porcine experiments, which are aortic arch and abdominal aortic pressure waveforms. In this analysis, a measured continuous abdominal aortic pressure waveforms, P_{abao}, was used for reservoir-excess separation. The continuous waveforms were first split into individual heart beats for the

beat-to-beat pressure contour analysis. For each beat, a reservoir-wave separation was applied and each pressure components were identified. Calibration parameters were then calculated using Equations (4.12) – (4.14) for the aortic model and Equation (4.18) for the traditional method. Finally, the resulting four estimations of SV per beat are made using Equations (4.15) – (4.17), and (4.19).

Table 4.1 - Summary of interventions made for each pig in the experiment.

Pig No	**Volume Expansion**					**Dobutamine (µg/kg/min) Endotoxin (mg/kg)**		**Dobutamine/Endotoxin + Volume Expansion**	
Dobutamine Pigs									
	180ml	360ml	540ml	720ml	900ml	2.5	5	180ml	
2	✓	✓	✓	✓	✓	×	✓	×	
3	✓	✓	✓	✓	✓	×	✓	×	
5	✓	✓	✓	✓	×	✓	×	✓	
6	✓	✓	✓	✓	✓	×	✓	✓	
Sepsis Pigs									
	400ml					0.5		400ml	800ml
7	✓					✓		✓	×
8	✓					✓		✓	✓

4.3 Results

4.3.1 Identified Parameters and Investigated Range of Windkessel Parameters

The identified parameters RC_v and $Z_{ao}C_v$ from Equation (4.6), and the number of heart beats analysed for each pig are presented in Table 4.2. Table 4.3 shows the range of Windkessel model parameters obtained for each pig by forward simulating Equations (4.15) – (4.17) and (4.19), and using the measured left ventricular SV value. It can be seen that vasodilatory effect of dobutamine decreased systemic resistance, R, in all pigs and increased aortic compliance, C_v, in 3 of the pigs. The characteristic impedance, Z_{ao}, derived by the traditional method and

by using the excess pressure approach had the same trend of decreased values for dobutamine and increased value for the endotoxin cases.

Table 4.2 – Summary of identified parameters RC_v, $Z_{ao}C_v$, and number of heart beats analysed for each pig. Data are presented as the median [5^{th} – 95^{th} percentiles].

Pre-dobutamine/Sepsis period			
Pig No	RC_v **(s)**	$Z_{ao}C_v$ **(s)**	*No Heart Beats*
Pig 2	2.75 [2.30 – 3.32]	0.16 [0.13 – 0.21]	1944
Pig 3	1.22 [0.99 – 1.46]	0.10 [0.09 – 0.12]	3920
Pig 5	1.77 [1.39 – 2.29]	0.11 [0.09 – 0.17]	2427
Pig 6	1.11 [0.58 – 1.34]	0.21 [0.08 – 0.24]	1723
Pig 7	1.65 [1.25 – 2.06]	0.22 [0.15 – 0.25]	762
Pig 8	0.96 [0.82 – 1.30]	0.21 [0.18 – 0.25]	762
Dobutamine RM			
Pig 2	2.30 [1.69 – 3.30]	0.13 [0.10 – 0.17]	1012
Pig 3	0.89 [0.74 – 1.04]	0.12 [0.10 – 0.14]	1025
Pig 5	1.82 [1.45 – 2.21]	0.12 [0.10 – 0.14]	630
Pig 6	0.57 [0.40 – 0.75]	0.11 [0.06 – 0.15]	728
Endotoxin RM			
Pig 7	1.22 [1.03 – 1.63]	0.24 [0.18 – 0.28]	663
Pig 8	1.20 [0.95 – 1.94]	0.21 [0.15 – 0.34]	808

Table 4.3 – Investigated range of Windkessel parameters R, C_v, Z_{ao}, and $Z_{ao(trad)}$ for each pig. Data are presented as the median [5^{th} – 95^{th} percentiles].

Pre-dobutamine/Sepsis period				
Pig No	R **(mmHg.s/ml)**	C_v **(ml/mmHg)**	Z_{ao} **(mmHg.s/ml)**	$Z_{ao(trad)}$ **(mmHg.s/ml)**
Pig 2	3.87 [3.27 – 5.08]	0.70 [0.54 – 0.89]	0.24 [0.15 – 0.36]	2.08 [1.54 – 2.83]
Pig 3	3.77 [2.70 – 5.15]	0.31 [0.24 – 0.46]	0.31 [0.22 – 0.47]	2.41 [1.53 – 3.49]
Pig 5	2.44 [1.95 – 2.95]	0.73 [0.59 – 0.90]	0.16 [0.12 – 0.21]	2.06 [1.47 – 2.82]
Pig 6	1.25 [1.02 – 1.51]	0.95 [0.76 – 1.17]	0.23 [0.19 – 0.28]	0.95 [0.80 – 1.15]
Pig 7	0.67 [0.55 – 0.78]	2.39 [1.90 – 2.83]	0.09 [0.07 – 0.10]	0.43 [0.38 – 0.49]
Pig 8	0.89 [0.79 – 1.27]	1.11 [0.93 – 1.34]	0.19 [0.17 – 0.24]	0.74 [0.68 – 1.08]
Dobutamine RM				
Pig 2	3.03 [2.56 – 4.63]	0.72 [0.48 – 1.06]	0.16 [0.13 – 0.34]	1.52 [1.24 – 2.83]
Pig 3	1.25 [1.53 – 3.49]	0.72 [0.48 – 0.97]	0.17 [0.12 – 0.22]	0.86 [0.70 – 1.26]
Pig 5	2.06 [1.47 – 2.82]	0.87 [0.52 – 1.34]	0.13 [0.09 – 0.21]	1.15 [0.74 – 1.71]
Pig 6	0.95 [0.79 – 1.25]	0.62 [0.47 – 0.78]	0.18 [0.10 – 0.26]	0.95 [0.70 – 1.42]
Endotoxin RM				
Pig 7	0.64 [0.56 – 0.74]	1.82 [1.63 – 2.20]	0.13 [0.11 – 0.15]	0.52 [0.47 – 0.58]
Pig 8	1.34 [1.16 – 1.60]	0.88 [0.73 – 1.03]	0.23 [0.16 – 0.26]	1.13 [1.01 – 1.36]

4.3.2 Calibrated Parameter Values

Table 4.4 shows the pig-specific calibrated parameters calculated from Equations (4.12) – (4.14) and (4.18), using the first 10 measured SV values. It can be seen that calibrated parameters varied widely between subjects, for all of the parameters. This inter-subject variability suggests that using a generic population and/or demographic value could produce large errors in the estimation of SV for any specific subject, although relative trends might be unaffected.

Table 4.4 – Calibrated parameters R, C_v, Z_{ao}, and $Z_{ao(trad)}$ used for the estimation of SV in each pig.

Pig No	R (mmHg.s/ml)	C_v (ml/mmHg)	Z_{ao} (mmHg.s/ml)	$Z_{ao(trad)}$ (mmHg.s/ml)
Pig 2	3.32	0.67	0.28	2.02
Pig 3	2.82	0.31	0.30	1.99
Pig 5	1.66	0.78	0.17	1.06
Pig 6	1.02	1.01	0.21	0.85
Pig 7	0.55	2.39	0.08	0.38
Pig 8	0.89	1.00	0.20	0.74

4.3.3 Bland-Altman Results

The accuracy of SV estimated from Equations (4.15) – (4.17) and (4.19) using each of the calibrated parameters in Table 4.4 were analysed with Bland-Altman plots. Figure 4.4 displays four Bland-Altman plots for each pig showing the accuracy of each calibration method. Summary results showing the bias, and the 95% interval, as well as the average 95% range for all pigs are presented in Table 4.5. It is clear that there are significant differences in error for each calibration method, and that the error distributions shown are not necessarily normally distributed.

Pig 2

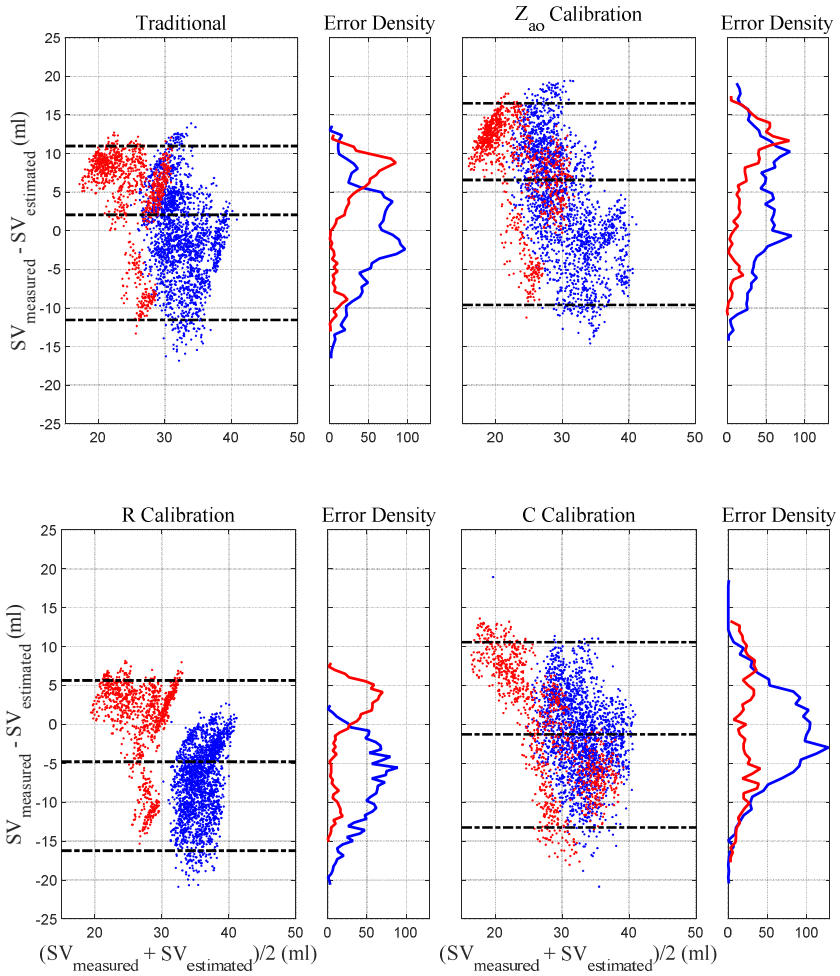
Traditional
Error Density
Z_ao Calibration
Error Density
R Calibration
Error Density
C Calibration
Error Density
SV_measured - SV_estimated (ml)
(SV_measured + SV_estimated)/2 (ml)

Pig 3

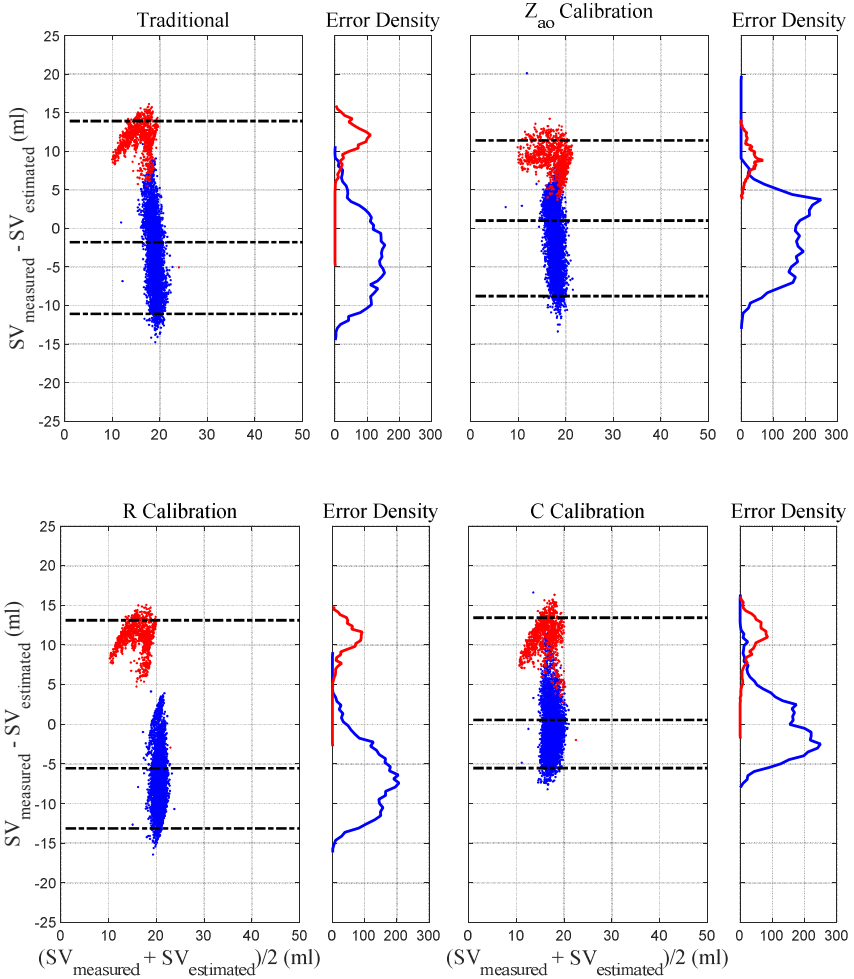
Traditional
Error Density
Z_ao Calibration
Error Density
R Calibration
Error Density
C Calibration
Error Density
SV_measured - SV_estimated (ml)
(SV_measured + SV_estimated)/2 (ml)

Pig 5

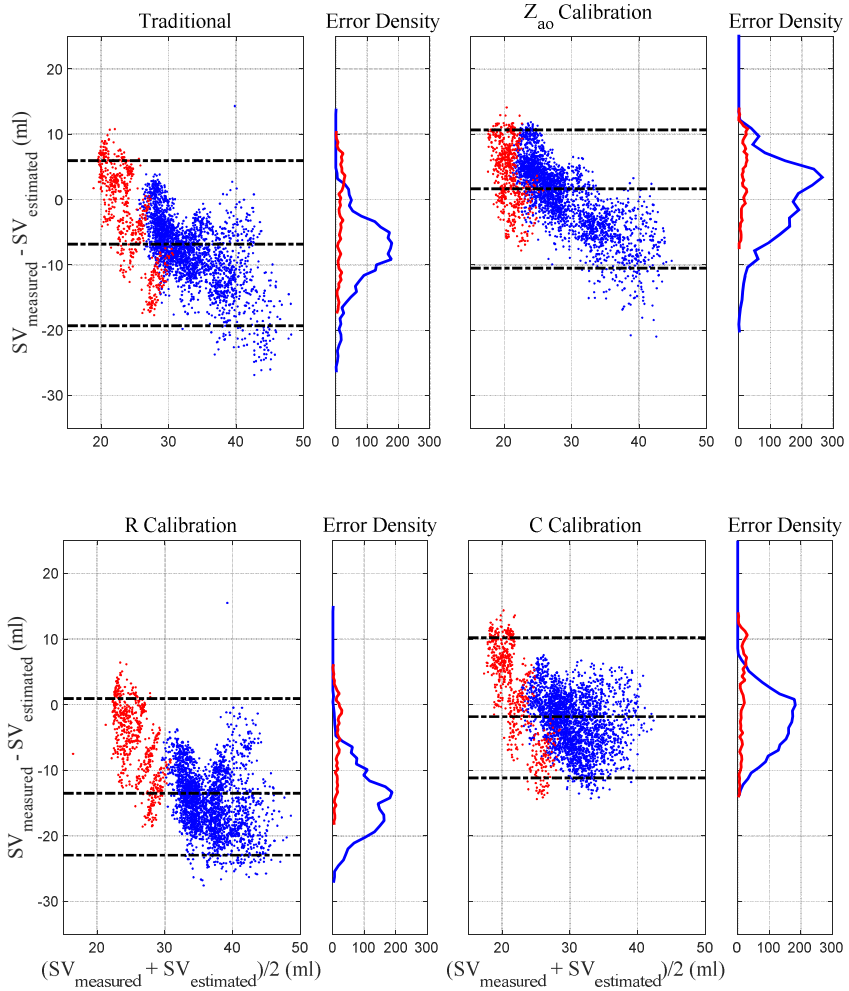
Traditional
Error Density
Z_ao Calibration
Error Density
R Calibration
Error Density
C Calibration
Error Density
SV_measured - SV_estimated (ml)
(SV_measured + SV_estimated)/2 (ml)

Pig 6

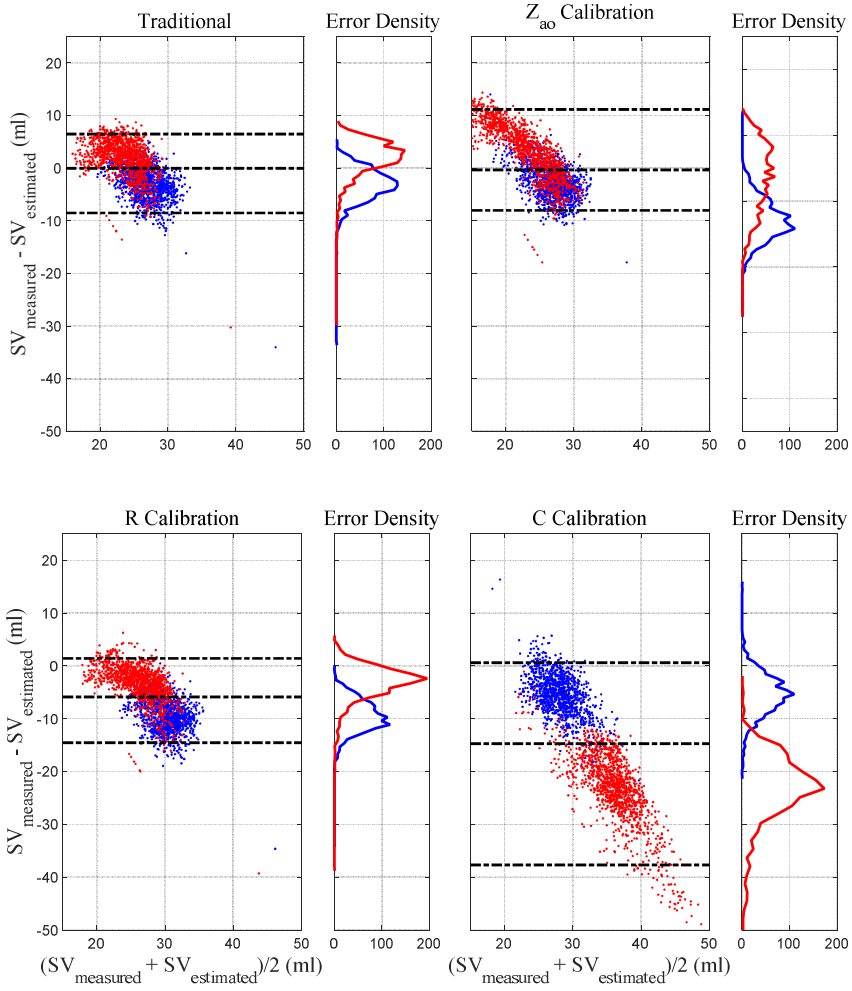
Traditional
Error Density
Z_ao Calibration
Error Density
R Calibration
Error Density
C Calibration
Error Density
SV_measured - SV_estimated (ml)
(SV_measured + SV_estimated)/2 (ml)

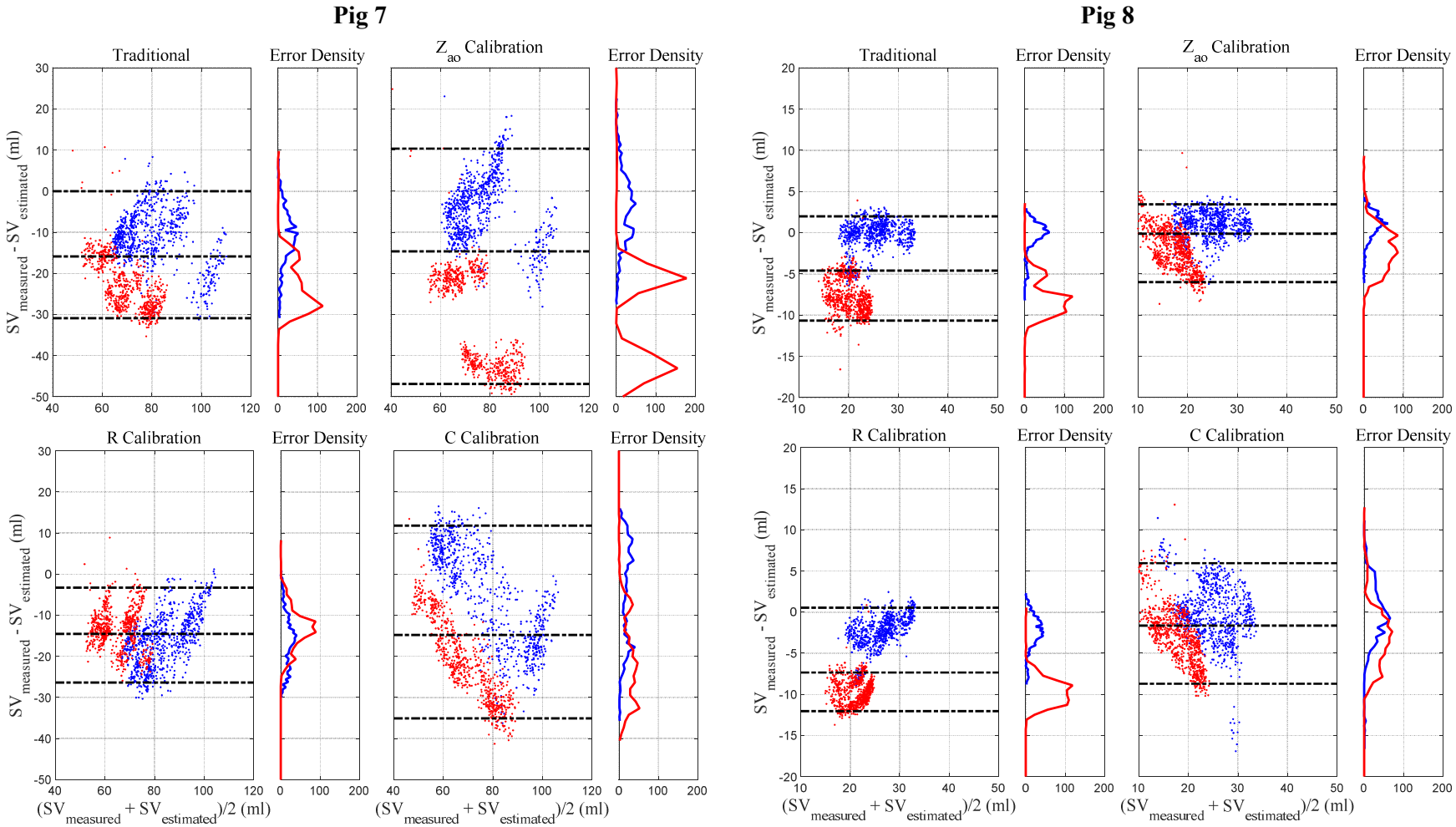

Figure 4.4 – Bland Altman plots showing agreement between measured and estimated SV for different calibration parameter. Pre-dobutamine/sepsis periods are shown with blue dots, and Post-dobutamine/endotoxin are shown with red dots. black dashed line showing the bias and 2.5th – 97.5th percentile and right panel showing the error distribution between measured and estimated SV values

Table 4.5 – Summary of Bland-Altman analysis showing bias, 95% interval, and average 95% range for each parameter. Data are presented as the bias [2.5-97.5th percentiles]. The calibration parameter having the best 95% range accuracy is shown in red.

	Calibration Parameter (ml)			
Pig No	***R* (mmHg.s/ml)**	**C_v (ml/mmHg)**	**Z_{ao} (mmHg.s/ml)**	**$Z_{ao(trad)}$ (mmHg.s/ml)**
Pig 2	-4.8[-16.2 – 5.7]	-1.3[-13.2 – 10.6]	6.6[-9.6 – 16.5]	2.0[-11.5 – 11.0]
Pig 3	-5.5[-13.1 – 13.1]	0.5[-5.5 – 13.4]	1.0[-8.7 – 11.4]	-1.8[-11.1 – 13.9]
Pig 5	-13.5[-22.9 – 0.9]	-1.8[-11.2 – 10.2]	1.6[-10.5 – 10.7]	-6.8[-19.3 – 6.0]
Pig 6	-5.9[-14.5 – 1.4]	-14.7[-37.7 – 0.6]	-0.3[-8.0 – 11.2]	0.0[-8.5 – 6.5]
Pig 7	-14.6[-26.4 – 3.3]	-14.8[-35.0 – 11.8]	-14.7[-46.9 – 10.4]	-15.9[-30.9 – 0.0]
Pig 8	-7.3[-12.1 – 0.5]	-1.6[-8.7 – 5.9]	-0.1[-6.0 – 3.5]	-4.6[-10.7 – 1.9]
	Average 95% range (ml)			
	20.60	27.31	25.55	21.89

4.3.4 Effect of Dobutamine and Sepsis on Aortic Pressure

The Bland-Altman analysis showed different accuracy for each of the calibration parameters. However, the optimal calibration parameter needs to be selected from clinically available surrogates. To analyse the relationship between the optimal parameter and observable data, changes in identified parameters RC_v, $Z_{ao}C_v$, and lower abdominal pressure, P_{abao}, from dobutamine/sepsis are shown in Table 4.6. The relative changes were calculated by mean (pre-dobutamine/endotoxin) minus mean (post-dobutamine/endotoxin) divided by mean (pre-dobutamine/endotoxin).

Table 4.6 – Effect of dobutamine and sepsis on clinical measurements. Relative change in P_{abao}, RC_v, and $Z_{ao}C_v$ are shown.

Pig No	ΔP_{abao} (mmHg)	ΔRC_v (s)	$\Delta Z_{ao}C_v$ (s)
Pig 2	-0.01	-0.16	-0.18
Pig 3	-0.49	-0.26	0.19
Pig 5	-0.10	0.02	0.06
Pig 6	0.46	-0.48	-0.48
Pig 7	-0.08	-0.26	0.10
Pig 8	-0.02	0.25	0.03

4.4 Discussion

4.4.1 Accuracy of Different Calibration Parameter

Table 4.5 and Figure 4.4 show optimal calibration parameters for estimating SV can be different for each pig. Pigs 2 and 7 had the best accuracy with R, Pig 3 was with C_v, Pigs 5 and 8 were Z_{ao}, and Pig 6 was best with the traditional method. This variability is due to dobutamine and endotoxin having different effects for each pig, even while the overall effect was broadly the same. Such inter-subject variability in response to care and/or dysfunction is typical.

As can be seen in Table 4.2, the degree of changes in Windkessel parameters depends on the individual response to intervention. The calibration parameter having the least changes produced greater accuracy for SV estimation. Overall, calibrating R with reservoir pressure showed the best overall 95% range accuracy, as R was the most stable parameter compared to other Windkessel parameters within these data.

Table 4.6 shows the impact on the abdominal pressure waveform and its characteristics, $P_{abao,}$ RC_v, and $Z_{ao}C_{v,}$ from dobutamine and endotoxin. The changes in Windkessel parameter values cannot be identified without SV, and thus, optimal calibration parameters must be selected from observable data. Pigs having relatively low changes in P_{abao} before and after dobutamine/endotoxin had better accuracy calibrating with R or Z_{ao}. Within the pigs having low P_{abao} changes, calibrating R had higher accuracy when P_{abao} and RC_v had the same trend, and Z_{ao} when relative changes in $Z_{ao}C_v$ was low. Pigs 3 and 6 having large variations in P_{abao} showed better results with compliance and traditional method, respectively.

There were potential relationships between measurable parameters $P_{abao,}$ $RC_{v,}$ $Z_{ao}C_{v,}$ and optimal calibration parameters. However, data from six pigs was not enough to identify strong patterns, and the physiological reasons behind these relations cannot be revealed until the

tendency shown in Tables 4.5 and 4.6 can be confirmed with larger sets of data. Further investigation is thus required to identify the relationships between different aortic pressure contours and stability of Windkessel parameters.

4.4.2 Comparison with the Traditional Method

Bland-Altman analysis in Figure 4.4 showed SV estimation from aortic pressure waveform can be improved using the method described in this chapter. Five out of six pigs had higher accuracy than the traditional method. However, when sub-optimal parameters were chosen, accuracy can be significantly worse as it can be seen in Pig 6 using C_v and Pig 7 using Z_{ao} and C_v.

The traditional method of analysing the entire systolic pressure may work better under normal homeostasis. All three Windkessel model parameters contribute to the shape of systolic pressure curve, and baroreceptor regulation changes these parameters to maintain mean arterial pressure (Kougias et al., 2010). In such cases, SV stays relatively constant with the combination of parameter changes, and fixing one of the Windkessel parameter worsens the accuracy of SV estimation. On the other hand, errors are minimised when using one variable to represent the entire systolic pressure.

In the ICU, patients suffer from a diverse range of cardiovascular dysfunctions (Goldhaber and Elliott, 2003a, Goldhaber and Elliott, 2003b, Gowda et al., 2008, Landgarten et al., 2000), and abnormal homeostasis (Thames et al., 1993, La Rovere et al., 2008), all of which can vary significantly over time. Patient-specific arterial properties are constantly fluctuating from these conditions, and by providing a method that can be adjusted according to the given conditions, the approach presented can adopt and provide better results. The method can also be improved by combining known mechanisms of action of drugs used (Overgaard and Dzavik, 2008,

Scholz, 1984) via a pharmacokinetics/dynamics model, and/or the known impact on vascular properties from various dysfunctions (Bonate and Steimer, 2006).

The SV estimation method described in this chapter requires further analysis detailing the identification method for optimal calibration. Although the *R* calibration showed the best overall accuracy, the result may change with more data and thus conclusions cannot be drawn with the current data. However, the method shows the possibility and means of improving the accuracy of SV estimation and enhances the current understanding of arterial mechanics.

4.4.3 Limitations

The clinical applicability of the presented method is limited to patients having aortic pressure measurements. In most cases, radial arterial catheters are used for ICU patients requiring continuous blood pressure monitoring and aortic catheters are rarely used. However, arterial catheterization sites are determined by the perceived risk-to-benefit ratio. Thus, increasing the benefit from using aortic pressure waveforms may reverse this trend, turning potential risk into benefits (Cousins and O'Donnell, 2004). Additionally, models for estimating aortic pressure from radial arterial pressure may be developed in future, which would enhance the clinical applicability of this approach.

Another limitation is the inability of the method to capture Windkessel model parameter dynamics. Information on systemic resistance, compliance, and impedance are clinically important for diagnosis and treatment. Alterations in these parameters help clinicians unmask hidden dynamics and interactions in evolving patient condition (Dart and Kingwell, 2001). Despite its usefulness, the aortic model is structurally non-identifiable without the value of SV, and consequently, all of the model parameters cannot be uniquely identified using information from single pressure waveform alone, which led to the fixed calibration parameter approach

presented. To overcome this limitation, an extended aortic model is conceptualized and validated in Chapter 5.

4.5 Summary

The aortic model and reservoir-excess pressure separation method presented in this chapter allowed systemic resistance R and compliance C_v in the three element Windkessel to be calibrated for the estimation of SV using aortic pressure waveform. The method showed higher SV estimation accuracy can be achieved compared to the traditional method when optimal calibration parameters can be used. In addition, information from clinical data could potentially be used to identify the optimal calibration parameter for a specific condition, but with the limited number of pigs analysed, the strength of the relation could not be assessed in this study.

The presented method needs to be improved with more clinical data, covering various cardiovascular conditions. With larger data sets, a robust identification method can be formed for optimizing calibration. Thus, the model has the potential for improving SV monitoring system and diagnosis/treatment of cardiovascular dysfunctions in the ICU.

Chapter 5: Stroke Volume Estimation using Aortic Pressure Waveform and Pulse Wave Velocity

This chapter extends the aortic model presented in Chapter 4 by incorporating PWV measurement to improve continuous SV estimation. The subject-specific aortic dimension is calibrated instead of initially calibrating and fixing one of the Windkessel model parameters. This approach enables changes in systemic resistance, aortic compliance, and impedance to be determined. The water-hammer equation, with a physiological relationship identified between ventricular ejection time and aortic area, is used to calculate beat-to-beat characteristic impedance. Continuous SV is then estimated using the identified value of characteristic impedance with the excess component of the aortic pressure waveform. The accuracy of identified physiological parameters and estimated SV values are analysed, in comparison to directly measured values.

5.1 Introduction

The aortic model presented in Chapter 4 calibrates and fixes one of three specific Windkessel model parameter values to estimate SV. This approach prevents changes in one of systemic resistance, aortic compliance, and impedance from being captured. However, as seen in Chapter 4, all three parameters are clinically important and equally necessary to minimize the

SV estimation error. In particular, in the ICU, changes in the hemodynamic state are expected and assuming constant hemodynamic parameters may not be suitable for patients undergoing significant physiological changes (Bein et al., 2007, Bendjelid, 2009). Inaccurate surrogate measures of SV and/or its trends in response to care and condition could lead to misdiagnosis, incorrect clinical treatment/decisions, and/or misinterpretation of patient response to therapy. Therefore, there is a need for accurate and robust methods of estimating SV that are reliable, even when hemodynamic properties are evolving rapidly.

This chapter presents a method for estimating dynamic Windkessel parameter values using measurements of aortic pressure and PWV, thus eliminating the limitation of requiring a constant Windkessel model parameter in Chapter 4. The value of PWV and calibrated aortic dimension are used to identify beat-to-beat aortic characteristic impedance with the water-hammer equation. The identified time-varying impedance value is then used to estimate SV with the excess pressure component. The distinct difference between this approach and the method used in many commercial SV monitors (Gödje et al., 2002, Porhomayon et al., 2012b) is that PWV measurements are used to improve the capacity of pressure contour analysis.

Pressure contour analysis has traditionally been purely based on the geometry of the pressure waveform alone (Esper and Pinsky, 2014). Consequently, the weaknesses associated with monitoring SV were always found during hemodynamic instability (Camporota and Beale, 2010). However, it is hemodynamic instability that is the exact point where monitoring SV becomes essential to patients.

To overcome the limited information available solely from pressure measurements, the method presented in this chapter couples pressure and PWV measurements to improve the analysis of the circulatory system. To investigate the accuracy of the method, Bland-Altman analyses are

performed between measured and estimated SV. In addition, correlation coefficients between identified Windkessel model parameter values and calculated parameter values using measured SV values are analysed to assess trend accuracy.

5.2 Method

Porcine experimental data from Chapter 4 was used for this analysis. A measured continuous abdominal pressure waveform, P_{abao}, was used as aortic pressure, and first split into individual heart beats for beat-to-beat pressure contour analysis. For each beat, a reservoir-excess separation was applied with the new parameter identification method utilising the PWV measurement. Aortic characteristic impedance was then calculated by solving the water-hammer equation. Finally, the excess component of the pressure is used with this calculated value of aortic characteristic impedance to estimate beat-to-beat SV.

5.2.1 Extended Aortic Model

With the additional information from PWV measurements, the ODE described in Chapter 4 (Equation 4.5) can be rearranged to include aortic compartment length. The ODE for the combined reservoir-excess and three element aortic model is defined:

$$\frac{dP_{res}(t)}{dt} = \frac{P_{ex}(t)}{Z_{ao}C_V} - \frac{P_{res}(t) - P_{cvp}}{RC_V} \tag{5.1}$$

Equation (5.1) can be modified using Equation (3.2), derived by Bramwell-Hill, and the water-hammer equation by relating PWV and $Z_{ao}C_v$ (Hughes and Parker, 2009). Aortic volumetric compliance, C_v, can be written in the form, $C_v=C_AL_{ao}$, and thus distensibility is written, $D = C_A/A_{ao}$, where C_A, L_{ao}, and A_{ao} are compliance per unit length of aorta, aortic length, and aortic

cross-sectional area, respectively. The Bramwell-Hill and water-hammer equations can then be combined to give:

$$Bramwell - Hill: \ PWV^2 = \frac{A_{ao}}{\rho C_A} \tag{5.2}$$

$$water - hammer: \ PWV = \frac{Z_{ao} A_{ao}}{\rho} \tag{5.3}$$

$$\frac{PWV}{L_{ao}} = \frac{1}{Z_{ao} C_V} \tag{5.4}$$

Both the Bramwell-Hill and the water hammer equations are derived from conservation of momentum for flow within an elastic tube (Butlin, 2008). The equations are derived by assuming insignificant change in cross-sectional area and without any reflection of the propagating wave. These assumptions may not be true for aorta as cross-sectional area can be changed to accommodate approximately 50% of SV (Metafratzi et al., 2002), and aortic impedance can vary as the wave propagate away from the ventricle with aorta gradually stiffening (Westerhof et al., 2015b). However, obtaining continuous information on changes in aortic cross-sectional area and the reflected wave are clinically difficult. Thus, given the limitations on clinically available metrics, the relationships given by the Bramwell-Hill and the water hammer equations are assumed to be valid for aorta in this work. The relationship given in Equation (5.4) can be substituted into Equation (5.1) where the ODE can now be rewritten as:

$$\frac{dP_{res}(t)}{dt} = \frac{PWV}{L_{ao}} P_{ex}(t) \ - \frac{P_{res}(t) - \ P_{cvp}}{R C_V} \tag{5.5}$$

The differential equation now includes the value of PWV which can be used to identify the subject-specific aortic characteristic length instead of, $Z_{ao}C_v$. This allows a more accurate estimation of relative changes in reservoir pressure as aortic length is a constant physical parameter. Solving Equation (5.4) with the initial condition of, $P_{res}(0) = P_{ao}(0)$, at the beginning of a heartbeat yields:

$$P_{res}(t) = e^{-(\alpha+\beta)t}\left(\int_0^t e^{(\alpha+\beta)t'}\left(\alpha P_{ao}(t') + \beta P_{cvp}\right)dt' + P_{ao}(0)\right) \tag{5.6}$$

Where, $\alpha = PWV/L_{ao}$, and $\beta = 1/RC_v$, respectively.

5.2.2 Parameter Identification

Parameter values, L_{ao} and β, were identified from the measured pressure waveform, P_{ao}. The diastolic condition given in Equation (4.7) with the value of PWV were used to identify both parameters. By performing a grid search for, L_{ao} and β, the discrepancy between Equation (5.6) and measured diastolic pressure decay was minimized. An example of the error surface produced from a grid search for a single beat is shown in Figure 5.1.

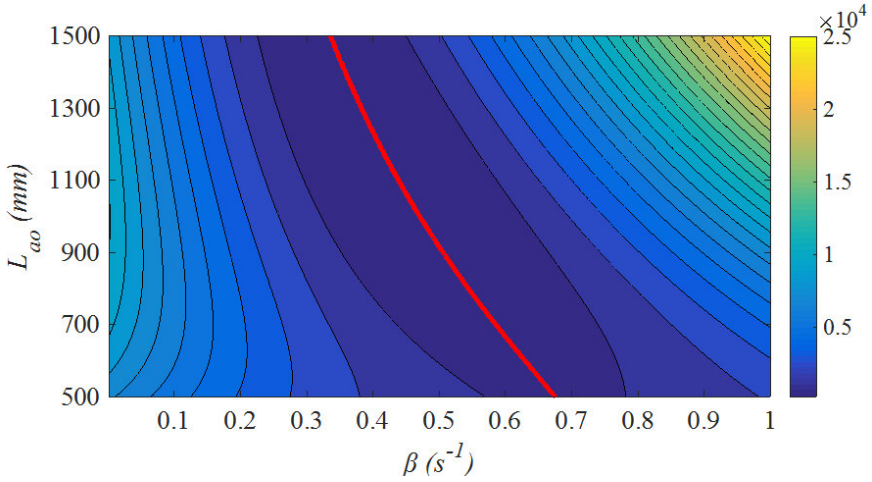

Figure 5.1 – Error surface showing the discrepancy between diastolic $P_{abao}(td<t<tf)$ and calculated P_{res} with Equation (5.5) using different values of L_{ao} and β. The red line represents optimal parameter L_{ao} for a given β.

It can be seen in Figure 5.1 that the surface is convex so an optimal value of L_{ao} could be identified for each value of β. To identify the most suitable set of parameters, L_{ao} and β, from the sets of optimal parameters identified by grid search, further weights were added to the ESP to improve practical identifiability (Pironet et al., 2016). The constraints given in Equation (4.9) were modified to suit parameter identification for Equation (5.6). At ESP and the aortic valve closure time, the blood flow entering the aorta from the ventricle is zero, and consequently, the excess pressure at this point must be zero. Implementing this condition, the discrepancy between calculated end systolic pressure using the identified optimal sets of parameters, and measured end systolic pressure were minimized to select an optimal set of parameters, L_{ao} and β, for a given pressure waveform. An example error curve for this optimization process is shown in Figure 5.2

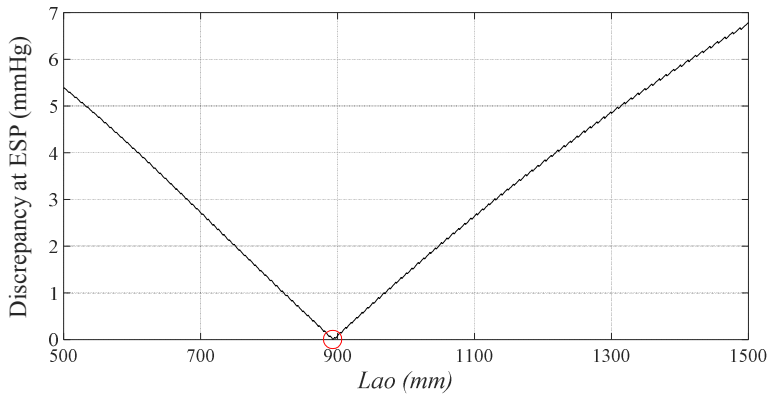

Figure 5.2 – The error curve showing the discrepancy between P_{abao} at ESP and calculated P_{res} at ESP using optimal sets of L_{ao} and β identified by grid search. The red circle shows the identified optimal parameter L_{ao} for a given pressure waveform.

The parameter identification process described above was used for the first 10 beats of the experiment for each pig. Once 10 values of L_{ao} were identified for each pig, the values were averaged to give a representative L_{ao} for each pig over the rest of the experiment. L_{ao} was held constant because this anatomical length is not expected to change with condition.

Using this fixed, subject-specific representative value of L_{ao}, β was optimized using the condition defined in Equation (4.7) for each heart beat and pressure waveform. The calculated P_{res} for each pressure waveform were then used to determine P_{ex} and, subsequently, used to calculate aortic flow and SV.

5.2.3 Aortic Characteristic Impedance Estimation

5.2.3.1 Calibration of Aortic Area

For this analysis, the first 10 beats of measured left ventricular SV values from the admittance catheter were used to calibrate A_{ao} for each pig. Identified P_{ex} and measured, SV = $\int_0^{t_d} Q_{in}$, were substituted into Equation (4.4) to calculate Z_{ao}. Using these Z_{ao} values, A_{ao} were determined from Equation (5.4) using a measured value of PWV. In this analysis the density of blood was assumed constant at 1050 kg/m^3 (Trudnowski and Rico, 1974). The average value of A_{ao} for the first 10 beats was used as a subject-specific representative value and to estimate aortic characteristic impedance, Z_{ao}, for the rest of the experiment.

5.2.3.2 Relationship between Model derived Aortic Area and Ejection Time

A previous study identified a relationship between ejection time and PWV (Salvi et al., 2013). It showed PWV, influenced by variation in ejection time, may provide inaccurate representation of aortic distensibility. Consequently, the changes in aortic characteristic impedance, Z_{ao}, calculated using PWV and A_{ao} from Equation (5.3) can be effected by this factor. To minimize the error in PWV from changes in ejection time, the relationship between model derived aortic area, A_{ao}, and ejection time were examined.

To capture the effect of ejection time on PWV over the course of an experiment, the relationship between A_{ao} calculated from Equation (5.3) using the measured SV and ventricular ejection time identified from the pressure waveform were analysed. The duration of systole is

used as the ejection time in this analysis. Figure 5.3 shows the regression line minimizing the geometric mean deviation between relative changes in A_{ao} and the inverse of ejection time for all pigs as a percentage change in relation to initial part of the experiment. Regression using geometric mean deviation was applied as both parameters were expected to have measurement error (Brace, 1977).

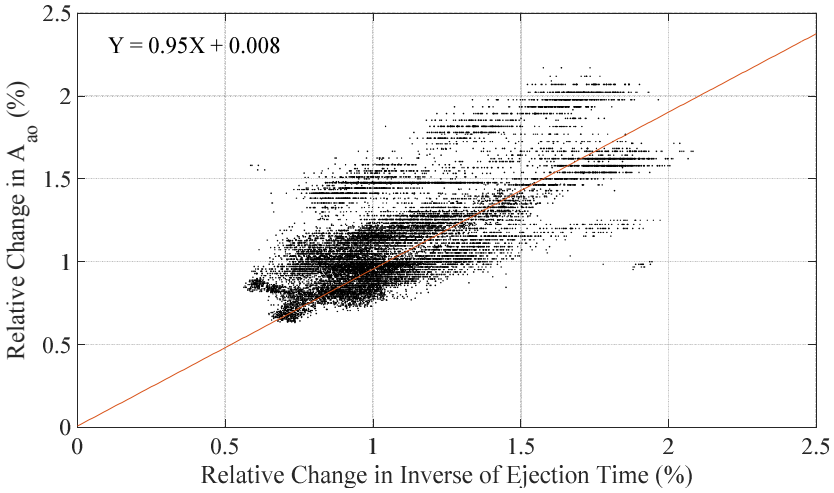

Figure 5.3 – Correlation plot showing relationship between relative change in aortic area, A_{ao}, and inverse of ejection time.

The relationship revealed a positive linear correlation between model derived aortic area, A_{ao}, and the inverse of ejection time. Assuming A_{ao} is a relatively constant physiological parameter, the effect of inverse of ejection time on aortic area, A_{ao}, showed a nearly 1:1 ratio. This relationship was applied to calibrate A_{ao} to identify more accurate values of Z_{ao}, yielding.

$$\frac{A_{ao}}{A_{ao,0}} = \frac{Ejection\ Time_0}{Ejection\ Time} \tag{5.7}$$

$$Z_{ao} = \frac{\rho PWV}{A_{ao,0}} \frac{Ejection\ Time}{Ejection\ Time_0} \tag{5.8}$$

Where the subscript zero refers to the calibrated value. The calculated aortic characteristic impedance, Z_{ao}, from Equation (5.8) and P_{ex} from Equations (4.1) and (5.6) were then used to estimate SV.

5.2.3 Stroke Volume and Windkessel Parameter Estimation

The identified value of Z_{ao} from Equation (5.4) and P_{ex} from the measured pressure waveform can now be used to estimate beat-to-beat SV for the entire experiment.

$$SV_{estimate} = \frac{1}{Z_{ao}} \int_{0}^{tf} P_{ex}(t)dt \tag{5.9}$$

The benefit of the method described in this chapter is that changes in aortic model parameters can also be tracked. The identified parameters RC_v and $Z_{ao}C_v$ for each heart beat combined with the estimated values of aortic characteristic impedance from Equation (5.4) allow all model parameters to be determined on a beat-to-beat basis. Aortic compliance was identified by, C_v=$Z_{ao}C_v$/Z_{ao}, and resistance was identified by, R= RC_v/C_v.

The aortic model can now reveal main cardiovascular dynamics responsible for changes seen in aortic blood pressure measurements. This ability is very important for correct diagnosis and optimizing treatment. Monitoring of the model outputs allow precise titration of fluid, inotropes, and vasoactive drugs by providing 'direct' physiological response.

The estimated SV is compared against directly measured SV from the admittance catheter using Bland-Altman plots. In addition, the estimated parameter values were compared against calculated values from Equations (4.12) – (4.14) using the measured SV. A schematic of processes involved for estimating SV with the aortic model is outlined in Figure 5.4.

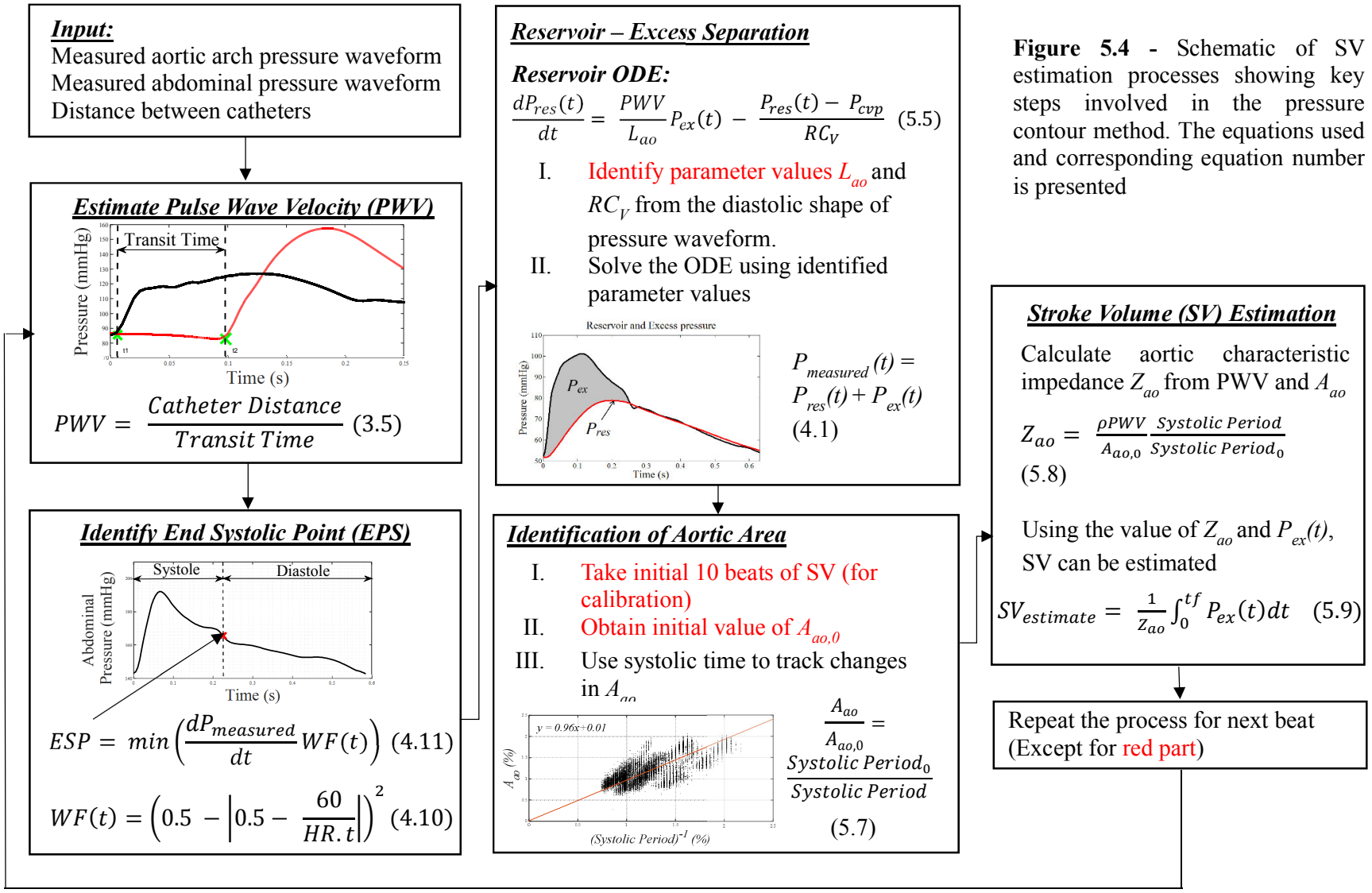

Figure 5.4 - Schematic of SV estimation processes showing key steps involved in the pressure contour method. The equations used and corresponding equation number is presented

5.3 Results

The identified values of L_{ao} and $A_{ao,0}$ for each pig are shown in Table 5.1. Table 5.2 summarizes the correlation coefficients (R) between estimated Windkessel model parameters and those directly calculated using the measured SV value, analysing trend accuracy. Bland-Altman plots comparing SV estimated using Equation (5.9) and SV measured from the admittance catheter are presented in Figure 5.4. The summary of bias, the 95% interval, and precision accuracy calculated as 95% range divided by mean SV for each pig are shown in Table 5.3. In addition, time series showing measured and estimated SV in the last RM period, the most distant point from calibration and thus a potential worst case, for each pig, are shown in Figure 5.5.

Table 5.1 – Summary of identified parameters, L_{ao} and $A_{ao,0}$, for all pigs.

	Pig 2	***Pig 3***	***Pig 5***	***Pig 6***	***Pig 7***	***Pig 8***
L_{ao} *(m)*	0.88	0.41	0.89	0.91	0.73	0.68
$A_{ao,0}$ *(mm^2)*	201	269	473	163	436	207

Table 5.2 – Summary correlation coefficients (R) between estimated and directly calculated Windkessel model parameters.

Pig No	***R* (mmHg.s/ml)**	**C_v (ml/mmHg)**	**Z_{ao} (mmHg.s/ml)**
Pig 2	0.54	0.74	0.62
Pig 3	0.95	0.93	0.91
Pig 5	0.76	0.81	0.70
Pig 6	0.76	0.65	0.51
Pig 7	0.17	0.58	0.58
Pig 8	0.87	0.68	0.65

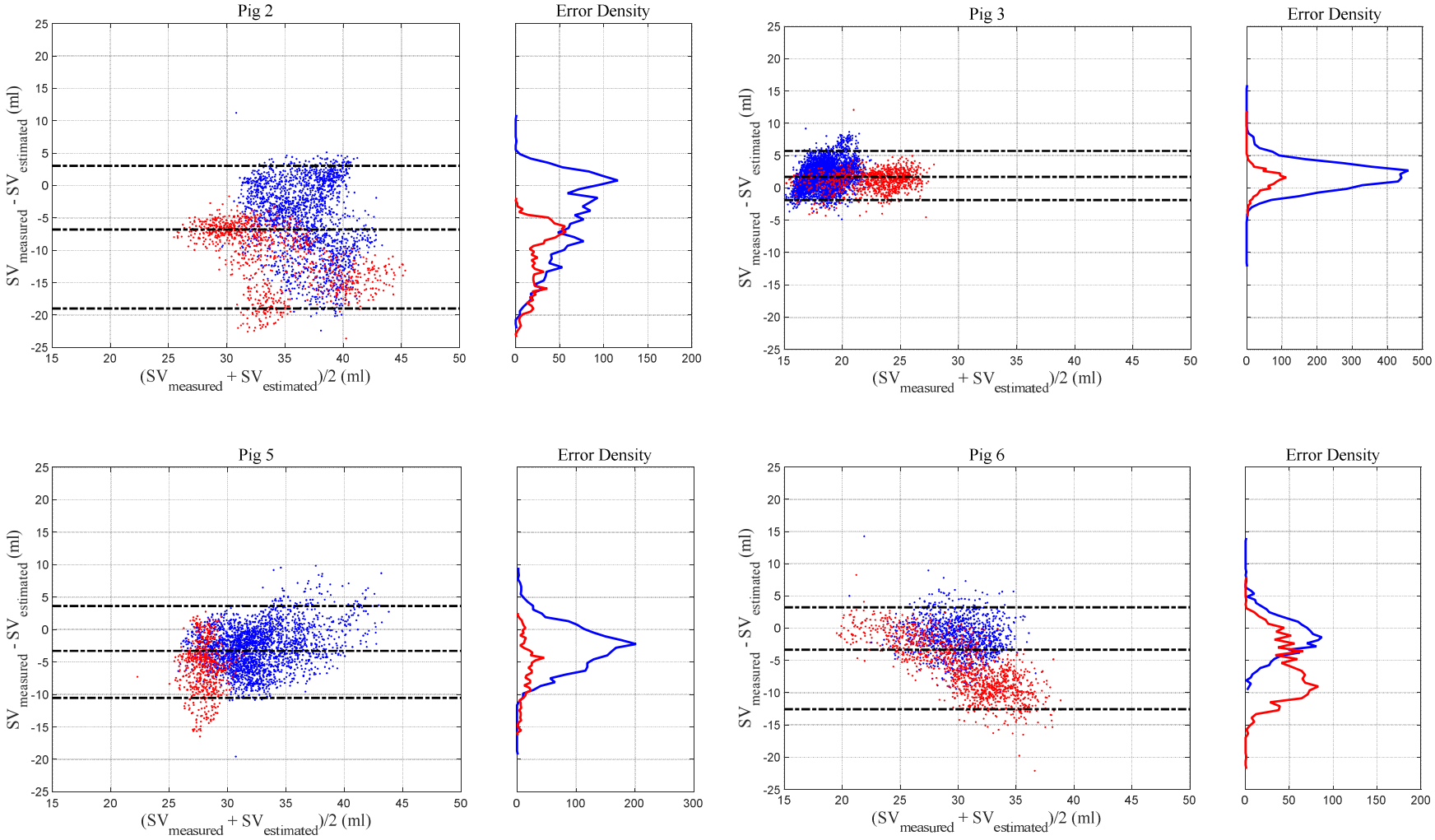
Pig 2
Error Density
Pig 3
Error Density
Pig 5
Error Density
Pig 6
Error Density
SV measured - SV estimated (ml)
(SV measured + SV estimated)/2 (ml)

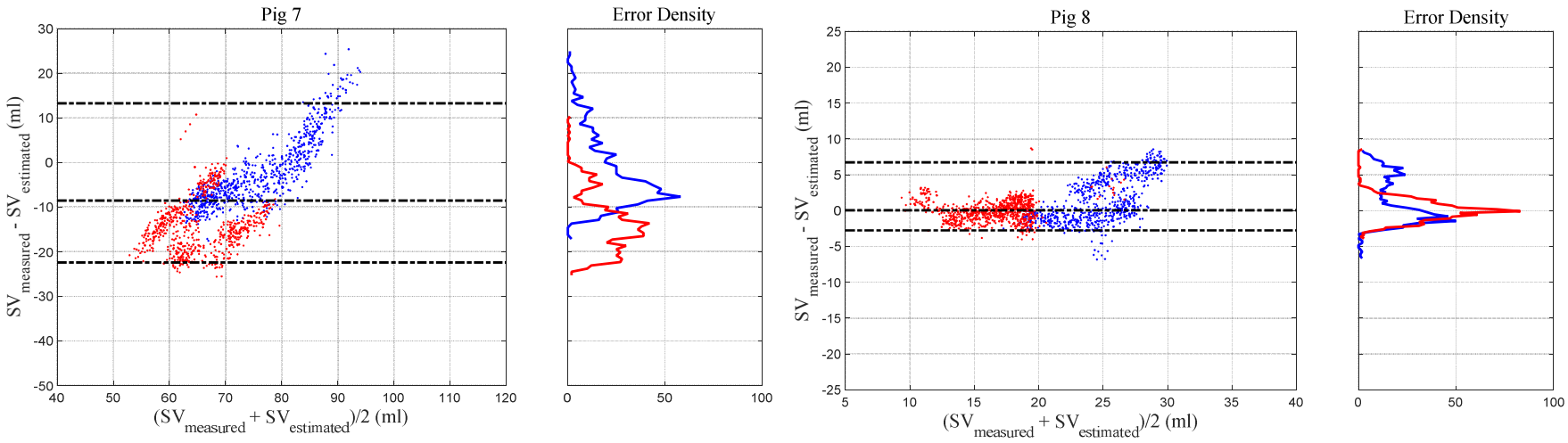

Figure 5.5 - Bland Altman plots showing agreements between measured and estimated SV for each pig. Pre-dobutamine/sepsis periods are shown with blue dots, and post-dobutamine/endotoxin are shown with red dots. Black dashed line showing the bias, 95th percent interval and right panel showing the error distribution between measured and estimated SV values.

Table 5.3 – Summary of Bland-Altman analysis for each pig. Data are presented as bias [95th percent interval].

Pig No	***Bland-Altman results** (ml)*	***Precision** (%)*
Pig 2	-6.8 [-17.7 – 2.2]	+27, -34
Pig 3	1.7 [-1.3 – 4.9]	+21, -18
Pig 5	-3.3 [-9.2 – 2.2]	+22, -23
Pig 6	-2.7 [-11.4 – 3.9]	+22, -31
Pig 7	-8.5 [-22.4 – 13.2]	+33, -21
Pig 8	-0.0 [-2.7 – 6.7]	+33, -14

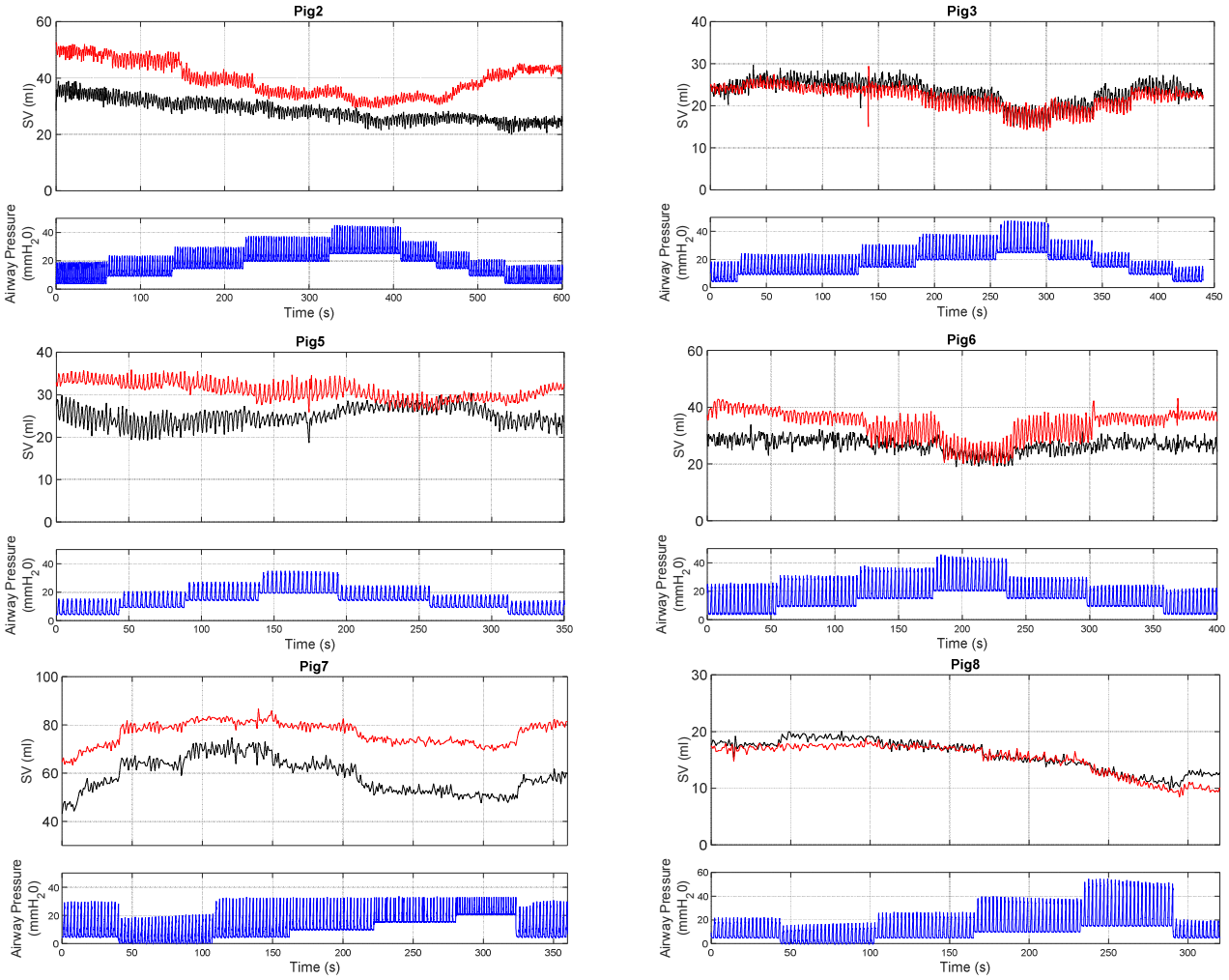

Figure 5.6 – Time series plot showing measured and estimated SV in the last RM period of the experiment for each pig. Top Panel: Measured SV from admittance catheter (black line) and estimated SV using equation (13) (red line). Bottom Panel: simultaneously measured airway pressure showing PEEP changes during recruitment manoeuvers RM (blue line).

5.4 Discussion

5.4.1 Accuracy of Windkessel Parameters and SV estimation

The correlation coefficients shown in Table 5.2 represent the similarity of estimated and calculated Windkessel parameter trends using direct SV measurement. The results showed all Windkessel parameters can be captured accurately with correlation coefficients above R=0.5 for all pigs except for systemic resistance, *R*, in Pig 7. The ability of the method to capture aortic characteristic impedance, systemic resistance, and compliance provides great potential for not only monitoring SV, but capturing the underlying physiological change that caused modification in SV, and thus, improving treatment decisions in critical care.

The Bland-Altman results in Figure 5.5 and Table 5.3 demonstrate the capability of the method to capture the absolute value of SV. Despite all the significant hemodynamic changes made by dobutamine and endotoxin, the 95% range was within approximately ±30% for all pigs. Thus, these results demonstrate that this method is capable of estimating clinically acceptable absolute SV values according to criteria from Critchely and Critchely (1999).

Trends in response to care and condition may be more important, clinically. The ability of the method to capture SV trends is shown in Figure 5.6. The figure shows the last RM period of the experiment where one would expect to find the largest difference in the hemodynamic conditions as it is furthest in time and condition from any calibration. It can be seen that PEEP induced SV trends were correctly captured in most cases. The method was able to capture both 'affected' and 'unaffected' (Pig 3) cases, which has clinical importance in preload assessment (Monnet and Teboul, 2013). In addition, SV variability induced from individual breath (Shekerdemian and Bohn, 1999) was correctly captured.

It can be noted that the method over-estimated the trend for Pig 6, had a large off-set for Pig 7, and made incorrect estimation for Pig 2 during PEEP reduction. Pig 6 had an extremely low blood pressure, of approximately 45 mmHg at the beginning of the experiment, where the method was calibrated and had the biggest change, almost a twofold increase, in the mean pressure during the experiment, which can be seen in Table 3.1. In such a case, the method was not able to capture the dramatic change in aortic dimension, and thus, deviated from true SV value. In Pig 7, the changes in SV from PEEP were accurately captured. However, the significant increases in aortic characteristic impedance from endotoxin were incorrectly captured. In this case, SV was reduced with the introduction of endotoxin with little modification to PWV or ejection time. This effect produced little to no change in model derived aortic characteristic impedance, and consequently, created the SV off-set seen in Figure 5.6. The error seen in Pig 2 during PEEP reduction was not able to be resolved as the value of measured SV remained at a reduced value, while all physiological parameters returned to pre-RM values. A possible reason for this could be that the SV reduction cause by PEEP changes shifted the location of admittance catheter within the ventricle, resulting in measurement error of SV. Despite these errors and offsets, the overall SV trends were captured in most of the RM period.

The method described in this chapter still requires improvement in accurately estimating the aortic characteristic impedance to minimise some of the errors in these results. Further investigations are necessary to determine the sources of error, and thus, appropriate corrections can be made to the model. Despite these limitations, the model presented in this chapter showed significant improvement compared to the Bland-Altman result shown in Figure 4.4, especially in Pigs 3, 5, and 8. In addition, the method overcame the inability to capture time-varying Windkessel model parameters, which are clinically essential for correct diagnosis and optimal treatment.

5.4.2 Pressure Contour Analysis

There are several methods currently available for estimating continuous SV by pressure contour analysis (Montenij et al., 2011). In general, Windkessel models are used and parameters involved in the model are identified from the single pressure waveform and/or patients' demographic/physical characteristics (Thiele and Durieux, 2011). The significant improvement of the method presented over conventional methods is that PWV measurements are integrated into pressure contour analysis to accurately capture the dynamics of time-varying model parameters, which are needed to obtain SV more reliably.

PWV measurements are related to arterial distensibility (Bramwell and Hill, 1922) and relative changes within a subject provide additional information on the cause of changes in the characteristics of the pressure waveform. A combination of changes in the value of PWV and changes in the shape of diastolic pressure decay for a given aortic dimension gives a better approximation of the time-varying arterial reservoir function. The reservoir pressure waveform estimates the minimum pressure that ventricle must provide to induce flow in to the artery (Parker et al., 2012) and is closely related to arterial impedance (Milnor, 1975). By assigning the correct components of the pressure waveform to each of the Windkessel parameters, and with added data inputs, the method is capable of capturing accurate physiological conditions and their changes.

5.4.3 Estimation of Aortic Dimension

In this work, the aortic dimension was estimated by assuming the aorta behaved as a simple cylindrical tube having uniform properties and pressure along it. In reality, the properties are non-uniform and each segment of aorta has different pressure contours. However, to obtain such a large amount of information in a clinical setting is impractical, if not impossible. These assumptions thus produce error in the estimation of SV, but are necessary in developing a

method based on clinically accessible and reasonable measurements. In the ICU, measurement of aortic area could be obtained using echocardiography (Robson et al., 1988) without additionally invasive procedures, and its value could be used to calibrate the model without SV measurements.

The identified values of L_{ao} and calibrated values of $A_{ao,0}$ for each pig are shown in Table 5.1. These values represent an estimate of aortic dimensions for a given value of pressure contour and PWV. It is largely affected by the absolute value of PWV and SV values used to calibrate the method. Since even the reference values are expected to have error of approximately ±20% (Peyton and Chong, 2010), the identified values of aortic dimension may not be entirely realistic. However, given the large errors of reference values, the resulting values are of use, as are the resulting SV values.

The important part of this calibration is to give an estimate of the dimension under given conditions and to use the relative changes in the measurements to track the trends of hemodynamic parameters. In a clinical environment, the absolute value of SV is often not of great importance. However, the relative changes in SV for different patient conditions and in response to therapy is of major clinical significance (Marik, 2013). From this point of view, the method has shown the ability to sufficiently track the trends of SV (Fig 5.6) under the assumptions made.

5.4.4 Relationship between Model Derived Aortic Area and Ejection Time

The identified relationship shown in Figure 5.3 uses A_{ao} derived from Equation (5.2) with aortic characteristic impedance calculated using the measured value of SV. In the experiment, true aortic diameter was not measured and consequently, the exact rationale behind the relationship between aortic area and systolic period was not able to be determined. This limitation is due to

the possibility that the relationship may represent correlation between systolic periods with other physiological variables.

Previous studies have identified the relationship between heart rate/ejection time and aortic PWV (Lantelme et al., 2002). The relationship can be explained by stiffening of the aortic wall due to viscoelastic properties (Salvi et al., 2013). The water hammer equation does not have terms to describe the energy loss due to hysteresis of the aorta, and thus could produce incorrect values of Z_{ao}, in turn affecting estimated SV.

To identify the exact source of the relationship presented in Figure 5.3, accurate measurements of time-varying aortic area are required. Such measurements will produce a stress-strain relationship explaining the time-dependent mechanisms associated with arterial distensibility/stiffness. However, whether the relationship is due to the viscoelastic properties or not, the relationship was still useful in providing an accurate estimation of SV with the hemodynamic conditions changed by dobutamine/endotoxin, and thus, it was used for the method presented until better data are available in subsequent experiments.

5.4.5 Limitations

The experimental data used here involved highly invasive methods to obtain PWV, requiring two pressure measurements along the aorta, which is currently uncommon in the critical care environment. However, the results from this analysis demonstrates the possibilities for more accurate estimation of SV if PWV can be estimated by this approach or a different one. In addition, a specially designed double-lumen catheter having two pressure sensor (Harley et al., 1969) could be used obtain accurate aortic PWV in a non-additionally invasive fashion, rendering it more clinically feasible. The aortic arch pressure measurement was used only for the purpose of identifying the transit time and the information from its contour was not used.

Therefore, this measurement can be replaced with less invasive measurements such as ECG to detect another pulse location (Loukogeorgakis et al., 2002). Previous studies show evidence for a strong relationship between invasive and non-invasive PWV measurements (Horvath et al., 2010), and thus the method is expected to have negligible influence from use of alternative PWV measurements. Chapter 8 further discusses and investigates the accuracy of estimating PWV using ECG measurements, improving the clinical applicability of the method.

5.5 Summary

The method presented in this chapter accurately estimates and tracks SV trends even when hemodynamic properties are significantly altered. PWV measurements, which are usually available in ICU or can easily be obtained in a non-additionally invasive way, were integrated into pressure contour analysis to overcome weaknesses associated with conventional methods for estimating SV. The additional information gained by PWV allowed precise estimation of Windkessel parameters and thus, accurate estimation of SV. The Bland-Altman plots showed SV error of within approximately ±30% between estimated SV and the reference SV across all pigs, demonstrating the clinical applicability of the method. In addition, the method requires only one calibration per subject offering less workload for beside clinicians and nurses. The method presented can track accurate and clinically important changes in patients' haemodynamic state providing essential information for correct diagnosis and optimal care.

Chapter 6: Comparison of SV Accuracy with PiCCO and Wesseling Models

This chapter compares the accuracy of SV estimation between the aortic model presented in Chapter 5, a nonlinear three-element model developed by Wesseling *et al* (Wesseling et al., 1993), and the PiCCO system from PULSION (Oren-Grinberg, 2010). Parameters involved in the nonlinear three-element model were identified by minimizing squared error between SV values from the admittance catheter/flow probe and the nonlinear model output. SV measurements from the PiCCO device were obtained every 12 seconds. In addition, PiCCO device was calibrated with thermodilution measurements in between clinical interventions. Accuracy of the three techniques is compared using Bland-Altman analysis and estimated SV trends from each techniques is discussed.

6.1 Introduction

There are many commercial devices available for continuously estimating SV using the pressure contour method (Porhomayon et al., 2012a). The most commonly used commercial devices are the: PiCCO system (Pulsion, Munich, Germany) (Oren-Grinberg, 2010); LiDCO system (LiDCO, Cambridge, UK) (Sundar and Panzica, 2010, Rhodes and Sunderland, 2005); and FloTrac system (Edwards Lifesciences, Irvine, CA) (Mayer et al., 2009). PiCCO and LiDCO both use indicator dilution measurements to calibrate the model for pressure contour analysis. FloTrac on the other hand uses demographic and physical characteristics of a patient

to identify values for the model. In general, indicator dilution calibrated systems have greater SV accuracy than non-calibrated systems (Hadian et al., 2010). A calibrated system has the advantage of correcting the model when estimated SV deviates from indicator dilution measurements due to hemodynamic instability or use of inotrope/vasoactive drugs, both of which are common in the ICU for patients with poor circulatory function.

The accuracy of continuously estimating SV with commercial devices has been validated against gold standard SV measurements (Bein et al., 2004). However, previous studies show contradicting results, varying from good accuracy achieved (Button et al., 2007, Della Rocca et al., 2003) to low accuracy when hemodynamic instability is present (Camporota and Beale, 2010, Bendjelid, 2009). For the calibrated systems, the necessity of frequent calibration during (unpredictable) instability suggests clinical impracticality and inaccuracy in continuously estimating SV from the arterial pressure waveform (Gruenewald et al., 2011).

Another widely known pressure contour method is the nonlinear three-element model developed by Wesseling *et al* (Wesseling et al., 1993). The accuracy of the model has been assessed in number of papers (Jansen et al., 1990, Jansen et al., 2001, Jellema et al., 1999, HARMS et al., 1999) and compared against different methods (De Wilde et al., 2007). Unlike the PiCCO and FloTrac systems, the underlying algorithms involved in the pressure contour method are fully described in the paper.

The PiCCO SV measurements were made in Pigs 5 and 6 from the dobutamine experiments and Pigs 7 and 8 from the endotoxin experiments. These data allow comparison of accuracy of SV estimation using different pressure contour methods. This chapter analyses the accuracy of three pressure contour methods, the: 1) PiCCO system; 2) Wesseling model; and 3) aortic pressure model developed in Chapter 5. They are compared to the admittance catheter/flow

probe direct measurements. Bland-Altman analysis between SV values estimated from three methods and measured SV assesses accuracy. Time-series plots demonstrate the trend accuracy of each method.

6.2 Method

6.2.1 PiCCO Measurement

Abdominal aortic pressure measurements for the PiCCO device were made by inserting a catheter from the femoral artery. The catheter location for the PiCCO was adjusted so that the pressure value was similar to that being measured with the other catheter in the abdominal aortic pressure. Central venous pressure measurement for the PiCCO system was made by inserting a pressure catheter from the jugular vein into the superior vena cava. Saline solution for thermodilution calibration measurements were also injected from the central venous catheter.

The PiCCO system was initially calibrated at the start of each experiment after all catheters had been placed. Re-calibrations of the PiCCO system were made between each of the clinical interventions shown in Table 4.1, ensuring optimal SV accuracy made by the PiCCO for each intervention. Each calibration involved administering 15ml of refrigerated saline into the central venous catheter and repeating the same process three times. The recorded temperature gradient at the abdominal aortic catheter site was used to estimate SV, thus calibrating the PiCCO system.

Continuous SV data from the PiCCO system was exported in MS excel format at the end of each experiment. The excel array was converted for analysis using MATLAB. Time on the

PiCCO device and Notocord were matched at the beginning of the experiment, so that estimated SV from all methods can be analysed on the same time line.

6.2.2 Nonlinear Three-Element Model by Wesseling

6.2.2.1 Wesseling Model

The electrical analogy of the three-element model for the Wesseling model is identical to Figure 4.1 without applying the reservoir-excess pressure hypothesis from Wang *et al* (Wang et al., 2003). The Wesseling model uses total systolic pressure minus end diastolic pressure level as a systolic area for computing aortic flow. This systolic area is defined:

$$P_w = \int_0^{t_d} (P_{ao}(t) - P_{ed})\, dt \tag{6.1}$$

Where P_w represents the systolic pressure component used for the Wesseling model, t_d is the end systolic time, P_{ed} is the end diastolic pressure, and $P_{ao}(t)$ is the measured abdominal aortic pressure waveform.

The main difference between the Wesseling pressure contour method and the aortic model presented in Chapter 5 is in the method for determining beat-to-beat characteristic impedance. The value of aortic area used in the Wesseling model is identified by employing the nonlinear pressure dependent aortic area relationship developed by (Langewouters et al., 1984). The relationship is also known as the arctangent aortic model, defined:

$$A_w(P) = A_{max}\left[0.5 + \frac{1}{\pi}\arctan\left(\frac{P - P_0}{P_1}\right)\right] \tag{6.2}$$

Where $A_w(P)$ is the pressure dependent aortic area used in the Wesseling model, P is the pressure, and the parameters, A_{max}, P_0 and P_1 define the characteristics of the aortic area function, which is the shape of arctangent function. A_{max} is the maximum aortic cross-sectional area at very high pressure, P_0 defines the position of the inflection point on the pressure axis, and P_1 defines the width between the points at one-half and three-quarter amplitude. The parameters A_{max}, P_0, and P_1 are defined using patient age and gender. The values and linear equations for these relationships are summarized in Table 6.1.

Table 6.1 – Summary of linear equations used for A_{max}, P_0, and P_1 in arctangent aortic model (Wesseling et al., 1993).

Parameter	F	M
A_{max}, cm^2	4.12	5.62
P_0, mmHG	72 – 0.89.Age	76-0.89.Age
P_1, mmHG	57 – 0.44.Age	57 – 0.44.Age

The compliance per unit length of aorta can be identified by differentiating Equation (6.2) with respect to pressure, $(C = dA/dP)$. The equation for aortic compliance derived from Equation (6.2) is written:

$$C_w(P) = \frac{A_{max}/\pi P_1}{1 + \left(\frac{P - P_0}{P_1}\right)^2} \tag{6.3}$$

Where $C_w(P)$ is the Wesseling model aortic compliance. The identified compliance and aortic area from Equation (6.2) and (6.3) can be used to calculate aortic characteristic impedance:

$$Z_w(P) = \sqrt{\rho/(A(P).C(P))} \tag{6.4}$$

Where $Z_w(P)$ is the pressure dependent aortic characteristic impedance used in Wesseling model. In this analysis, mean systolic pressure value were used in Equations (6.2) and (6.3) to

calculate aortic characteristic impedance for the beat. The calculated aortic characteristic impedance is then used to estimate beat-to-beat SV using systolic area defined in Equation (6.1), yielding.

$$SV_w = \frac{P_w}{Z_w(P_{mean})} \tag{6.5}$$

Where SV_w is the stroke volume estimated from Wesseling model.

6.2.2.2 Parameter Identification for the Wesseling Model

The information required for estimating SV using the Wesseling model are the arterial pressure measurements, gender, and age. However, the pressure dependent area relationships described in Table 6.1 were obtained using human aorta data (Langewouters et al., 1984), and thus, the relationship may not be suitable for use in pig data. There are similarities between human and porcine cardiovascular systems (Li et al., 2008), but the age and gender related cardiovascular changes are expected to be different.

To overcome this unidentifiable condition for the Wesseling model when using pig data, A_{max} and age were optimized by minimizing squared error between 'true' aortic characteristic impedance calculated using measured SV and Z_w, giving the best possible accuracy for the model in this work. The equation for P_0 was modified to, $P_0=74-0.89*Age$, taking the middle value of male and female. This optimization is described:

$$[A_{max}, age] = argmin_{[A_{max},age]}\left(\sum_{i=1}^{T_{beats}} (Z_{true,i} - Z_{w,i})^2\right) \tag{6.6}$$

Where T_{beat} is the total number of heart beats analysed in an experiment, and Z_{true} is the calculated aortic characteristic impedance using SV from the admittance catheter/flow probe.

Grid searches were applied by varying A_{max} and age from 2cm^2 to 8cm^2 with 1mm^2 resolution, and 1year to 125years with 1year resolution, respectively. The range for the grid search covers all of the physiological values observed in (Langewouters et al., 1984). The error surface obtained from grid searches are shown in Figure 6.1. The results are zoomed in to capture the surface around the minimum region.

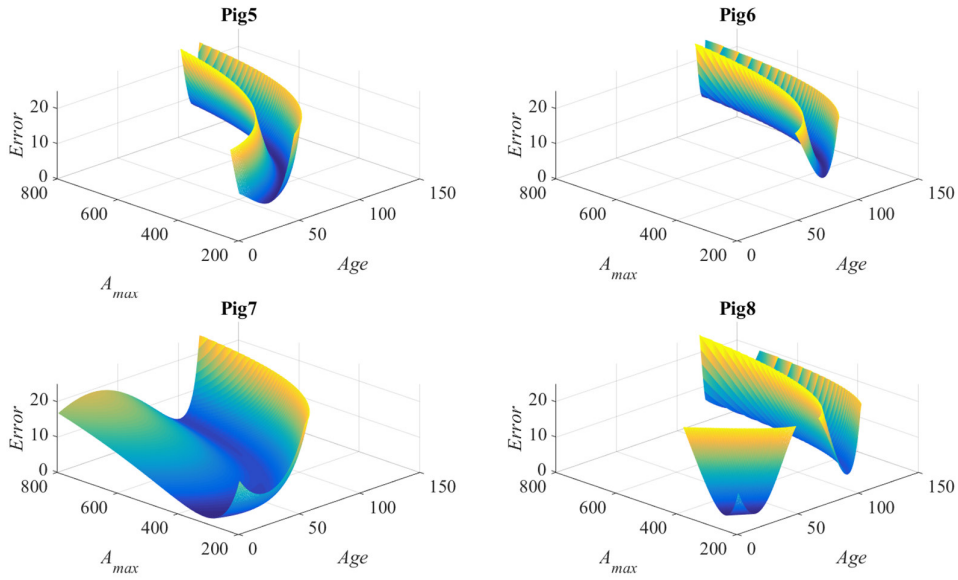

Figure 6.1 – Error surface produced from A_{max} and age grid search for each pig. Vertical axis on the plots represents sum of squared error between Z_{true} and Z_w for the entire experiment.

The error surface for each pig showed multiple combinations of A_{max} and age could be chosen to provide similar total error in aortic characteristic impedance, as shown by blue area in Figure 6.1. The calculated SV accuracy from any combinations of A_{max} and age within the blue area would be very similar. However, to give the best possible accuracy for the Wesseling model,

the A_{max} and age values giving the minimum error were chosen. Table 6.2 summarises the identified values of A_{max} and age for each pig.

Table 6.2 – Identified values of A_{max} and age for each pig from grid search.

Parameter	Pig 5	Pig 6	Pig 7	Pig 8
A_{max},mm^2	260	796	315	244
Age,year	50	121	1	1

The identified values in Table 6.2 were substituted in Equation (6.2) – (6.4) for beat-to-beat aortic characteristic impedance calculation. Using the identified aortic characteristic impedance with the systolic pressure area, SV was estimated from the Wesseling model using Equation (6.5). The estimated SV were then used for SV comparison.

6.2.3 Data Analysis

The estimated SV from the PiCCO system were only obtained every 12 seconds. Thus, SV estimated from the Wesseling model and from the aortic model of Chapter 5 were decimated to the same sampling frequency. For the decimation, the MATLAB function 'decimate(fir)' were used, which applies a 30th order Hamming window filter to the original waveform and reduces the sampling rate by a chosen factor. The decimated SV waveform from each method was then used to compare SV accuracy.

6.3 Results

The Bland-Altman plots comparing measured SV and estimated SV using the three methods are presented in Figure 6.2. The summary of bias, 95% interval, and the 95% range for each pig are shown in Table 6.3. In addition, time series showing decimated SV measurements from admittance catheter/flow probe and decimated SV estimated from the three different methods are shown in Figure 6.3.

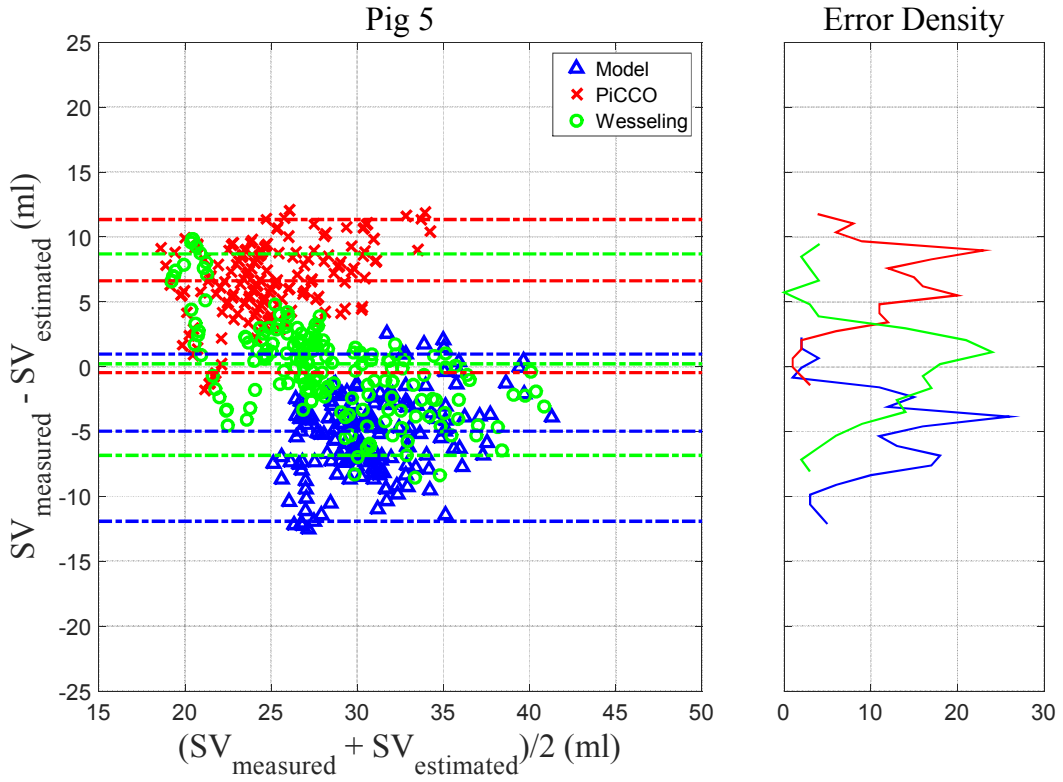
Pig 5
Error Density
Model
PiCCO
Wesseling
SV measured - SV estimated (ml)
(SV measured + SV estimated)/2 (ml)

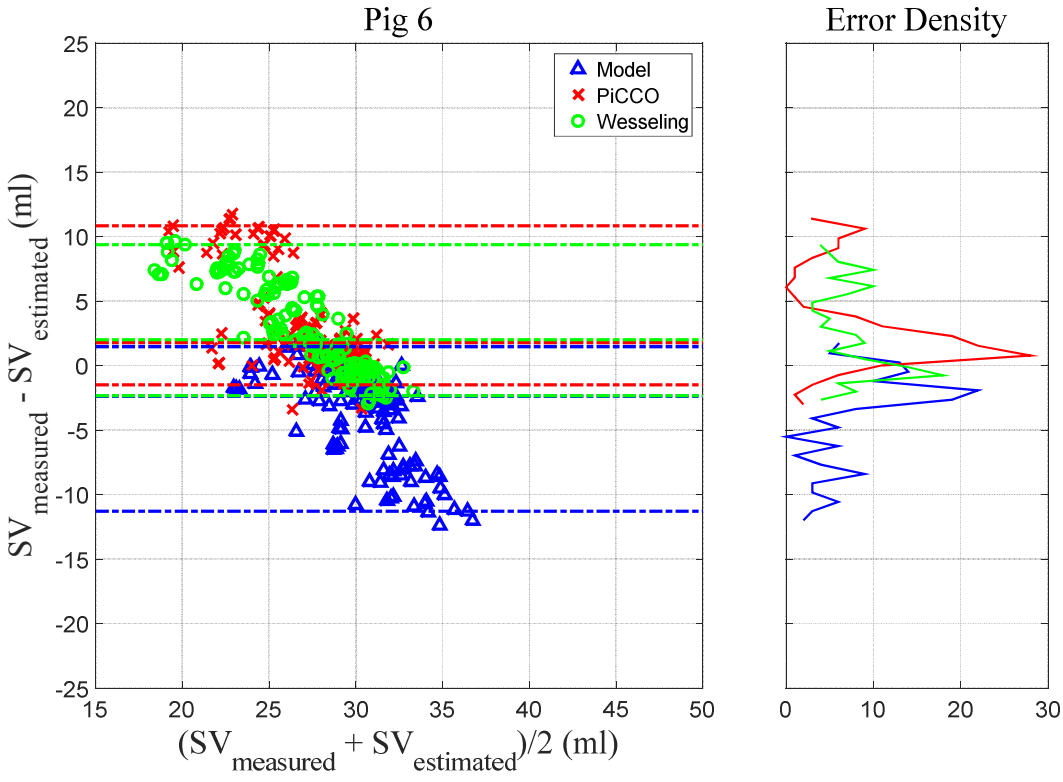
Pig 6
Error Density
Model
PiCCO
Wesseling
SV measured - SV estimated (ml)
(SV measured + SV estimated)/2 (ml)

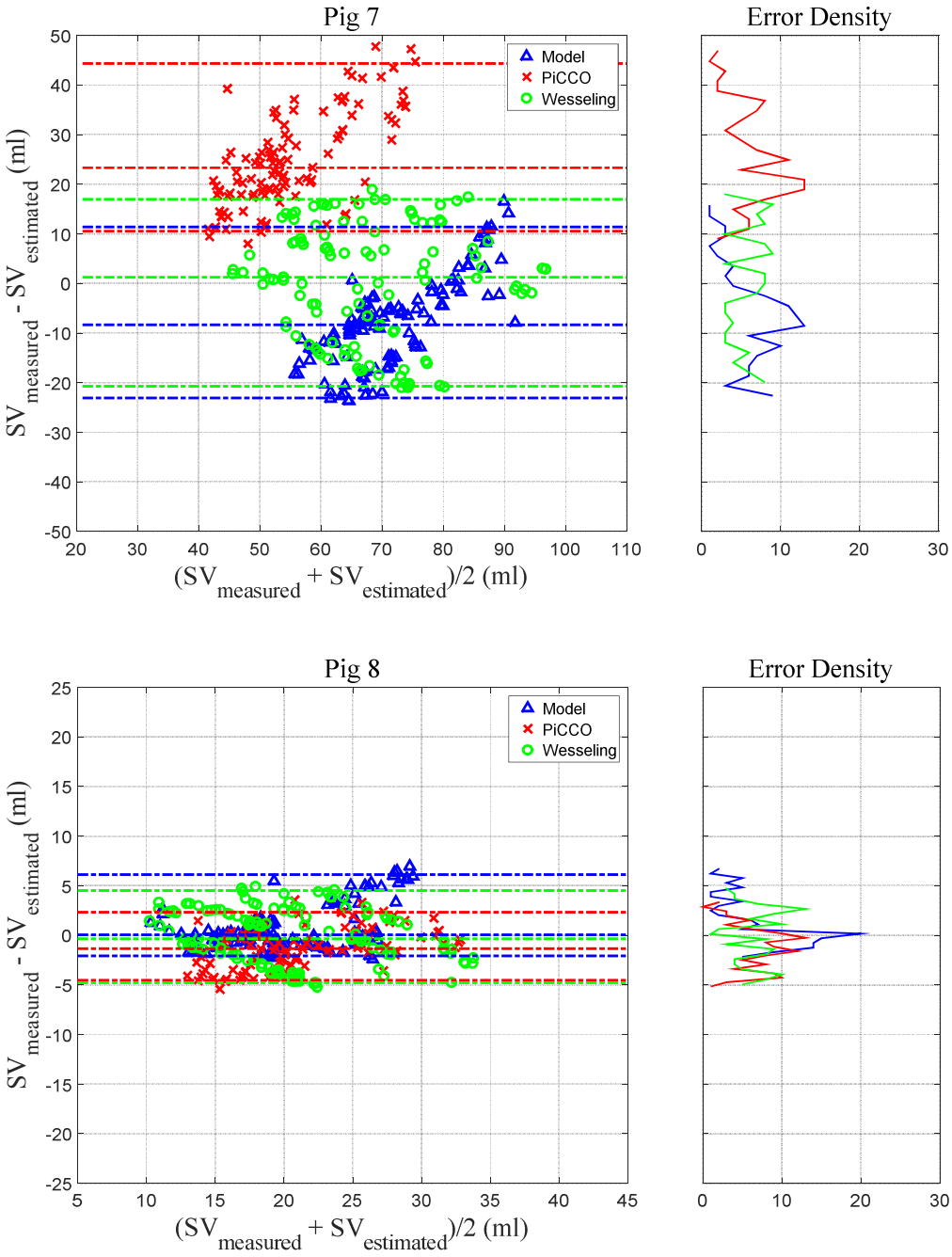

Figure 6.2 – Bland-Altman plots comparing agreement between SV from admittance catheter/flow probe and SV estimated from three pressure contour methods; 1) PiCCO (red cross), 2) Wesseling (green circle), and 3) the aortic model (blue triangle). The bias and 95th percentile for each comparison are shown with dashed line and error distribution are shown on the right panel.

Table 6.3 – Summary of Bland-Altman analysis for each pig and each pressure contour method. Data are presented as bias and 95% interval, and precision are presented as 95% range divided by mean SV in percentage.

The Aortic Model		
Pig No	***Bland-Altman results*** *(ml)*	***Precision*** *(%)*
Pig 5	-5.0 [-11.9 – 1.0]	+21, -25
Pig 6	-2.4 [-11.3 – 1.5]	+14, -31
Pig 7	-8.1 [-23.1 – 11.4]	+29, -22
Pig 8	0.0 [-2.1 – 6.1]	+30, -10
PiCCO		
Pig No	***Bland-Altman results*** *(ml)*	***Precision*** *(%)*
Pig 5	-0.5 [6.6 – 11.3]	+17, -25
Pig 6	1.8 [-1.5 – 10.8]	+31, -11
Pig 7	23.3 [10.5 – 44.4]	+31, -19
Pig 8	-1.3 [-4.5 – 2.3]	+18, -16
Wesseling Model		
Pig No	***Bland-Altman results*** *(ml)*	***Precision*** *(%)*
Pig 5	0.2 [-6.8 – 8.7]	+30, -25
Pig 6	2.0 [-2.3 – 9.4]	+26, -15
Pig 7	1.3 [-20.7 – 17.0]	+23, -32
Pig 8	-0.3 [-4.8 – 4.5]	+24, -22

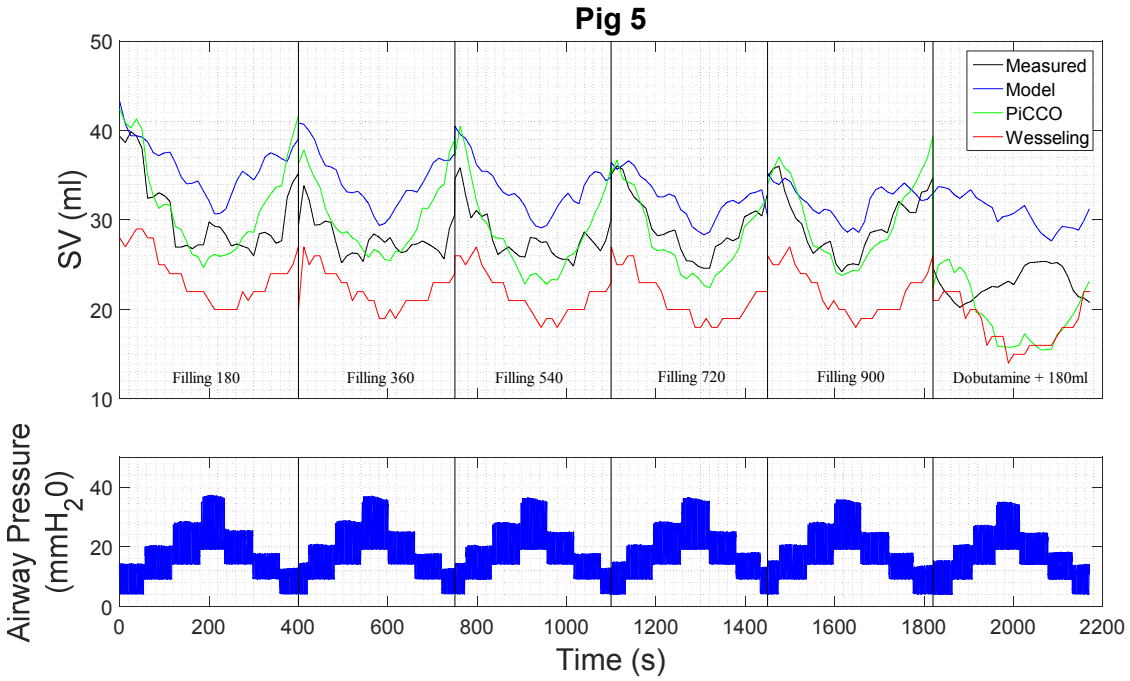

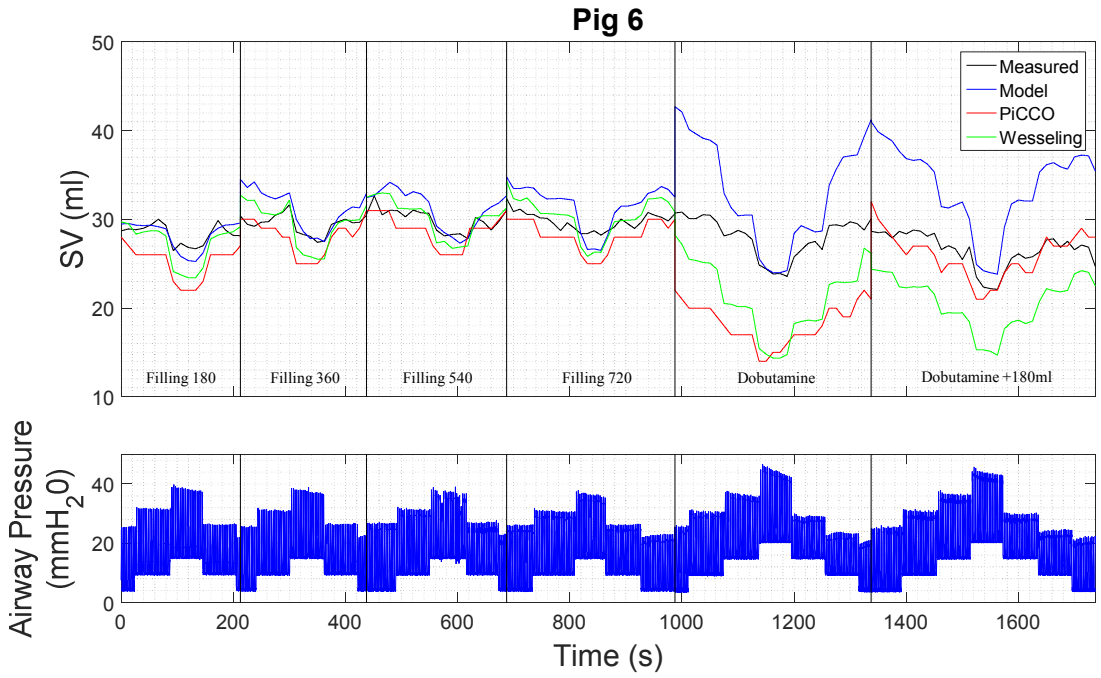
Pig 6
SV (ml)
Measured
Model
PiCCO
Wesseling
Filling 180
Filling 360
Filling 540
Filling 720
Dobutamine
Dobutamine +180ml
Airway Pressure (mmH20)
Time (s)

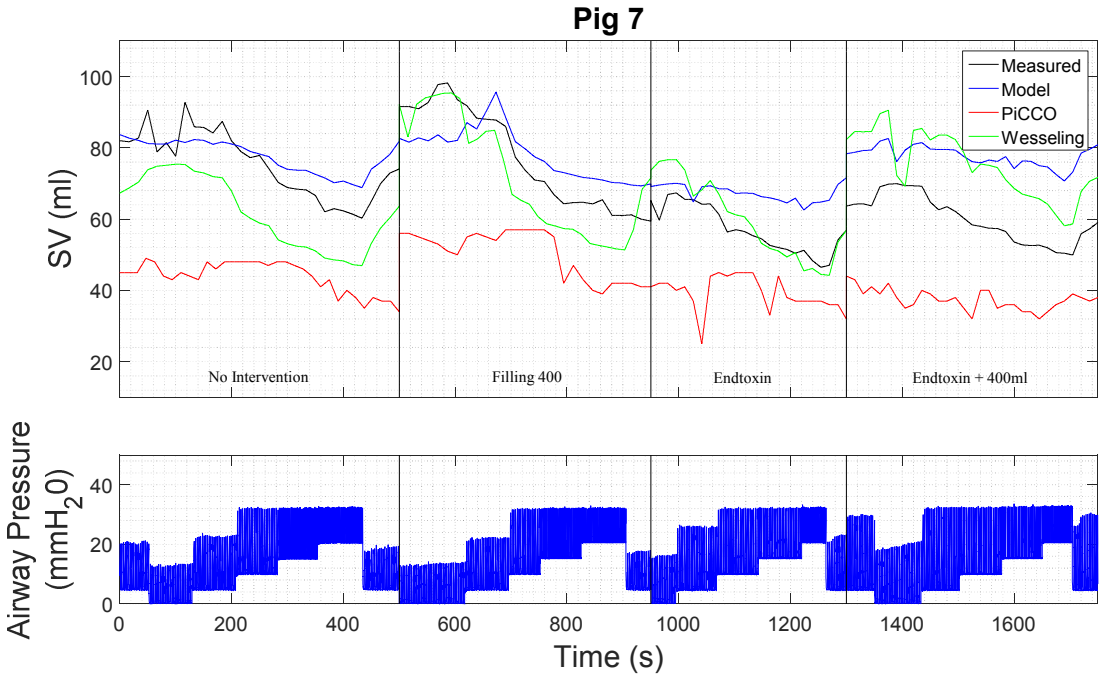
Pig 7
SV (ml)
Measured
Model
PiCCO
Wesseling
No Intervention
Filling 400
Endtoxin
Endtoxin + 400ml
Airway Pressure (mmH20)
Time (s)

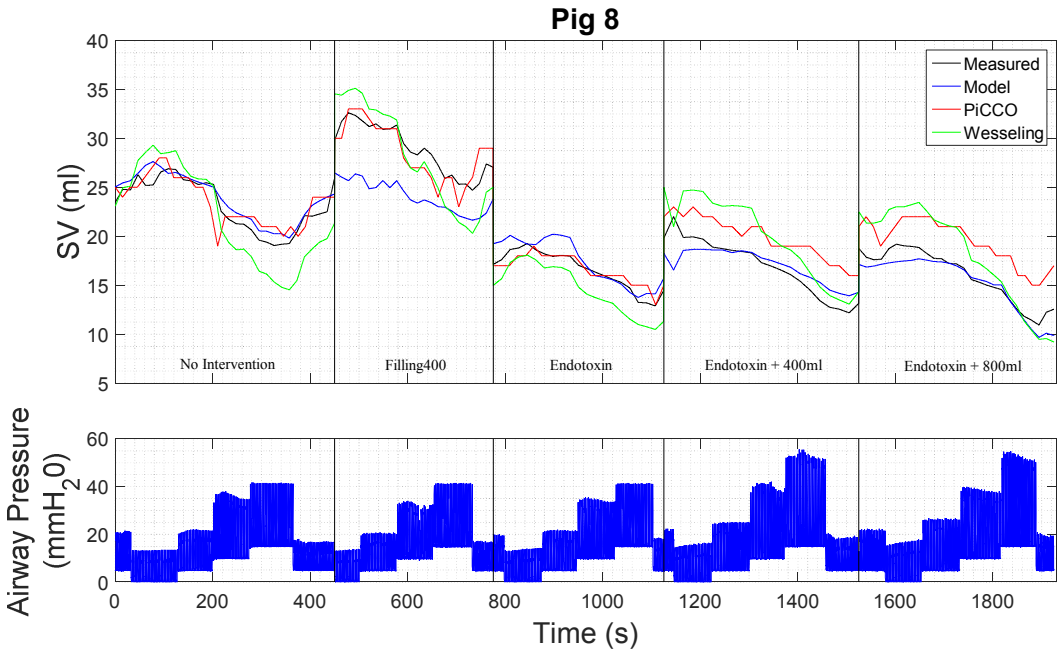

Figure 6.3 - Time series plots showing SV from admittance catheter/flow probe (measured) and estimated SV from three pressure contour methods 1)PiCCO (red line), 2)Wesseling (green line), and 3)the aortic model (blue line). Top panel shows decimated SV waveforms in RM period after each clinical interventions. Bottom panel shows airway pressure measured by the ventilator. PiCCO thermodilution calibration were made in between each clinical interventions (vertical black line).

6.4 Discussion

6.4.1 Accuracy of Each Method

The Bland-Altman results from the three different pressure contour methods showed similar accuracy across all pigs, as shown in Figure 6.2 and Table 6.3. The accuracy calculated as the 95% range divided by mean SV were all within ±31%, demonstrating clinically acceptable estimates of SV by each method (Critchley and Critchley, 1999). All of the methods were capable of capturing SV changes induced by the RMs. However, in some of the RM periods, accuracy was reduced, especially in the post-dobutamine periods. The time-series plots in Figure 6.3 display the details of possible errors introduced.

SV estimated from the PiCCO and Wesseling model during the dobutamine RM period in Pig 5 showed decreases in SV estimated with increasing PEEP, while the aortic model and admittance SV had minimal change induced by, increasing PEEP in this case, despite expectations. The PiCCO and Wesseling model estimate of SV suggest Pig 5 is preload responsive as SV variation is achieved with preload changes induced by the RM (Hofer et al., 2008). On the other hand, SV estimated by the aortic model suggests a non/less-preload responsive case compared to pre-dobutamine period. This lack of response was also seen in the measured SV from the reference admittance catheter. In clinical situations, this error seen in the PiCCO and Wessling model could lead to overloading the patient with extra fluid when the patient is no longer fluid responsive (Monnet and Teboul, 2013). Hence, the ability to track the measured SV changes is important.

SV estimated from the three pressure contour methods were different from each other during the dobutamine RM period in Pig 6. The PiCCO was able to capture the absolute SV trend induced from RM, but was offset by approximately -10ml. The error seen in the PiCCO outputs could be due to inaccurate thermodilution calibration made at the start of dobutamine administration. It can be seen that this error was removed at the start of the 'dobutamine+180ml' RM period as another thermodilution calibration was made between the two dobutamine RM.

The Wesseling model and aortic model both overestimated the SV trends induced by the RM. In addition, SV estimated from the aortic model was overestimated by approximately +10ml at the beginning and the end of the RM. The overestimation in SV by the Wesseling model and the aortic model are due to fixed model parameters. Pig 6 had the most significant increase in measured aortic pressure, and consequently, the arctangent model in the Wesseling model and a fixed value of the aortic area in the aortic model were not able to capture the dramatic change in aortic dimension induced, in this period.

The PiCCO estimated SV in Pig 7 was significantly lower than the SV directly measured by the aortic flow probe. Thermodilution calibrations for PiCCO were made several times during the experiment, and the SV value obtained from the calibrations were consistently 20-30ml lower than the SV obtained from the integral of the aortic flow directly measured by the flow probe, unlike the case seen in Pig 6 where the thermodilution value deviated only once. With both flow probe and thermodilution SV measurements being equivalent to the research and clinical gold standard (Smartt, 2005, Yang et al., 2013), the justification of the 'true' SV value in such cases is very difficult. However, the SV trends measured by the flow probe are still useful as it captures decreases or increases in SV. The Wesseling model method captured the SV trends accurately, while the aortic model and PiCCO were less accurate in the endotoxin RM, for this pig.

In Pig 8, all three methods displayed similar results with little to no bias compared with SV measurement from the flow probe, and all methods captured SV changes from the RM accurately throughout the entire experiment. There were minor underestimations made by the aortic model in the 'Filling400' section, but SV accuracy in the endotoxin periods was very high. In addition, the Wesseling model and PiCCO SV were overestimated in the last two RMs.

Overall, the accuracy of SV estimated by each method was very similar. The only difference between each method was in the way the pressure contour was calibrated. The Wesseling method was calibrated using the entire SV waveform giving the optimal result. The PiCCO device was calibrated each time an intervention was made. The aortic model was calibrated only once at the beginning of the experiment and thus had the least amount of information available, and is thus potentially the most clinically realistic. The results showed models/algorithms used to estimate SV for each method computes acceptable SV with sufficient calibration frequency.

6.4.2 PiCCO

The accuracy of the PiCCO device has been investigated in a number of studies (Bajorat et al., 2006, Rödig et al., 1999, Østergaard et al., 2006). However, some studies indicate inaccuracies for continuously estimating SV with this system under hemodynamic instability or during inotrope/vasoactive drug use (Halvorsen et al., 2006, Yamashita et al., 2008, Yamashita et al., 2007), which is exactly when it is most clinically useful and necessary. In addition, due to these inaccuracies, re-calibration of the PiCCO system is recommended whenever cardiovascular properties are expected to change (Rödig et al., 1999, Bendjelid, 2009), which is a difficult proposition to predict and to act upon when it occurs.

There are two main potential causes for the error produced in SV estimated by the PiCCO: 1) inability to correctly capture hemodynamic properties; and 2) error introduced from inaccurate thermodilution calibration measurement. The physiological model and algorithms used to estimate SV for the PiCCO are unknown. However, based on several studies done on the accuracy of PiCCO during hemodynamic instability (Boyle et al., 2007, Halvorsen et al., 2006, Rödig et al., 1999), it is clear that the model parameters used for pressure to flow conversion deviate from the true hemodynamic values as vascular properties change from the calibrated points. These results demonstrate the limited ability of obtaining changes in vascular properties, such as aortic characteristic impedance, compliance, and systemic resistance from pressure measurements alone.

The second error introduced in PiCCO is from the reference/calibration measurement. This error is due to thermodilution measurements having an approximately ±20% error in estimating SV, even with an accurate method using a Pulmonary Artery Catheter (PAC) (Yang et al., 2013). The PiCCO device uses transpulmonary thermodilution methods, and thus, could produce incorrect SV trends when the device is re-calibrated. This effect can be seen in the first

dobutmine RM period in Pig 6, where the PiCCO system showed significantly decreased SV, while the SV from the admittance catheter stayed constant. With the large error in the reference measurements, frequent model calibration could lead to incorrect SV trends.

Calibration error is reduced in PiCCO as it uses three thermodilution measurements per calibration (Gondos et al., 2009). As a result, there were only one obvious error seen from 17 calibrations performed across all pigs, as shown in Figure 6.3. With the PiCCO system calibration measurements being very close to the admittance/flow probe SV value, the PiCCO SV estimates obtained are considered to be at its optimum accuracy, and clinically such frequent calibration would not be expected, leading to reduced accuracy.

6.4.3 Wesseling Model

The Wessling model is used as the basis for several commercially available uncalibrated pulse contour devices (Truijen et al., 2012), and is a well-known model in the cardiovascular field. Wesseling *et al* introduced a method for identifying characteristic impedance by defining the pressure-area relationship in Equation (6.4). This relationship provides a method to compute aortic flow from pressure, thus making SV estimation possible. Moreover, the equation links aortic characteristic impedance and compliance, revealing interactions between changes in hemodynamics and vascular properties.

The arctangent model developed by (Langewouters et al., 1984), were combined in a Wesseling model to develop a SV estimation method requiring no SV calibration. The arctangent model uses population derived aortic wall properties for describing the pressure-area relationship. The model requires the patient's age and maximum cross-sectional area, A_{max}, as input parameters to determine subject-specific relationship. The relationship is used to calculate aortic

compliance and area, which is then used to identify aortic characteristic impedance using Equation (6.4).

In this analysis, age and A_{max} were optimised for the pig experiments to give the best SV estimate. The identified pressure-area relationship from optimization provides the best subject-specific representation of the aorta for the given SV data. In reality, such optimization is not possible, and the arctangent model would introduce larger errors, as a result, depending on the strength of population derived relationships used in the model for any given subject.

The optimized Wesseling model correctly captured SV trends induced from PEEP changes, dobutamine, and endotoxin. The result demonstrates the ability of the nonlinear three-element Windkessel model combined with aortic characteristic impedance determined from the arctangent model and Equation (6.4). However, if age and A_{max} were changed from the optimal value, the model error could increase rapidly, as can be seen in Figure 6.1.

6.4.4 Aortic Model

The aortic model presented in Chapter 5 resulted in similar SV accuracy compared against the clinically accepted PiCCO system with multiple calibrations during the experiment, and the Wesseling model optimised for the SV data. The results show ability of the aortic model for continuous accurate estimation of Windkessel model parameters, and thus accurate estimation of SV in all conditions tested. The model requires only a single calibration, and minimises the possible error introduced from re-calibration with the reference measurement.

The aortic characteristic impedance calculation using Equation (5.3) for the aortic model is similar to Equation (6.4) for the Wesseling model. However, the aortic model uses PWV measurement instead of the arctangent model for describing aortic pressure-area relationship.

The PWV captures aortic distensibility (Bramwell-Hill equation), and given a calibrated aortic area, pressure-area relationship is obtained. The use of PWV measurement removes the potential error associated with population derived relationships. Thus, the aortic model accurately estimates SV, even when vascular system is significantly altered/modified as vascular properties are continuously monitored through PWV measurement.

6.5 Summary

The accuracy of three pressure contour methods: 1) PiCCO; 2) Wesseling; and 3) the aortic model presented in Chapter 5 are compared in this chapter. The result showed all methods are capable of accurate continuous SV estimation, provided model parameters are adequately calibrated. The PiCCO device was calibrated multiple times during the experiment and Wesseling method was optimised to the SV data. In contrast, the aortic model required only a single calibration, demonstrating its ability to capture changes in cardiovascular parameters, and thus provide accurate continuous SV without the need for frequent re-calibration.

The aortic model requires less calibration as information from both PWV and pressure measurements are used. The PWV measurement provides continuous information on aortic wall properties and removes the need for population approximation. The changing property of the aortic wall is measured instead of fixed or estimated, thus the aortic model is capable of accurate SV estimation even during significant hemodynamic modification induced by dobutamine, and endotoxin.

The additional PWV measurement required by the aortic model can be seen as a disadvantage, as the PiCCO and Wesseling methods need only pressure waveform. However, reduced probability of misdiagnosis and incorrect treatment from accurate SV monitoring could outweigh the model disadvantage. In addition, the frequent calibration and/or subject-specific

optimisation required by the other methods is clinically impractical. The primary source of error during hemodynamic instability is the main time when SV estimation is most clinically necessary. Further investigation of the model using post-hoc human data would reveal the clinical applicability and usefulness in the critical care environment.

Chapter 7: Estimation of Changes in Contractility and Mechanical Efficiency for Monitoring Inotrope Therapy

Contractility and mechanical efficiency of the heart are essential for optimizing/titrating treatment involving inotropes. However, current methods of identifying these parameters involve highly invasive procedures and are not clinically feasible. Thus, this chapter investigates the relationship between contractility, mechanical efficiency and output parameters from the extended aortic pressure model presented in Chapter 5. The goal is to minimise invasive measurements, while enabling more optimal inotrope therapy. The strengths of these relationships for contractility, E_{es} - PWV, ventricular arterial coupling ($1/E_{es}C_V$) - aortic characteristic impedance, Z_{ao}, and mechanical efficiency - ratio of aortic compliance to impedance, (C_V/Z_{ao}), are analysed using the data from the dobutamine experiments.

7.1 Introduction

Inotropes are used in the ICU for management of heart failure and administered if hemodynamic properties cannot be improved with "standard care", such as fluid resuscitation (Felker and O'Connor, 2001). In such cases, the decompensating heart requires stimulation of adrenergic receptors to improve cardiovascular performance and oxygen delivery to restore adequate organ perfusion (Overgaard and Dzavik, 2008). Adrenergic agonists/blockers in the

inotrope stimulate/block adrenergic receptors, modifying cardiac function and/or vascular tone to change CO, blood pressure, and systemic resistance (Metra et al., 2011).

The effects of inotropes can be broken down into three main physiologic changes: 1) chronotropic (rate); 2) Inotropic (strength); and 3) vasoconstriction/dilation. A given inotrope binds/blocks each of the alpha, α, and beta, β, adrenergic receptors (α_1, α_2, β_1, β_2, and β_3) to a different degree, and thus, the overall effect varies depending on the specific drug (Francis et al., 2014). Selection of suitable drug type is often made with knowledge of the drug from past studies and/or types of agonists/blockers within the drug (Garg et al., 2012). However, pharmacokinetics and pharmacodynamics of the drug can be significantly different between individuals (Lehtonen et al., 2004), and thus, desirable outcomes may not be achieved unless the quantifiable patient-specific effects of inotropes can be monitored appropriately.

To capture the patient-specific effects of inotropes, changes in Heart Rate (HR), myocardium contractility, and arterial compliance need to be monitored (chronotropy, inotropy, and vascular tone). HR is measured relatively easily from electrocardiography or photoplethysmography, and changes in arterial compliance can be measured from central pressure measurement combined with the aortic model described in Chapter 5. However, a method for measuring contractility requires information from the pressure-volume (PV) relationship within the ventricle at various levels of preload (Sagawa, 1978), and is highly invasive.

For this reason, assessments of contractility are very rare in ICU despite their importance for capturing patient-specific inotrope response. In addition, many clinical trials of inotrope therapies do not include this parameter for the analysis due to the difficulty in obtaining the

parameter value (Lobo et al., 2006, Modine et al., 2005). Hence, there is a clinical need for a non-additionally invasive assessment.

Another important parameter to be monitored for inotrope therapy is the mechanical efficiency (ME) of the heart (Knaapen et al., 2007). ME is calculated as stroke work (SW) divided by pressure volume area (PVA) which is defined by the sum of total area under the end systolic pressure volume relationship (A_{ESPVR}) and SW.

$$ME = \frac{SW}{PVA} \tag{7.1}$$

$$PVA = SW + A_{ESPVR} \tag{7.2}$$

PVA represents the total mechanical energy generated by the heart per beat and the efficiency, ME, shows the amount of energy received by the arterial system per total energy produced by the heart (Westerhof, 2000).

Inotropes increase contractility of the heart. However, if ME is altered with changes in ventricular-arterial (VA) coupling, which is the ratio of arterial elastance to contractility (Pittarello et al., 2004), it could have adverse effects in the failing heart as the added energy expenditure of the heart can be insufficiently transferred to the vascular system. Therefore, ME needs to be monitored along with the key metrics to properly capture and assess effectiveness of these drugs.

In this chapter, clinically measurable metrics such as PWV and Windkessel model parameters of the vascular system are investigated to see whether changes in contractility and ME of the heart can be captured during inotrope therapy. Relationships between invasively measured contractility and ME from the admittance catheters with clinically measurable metrics from

aortic pressure measurements are analysed to assess the accuracy of these surrogates against highly invasive direct measurement. Identified relationships between these parameters would provide a basis for a less invasive method to capture drug response and efficacy, and could improve current inotrope therapy by offering better metrics with which to titrate inotropes to a more optimal level.

7.2 Method

7.2.1 Measurement of Contractility

Contractility of the heart can be defined at any given time in systole as it is defined by the ratio of ventricular pressure to volume (Suga and Sagawa, 1972) or time-varying elastance, $E_{vent}(t)$ of cardiac muscle;

$$E_{vent}(t) = P_{vent}(t)/(V_{vent}(t) - V_d) \quad (7.3)$$

Where E_{vent}, P_{vent} and V_{vent} are ventricular elastance, pressure, and volume, respectively, and V_d is the ventricular volume at zero pressure (Sagawa, 1981).

The pressure within the ventricle during isovolumetric relaxation does not represent pressure resulting from the ventricular contraction. Consequently contractility calculated from Equation (7.3) can only be valid during systole. An example of a typical time-varying elastance profile for a single heartbeat is shown in Figure 7.1.

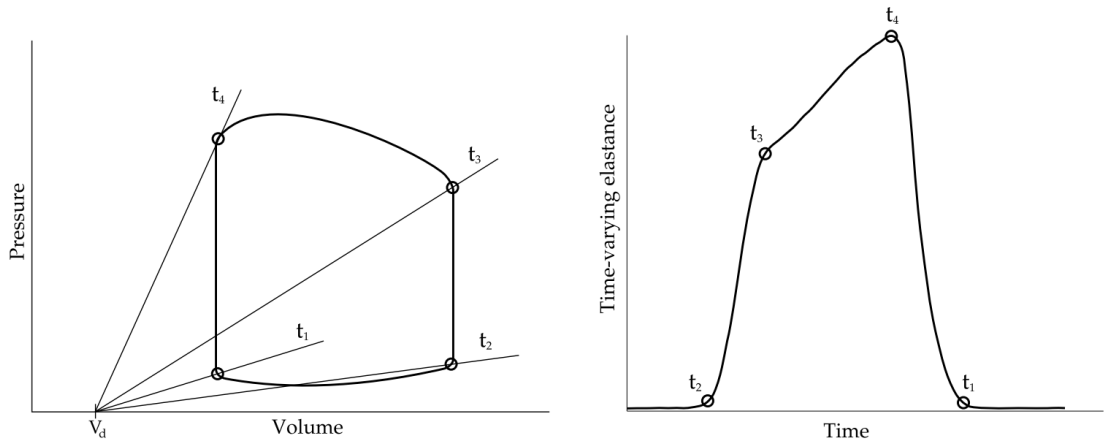

Figure 7.1 - Left Panel: Ventricular PV loop showing various ratios of pressure and volume during one cardiac cycle and the slopes represents the contractility $E_{vent}(t)$. Right Panel: Time-varying elastance curve shown in the time domain. Ventricular elastance calculated using Equation 7.1 are shown, however, elastance from t_2 to t_3 does not represent the true value. Figure from (Stevenson, 2013).

In this analysis, the maximum value of $E_{vent}(t)$ during a cardiac cycle was chosen to represent contractility for a given heartbeat as maximum contractility is the value most commonly used for assessment of contractility in clinical settings (Kass, 1992). The maximum contractility of the heart is reached at end-systole, and is located at point t_4 in Figure 7.1. Equation (7.3) can now be modified to give beat-to-beat end systolic contractility, defined:

$$max(E_{vent}(t)) = E_{es} = P_{vent}(t_{es})/(V_{vent}(t_{es}) - V_d) \quad (7.4)$$

Where t_{es} is the time at end-systole. To determine $P_{vent}(t_{es})$, and $V_{vent}(t_{es})$, end-systolic time, t_{es}, was identified as the time when product of maximum $V_{vent}(t)$ minus $V_{vent}(t)$, and $P_{vent}(t)$ reaches maximum, representing t_4 in Figure 7.1.

$$t_{es} = t \text{ @ } \max((\max(V_{vent}) - V_{vent}(t)) \; . \; P_{vent}(t)) \quad (7.5)$$

Using the identified end-systolic point on the PV loop, V_d in Equation (7.3) was identified using the data from the first RM of the experiment. RMs provide sufficient preload variation to identify a linear relationship, $P_{vent}(t_{es}) = mV_{vent}(t_{es}) + b$, and using this linear equation, V_d was determined for each pig. The example of multiple PV loops obtained from a RM and the identified linear relationship is shown in Figure 7.2.

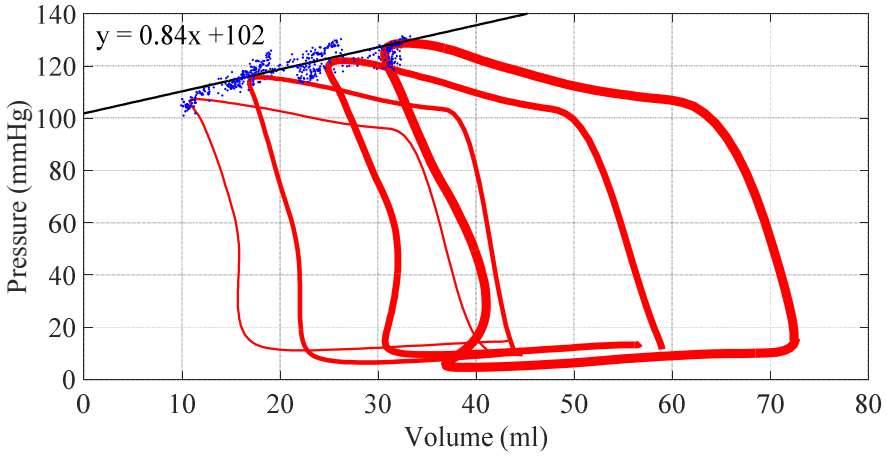

Figure 7.2 – End-systolic pressure volume relationship obtained from RM. Beat-to-beat identified end-systolic points are shown with blue dots. PV-loop obtained at PEEP 5, 10, 15, and 20 are shown with red line (thick to thin, respectively). Regression line representing ESPVR is shown with black line with corresponding linear equation at top left corner.

As can be seen in Figure 7.2, V_d is a negative value and does not represent 'true' ventricular volume when pressure is zero. This outcome is due to ESPVR curve being nonlinear in the nonphysiologic range at low ventricular volume (Oommen et al., 2003). In reality, "dead space volume" or volume that exists within the ventricle at zero pressure is a positive value. However, it is assumed for this analysis that the ESPVR line can be treated as linear within the physiological range (Senzaki et al., 1996). Negative values of V_d are non-physiological, but are a necessary assumption in obtaining beat-to-beat contractility within the physiological range (Senzaki et al., 1996). Once theoretical V_d is identified for each pig, beat-to-beat

contractility can be calculated using Equation (7.3) with $P_{vent}(t_{es})$ and $V_{vent}(t_{es})$ identified from Equation (7.5) for each beat.

7.2.2 Measurement of Mechanical Efficiency

Total mechanical energy produced by the heart from contraction can be defined as the energy received by the arterial system plus the remaining elastic potential energy of the heart when the aortic valve closes. This elastic potential energy can be determined from the area under the ESPVR line on a PV plot, similar to determining potential energy stored in a spring on a force-displacement plot. Figure 7.3 shows the two energy components on a ventricular PV diagram.

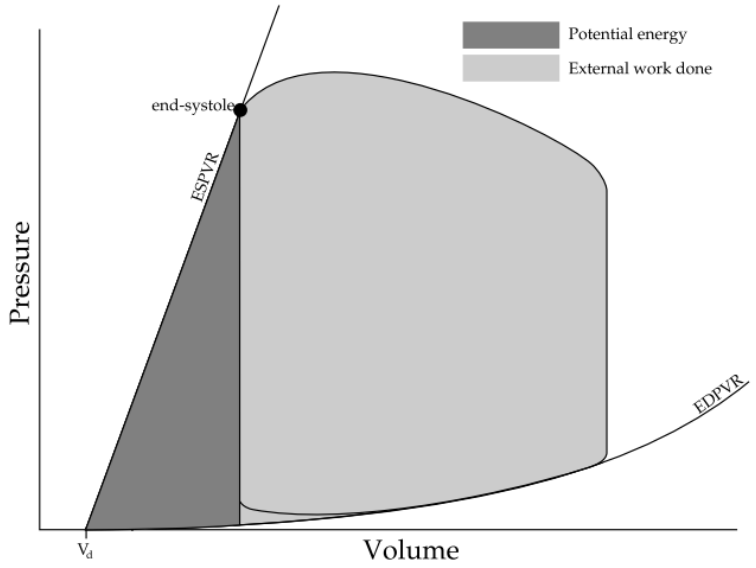

Figure 7.3 – The total mechanical energy produced by the heart from contraction. Light grey area shows the energy received by the arterial system (external work) and dark grey area shows the remaining elastic potential energy of the heart at end systole. Figure from (Stevenson, 2013).

The total energy produced by the heart, also known as PVA has been linearly correlated with oxygen consumption under various preload and afterload conditions (Suga et al., 1981). Thus, ME of the heart, which is the ratio of external work to PVA, also represents how well the heart

is utilizing oxygen to provide energy for the vascular system. To estimate the area of potential energy and external work done in Figure 7.3, these areas were simplified as a rectangle and a triangle.

$$SW = (P_{vent}(t_{es}) - P_{vent}(t_{ed})).(V_{vent}(t_{ed}) - V_{vent}(t_{es})) \quad (7.6)$$

$$PVA = (P_{vent}(t_{es}) - P_{vent}(t_{ed})).(V_{vent}(t_{es}) - V_d)/2 + SW \quad (7.7)$$

$$t_{ed} = \text{t @ min}((\max(V_{vent}) - V_{vent}(t)) \; . \; P_{vent}(t)) \quad (7.8)$$

where $t_{ed}=t_1$ and $t_{ed}=t_4$ in Figure 7.1

For the calculation of PVA, "dead space volume", V_d, was assumed to be zero, unlike the case for estimating contractility in Equation (7.3). This assumption is due to potential energy being the integral of the ESPVR curve, and thus, the true value of V_d, which is approximately zero, should be used. Using the obtained PVA, beat-to-beat ME was calculated using Equation (7.1).

7.2.3 Alternative Indices

7.2.3.1 Contractility

Contractility of the heart alters the blood flow within aorta, as more forceful contraction has greater capacity to produce higher flow (de Wildt and Sangster, 1983). However, flow rate through aorta is not directly proportional to contractility, as there are two other factors that could influence its rate: 1) ability of the aorta to absorb contractile force; and 2) initial potential energy of the aorta. If the aorta is very stiff, and thus, difficult to absorb energy from the heart (Chirinos, 2013), low flow is expected even with higher contractility. The same phenomenon is expected if the initial potential energy of the aorta is high yielding a lower energy difference

between the ventricle and aorta. To approximate the contractility from aortic flow, these two influences must be considered.

The output parameters of the aortic model presented in Chapter 5 can be used to measure these effects. Identified compliance, C_v, could assess the energy absorption potential/capacity of the aorta and the amount of excess pressure can reveal how easily the heart was able to overcome the potential energy of the aorta. Therefore, a parameter showing flow rate per unit compliance per unit of excess pressure can be hypothesised to provide an estimate of changes in contractility. PWV, as described by the water hammer relation in Equation (5.3), can be rearranged by substituting in Equation (4.4) to yield such a parameter.

$$PWV = Q_{in}/P_{ex}C_A \tag{7.7}$$

7.2.3.3 Mechanical Efficiency

The mechanical efficiency of a single heartbeat captures the ratio of energy received by the aorta or external work done by the heart to that of the entire energy produced by contractility of the heart. For a given contractility and a given magnitude of aortic pressure, the energy received by aorta is determined by the values of aortic characteristic impedance and compliance. Higher compliance for a given reservoir pressure increases energy stored by the aorta during systole, and reduced impedance for a given excess pressure increases SV during systole. Thus, the values of these two parameters influence the external work and ME of a heartbeat.

External work done can be explained by the sum of four energies within the aorta: 1) potential energy before ventricular ejection, PE_{ao}; 2) energy stored by aortic compliance during systole, E_{stored}; which is also the energy released during diastole by the aorta, 3) energy expended by aortic compliance during systole, $E_{expende}$; and 4) excess energy introduced by the ventricle to

accelerate flow, E_{ex}. Potential energy of the aorta is the energy that the heart must first overcome to start ejecting blood from the ventricle to aorta, through increase in contractility of the heart during systole. Once contractility is increased above potential energy of the aorta, energy is transferred into aortic compartment, where this energy is divided into three energies E_{stored}, E_{expend}, and E_{ex}. Figure 7.4 shows these energies of the aorta on PV loop of the left ventricle.

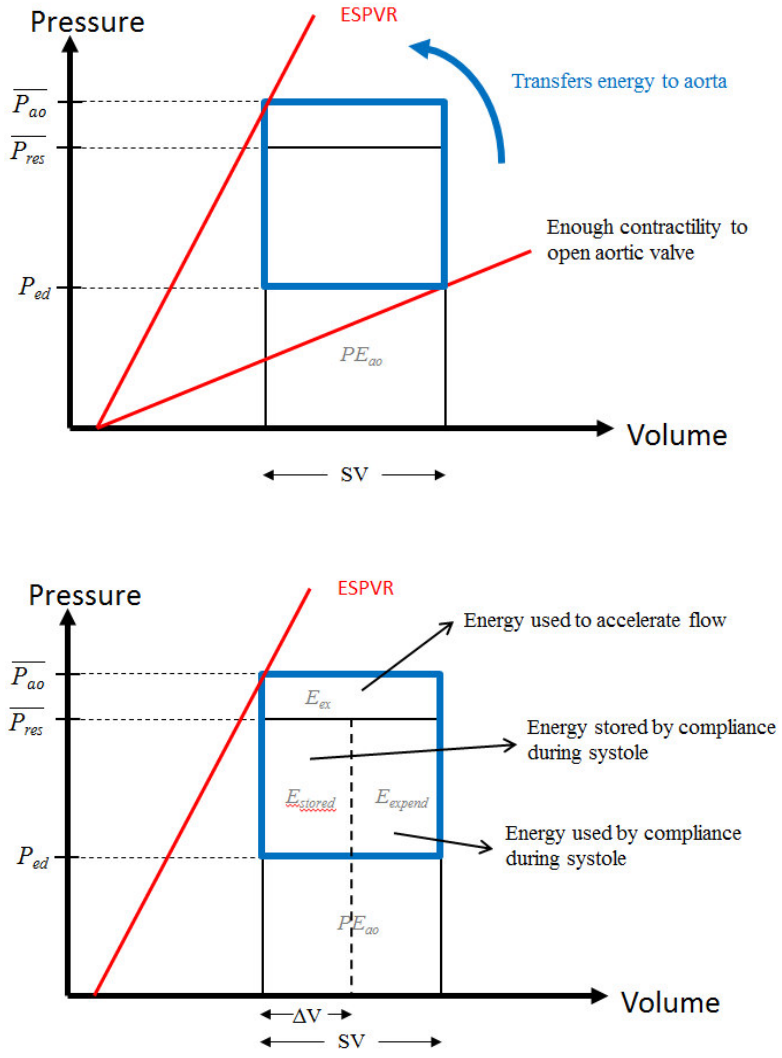

Figure 7.4 – Diagram showing four energies in the aortic compartment during systole on ventricular PV loop. Top panel shows increase in time varying contractility during systole (red lines). At aortic valve opening time, ventricular energy exceeds aortic potential energy to start transferring energy in to aorta. Blue rectangle shows the total energy transferred from the ventricle to aorta. Bottom panel shows three energy components within the total energy transferred, which are E_{stored}, E_{expend}, and E_{ex}

Relationships between impedance, compliance, SV, and each of these energy components are defined:

$$PE_{ao} = P_{ed}\, SV \tag{7.8}$$

$$E_{stored} = \overline{P_{res}}^{\,2} C_V - \overline{P_{res}} C_V P_{ed} \tag{7.9}$$

$$E_{expend} = \left(\overline{P_{res}} - P_{ed}\right) SV - E_{absorb} \tag{7.10}$$

$$E_{excess} = \frac{\overline{P_{ex}}^{\,2} T_s}{Z_{ao}} \tag{7.11}$$

Where T_s is systolic time interval and the overbar represents the mean value for systole.

These equations were derived from the definition of reservoir-excess pressure outlined by Wang et al. (2003), combined with aortic flow generated from each pressure component. The value of aortic characteristic impedance is determined from the water hammer relation in Equation (5.3), where changes in aortic compliance modify the value of PWV and impedance value. With increased aortic compliance, PWV is reduced and, consequently, aortic characteristic impedance is reduced. Equation (7.11) shows the increase in E_{excess} with reduced aortic characteristic impedance as more flow would be expected from the excess pressure. From an increased amount of total aortic flow, the rest of the external work done, as shown in Equations (7.8) - (7.10), is also increased. Thus, ME of the heart increases with increased compliance and reduced impedance by producing higher external work done for a given pressure and contractility. Figure 7.5 shows how each energy components relates to aortic characteristic impedance and compliance on a PV diagram.

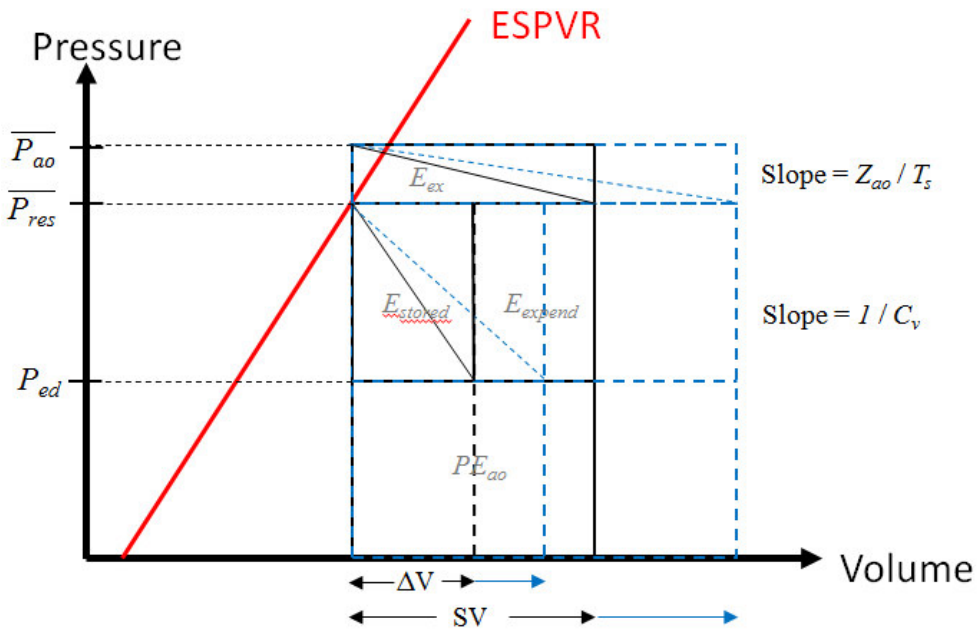

Figure 7.5 – Pressure-Volume diagram showing different components of external work done and its relations to impedance and compliance. Looking at the external work done enclosed by the black lines, rectangular section below P_{ed} shows the initial potential energy of aorta PE_{ao}. Middle rectangles in between P_{ed} and $\overline{\boldsymbol{P_{res}}}$ shows the sum of E_{absorb} and E_{expend} separated by volume absorbed by the aorta ΔV. Top rectangle section between $\overline{\boldsymbol{P_{res}}}$ and $\overline{\boldsymbol{P_{ao}}}$ shows the amount of E_{ex}. Slopes inside E_{absorb} and E_{ex} as shown in the figure relates to the value of impedance and compliance. The dashed blue line represents increased external work from reduced slopes.

Assuming that contractility is a function of aortic characteristic impedance and compliance multiplied together, so $E_{es} = f(Z_{ao}C_V)$, or E_{es} α PWV, as can be derived from the relation described in Section 7.2.3.1, and that the values of each parameter, Z_{ao} and C_V, determines the size of external work done, the ratio of compliance and impedance, C_V/Z_{ao}, could potentially track the ME of the heart. For a given contractility, $Z_{ao}C_V$, a set of solutions that results in a higher value of C_V/Z_{ao} indicates larger external work done. This result is similar to the definition of ME, which is a measure of the ability of aorta to absorb energy produced by contractility of the heart.

7.2.4 Data Analysis

Data from the four dobutamine experiments described in Chapter 4 (Pigs 2, 3, 5, and 6) were used to analyse the relationship between contractility, ME, and output parameters of the aortic model in Chapter 5. Measured continuous ventricular volume and pressure waveforms were first split into individual heart beats for the beat-to-beat PV loop analysis. The start of a beat was identified as the location of maximum ventricular volume. Theoretical dead space volume, V_d, in Equation (7.3) was estimated using the first RM for each pig and beat-to-beat contractility of the heart was calculated for whole duration of the experiment with fixed V_d. ME of the heart was determined using measured SW and PVA from PV-loop using Equation (7.6) and (7.7), respectively.

The values of PWV were obtained using the method described in Section 3.2.3. Windkessel model parameters of the aorta were identified using the aortic model in Chapter 5 with measured values of SV. Measured values of SV were used in this investigation to reveal the relationships between 'true' vascular properties and cardiac parameters. Moreover, it is important to provide correct evidence for clinical feasibility of the relationships, in the case where accurate Windkessel parameters could be identified using other methods and techniques (Cappello et al., 1995). To assess the accuracy of PWV and C_V/Z_{ao} for capturing changes in contractility and ME, respectively, correlation coefficients and regression coefficients using least-squares were analysed for each data set.

7.3 Results

7.3.1 Hemodynamic Changes from Dobutamine

To investigate the effectiveness of dobutamine for each pig, hemodynamic parameters for 10 heartbeats before and after dobutamine administration (steady-state) were analysed. Table 7.1

summarises the changes in maximum elastance, E_{es}, end-diastolic/systolic ventricular volume, V_{ed} and V_{es}, ventricular-arterial coupling (VAC), PVA, SW, ME, PWV, Z_{ao}, and C_V resulting from the administration of dobutamine. The value of VAC is determined as aortic elastance, ($1/C_V$), divided by contractility, E_{es}. The mean value of 10 heartbeats analysed are shown in Table 7.1, which eliminates any effect of beat-to-beat variability due to breathing cycle or other factors, so a direct change can be assessed due to dobutamine.

Table 7.1 – Summary of hemodynamic changes made by dobutamine. Data are presented as the mean of 10 heartbeat analysed.

10 Heartbeats Before Dobutamine										
Pig No	**E_{es} (mmHg/ml)**	**V_{ed} (ml)**	**V_{es} (ml)**	**VAC**	**PVA (mmHg.ml)**	**SW**	**ME**	**PWV (m/s)**	**Z_{ao} (mmHg.s/ml)**	**C_V (ml/mmHg)**
Pig 2	1.40	99	73	1.41	9318	3893	0.42	5.5	0.32	0.50
Pig 3	0.76	58	43	5.8	3578	1519	0.42	6.4	0.28	0.23
Pig 5	0.80	71	37	2.0	5700	3676	0.65	8.4	0.17	0.62
Pig 6	1.44	73	46	0.78	2516	1349	0.53	3.9	0.25	0.91
10 Heartbeats After Dobutamine										
Pig No	**E_{es} (mmHg/ml)**	**V_{ed} (ml)**	**V_{es} (ml)**	**VAC**	**PVA (mmHg.ml)**	**SW**	**ME**	**PWV (m/s)**	**Z_{ao} (mmHg.s/ml)**	**C_V (ml/mmHg)**
Pig 2	1.85	78	44	0.79	8791	5315	0.6	6.4	0.20	0.70
Pig 3	0.83	51	29	3.2	3729	2209	0.59	6.8	0.16	0.37
Pig 5	0.80	43	19	2.0	3524	2546	0.72	8.4	0.17	0.63
Pig 6	1.86	66	41	0.61	2789	1552	0.55	4.5	0.22	0.87

7.3.1 Correlation between Contractility and PWV

Correlation plots between measured contractility and PWV for each pig are presented in Figure 7.6. Correlation coefficient, linear regression line, and corresponding linear equation for individual pig are also shown in the plots. The correlation plots shows that contractility and PWV were more varied in the dobutamine RM period than the pre-dobutamine RM due to higher preload responsiveness achieved by higher inotropy of the heart. The variability around the regression line shows the level of intra-subject variability in each pig and each condition.

They also show that the regression line varies significantly for each pig, indicating significant inter-subject variability.

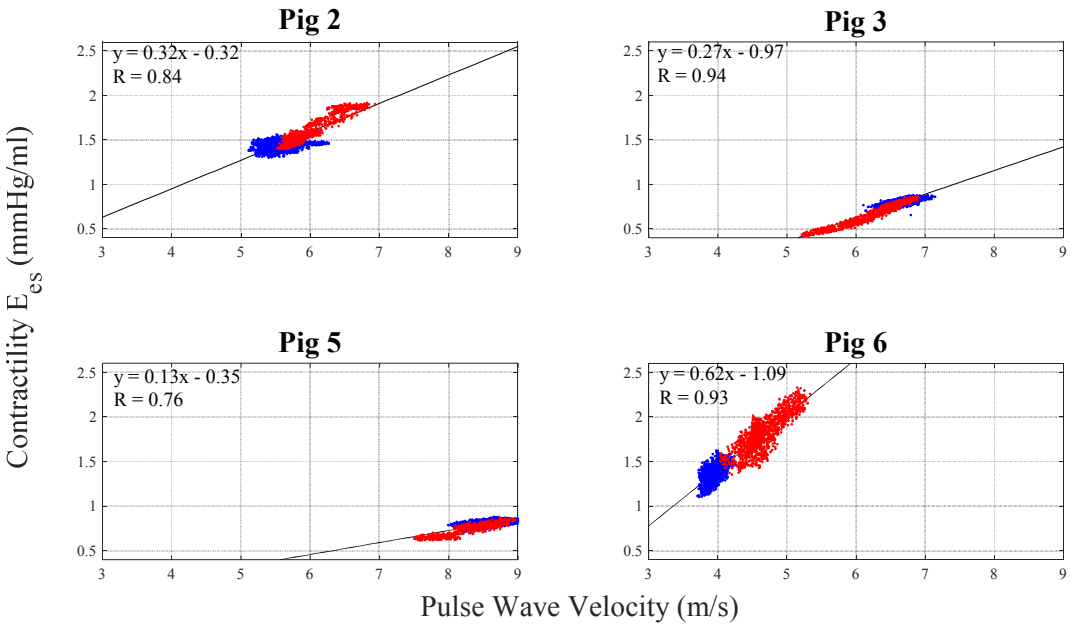

Figure 7.6 – Correlation plots showing relationship between contractility, E_{es}, and PWV. Correlation coefficient and linear equation are shown at top left corner. Pre-dobutamine RM period are shown with blue dots and post-dobutamine RM period are shown with red dots.

7.3.2 Correlation between Ventricular-Arterial Coupling and Impedance

As seen in Figure 7.6, contractility can adequately be expressed as a linear function of PWV. Using this linear relationship combined with compliance derived from the aortic model, impedance can be related to VA coupling. VA coupling is the ratio of aortic elastance and contractility, $1/E_{es}C$. Therefore, inverse of PWV divided by compliance, which is simply the impedance of aorta should also be correlated with VA coupling. In addition, past studies and results indicate the possibility of a relationship between these parameters (Bauernschmitt et al., 1999, Eaton et al., 1993). To investigate the relationship between impedance and VA coupling,

correlation plots relating these two parameters are shown Figure 7.7, which again show significant inter-subject variability, but much less intra-subject variation.

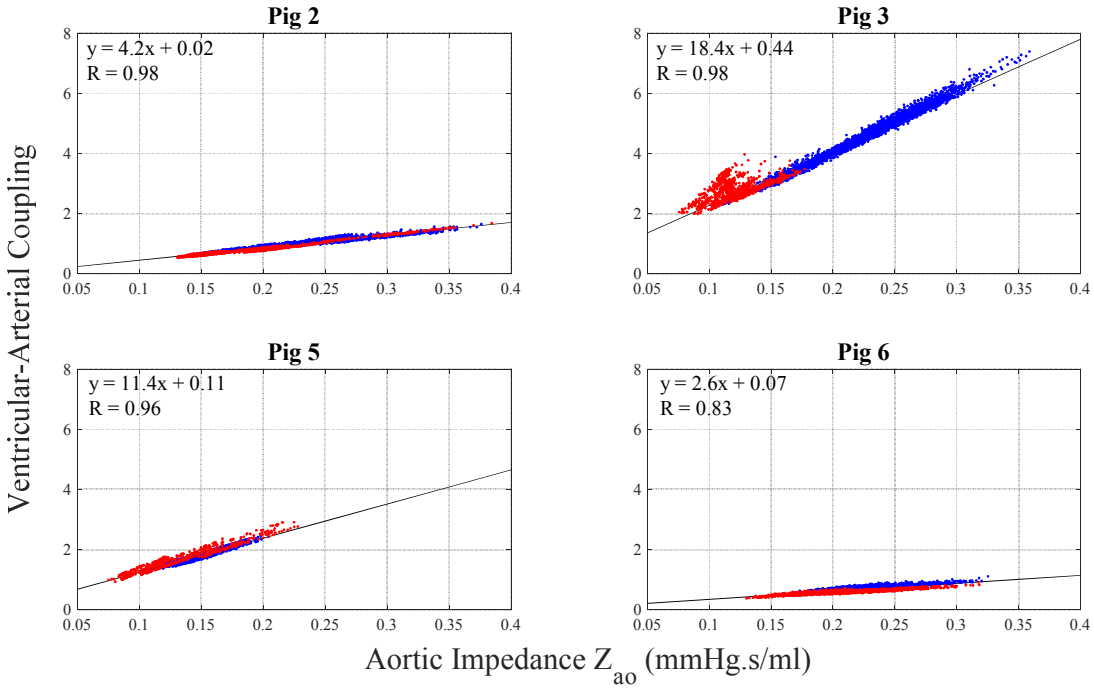

Figure 7.7 – Correlation plots showing relationship between VA coupling and aortic characteristic impedance, Z_{ao}. Correlation coefficient and linear equation are shown at top left corner. Pre-dobutamine RM period are shown with blue dots and post-dobutamine RM period are shown with red dots.

7.3.3 Correlation between Mechanical Efficiency and Ratio of Compliance and Impedance

Correlation plots between ME and the ratio, C_V/Z_{ao}, are presented in Figure 7.8. The analysis shows that the relationship between these parameters can be poor, for example in Pig 6. The relationship also showed that ME could plateau at certain level while there is still an increase in the ratio C_V/Z_{ao}.

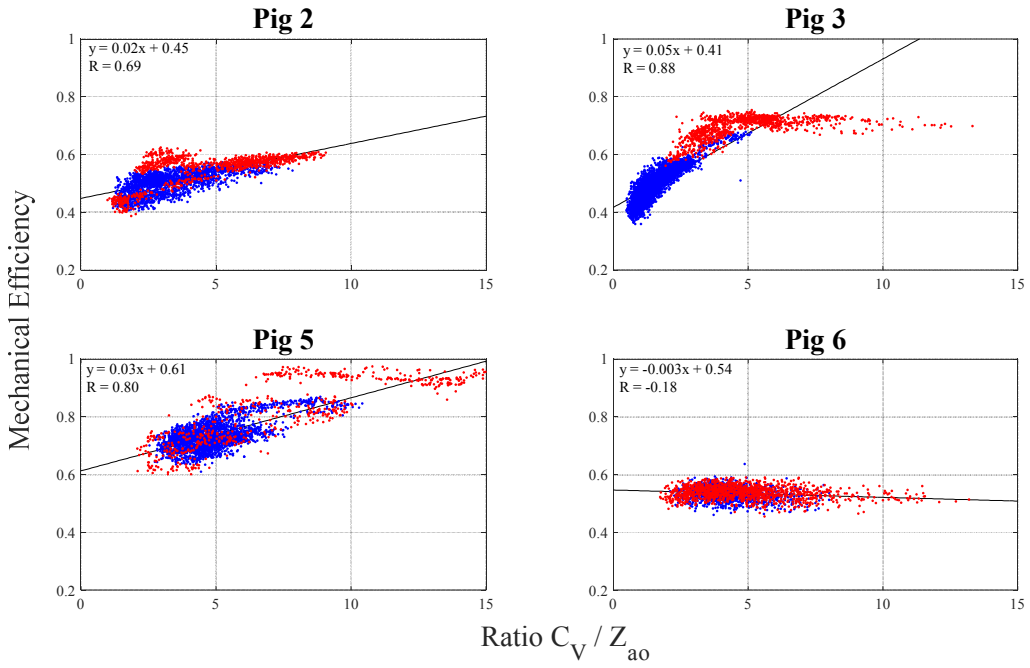

Figure 7.8 – Correlation plots showing relationship between mechanical efficiency and ratio of compliance and impedance, C_V/Z_{ao}. Correlation coefficient and linear equation are shown at top left corner. Pre-dobutamine RM period are shown with blue dots and post-dobutamine RM period are shown with red dots.

7.4 Discussion

7.4.1 Effect of Dobutamine

Dobutamine is a sympathomimetic drug with three main effects on the sympathetic nervous system. It is primarily a β_1 agonist, with β_2, and α_1 effects. Stimulation of the β_1 receptors increases contractility and heart rate, β_2 increases arterial compliance by relaxing vascular muscle, and α_1 has a vasoconstrictive effect (Garg et al., 2012). Patient response to each of these effect varies, , but dobutamine is a drug generally viewed as predominantly β_1, weak β_2, and minor α_1 stimulation (Ruffolo Jr, 1987). From this information, the benefit of inotrope therapy by dobutamine can be summarised:

- Increased SV by increasing contractility of the heart

- Increased compliance of the blood vessels to minimise systemic hemodynamic changes due to increased contractility
- Improved mechanical efficiency of the heart by modulating VA coupling

The expected hemodynamic improvements from dobutamine are relatively simple. However, complex and patient-specific differences in pharmacokinetics and pharmacodynamics of the drug could produce sub-optimal and sometimes undesired outcomes. As seen in Table 7.1, two out of four pigs (Pig 3 and 5) had minimal change in contractility and there was no change in compliance for Pig 5. The only change induced by dobutamine in Pig 5 was a reduction in SV, V_{ed}, and V_{es} caused by a significant increase in HR (Weissler et al., 1961). This increased HR can be seen as an undesired effect with decreased SW, delivering less energy to the vascular system per beat, and increased HR is related to increase cardiovascular risks (Hori and Okamoto, 2012). For these reasons, it is important to monitor the effectiveness of inotrope therapy, as continuing dobutamine administration for a patient who responds in a similar manner to Pig 5 could only result in higher chance of mortality without any benefit.

7.4.2 Relationships

7.4.2.1 Contractility and PWV

The results from Figure 7.6 demonstrate the ability of PWV for tracking changes made to contractility by dobutamine. Correlation coefficients between PWV and E_{es} were very high for all pigs, with the lowest coefficient value of R = 0.76 for Pig 5. The regression coefficients for each pig were different, showing estimation of changes in absolute value of E_{es} from PWV measurement alone is difficult, due to significant inter-subject variability.

The difference in gradient of the relationship for each pig could be due to inaccurate measurements of PWV. As seen in Figure 7.6, the relationships had higher gradient when PWV

was in the lower range and had lower gradient when PWV was in a higher range. PWV was calculated using the approximate distance between the catheters (40cm as described in Section 3.2.3), and the absolute value of PWV could be incorrect by a constant factor for each pig. If the approximated catheter distance were longer than the actual distance, calculated PWV values are higher with higher variability. In contrast, if the approximated catheter distance were shorter than the actual distance, the opposite would occur, potentially shifting the results to the left with a higher gradient on the correlation plots. Taking these inaccuracies into account, a population correlation between PWV and E_{es} may result in a similar gradient. To reveal the true population relationship between PWV and E_{es}, further investigations are necessary where exact catheter distance is known or can be measured accurately.

Individual differences in the relationship prevents capturing the absolute changes in contractility from PWV. However, it can be seen from Pig 5 in Table 7.1 that both PWV and contractility were constant before and after dobutamine administration, showing the clinical feasibility of the relationship in an unaffected case. The identified relationship, combined with the value of compliance from the aortic model, has the potential to improve dobutamine therapy in the clinical settings.

7.4.2.2 VA Coupling and Impedance

The results from Figure 7.7 shows VA coupling and Z_{ao} are highly correlated, with a lowest correlation coefficient R = 0.83 for Pig 6. Z_{ao} were highly accurate in capturing the increase and decrease of VA coupling. However, the difference in regression coefficients between each pig shown in Figure 7.7 prevents use of this relationship to capture changes in absolute value of VA coupling from Z_{ao}.

The reservoir-excess aortic model separates systolic aortic pressure waveform into excess pressure. Excess pressure represents the force producing ejection of blood out of the ventricle into the aorta, and reservoir pressure, which represents force pushing against the aortic valve (Hametner et al., 2014). Thus, the excess pressure results from the interaction between the ventricle and aorta. Converting this force into measures of elastance by dividing it by volume would yield a parameter representing VA coupling. The aortic characteristic impedance derived from the reservoir-excess aortic model captures this interaction, and was highly correlated with VA coupling.

The assessment of VA coupling is important for clinical diagnosis, selecting correct treatment, and optimizing cardiac energetics (Ky et al., 2013, Guarracino et al., 2013, Guarracino et al., 2014). In acute heart failure, reductions in contractility of the heart decreases the vascular compliance as a result of the normal response of the autonomic nervous system from reduced SV. The outcome is significantly decreased VA coupling with an inefficient cardiovascular system (Chantler and Lakatta, 2012, Asanoi et al., 1989).

For these conditions, inotrope therapy is necessary (Stevenson, 2003), and appropriate monitoring is required as inotropes may overcompensate and/or have adverse effects. Optimal VA coupling is achieved when $1/E_{es}C_V = 1$ (Sunagawa et al., 1985), and the relationship between Z_{ao} and VA coupling could thus be used to guide inotrope therapy. The results of this study show that it is difficult to capture the absolute value of VA coupling from Z_{ao} alone. However, if the relationship can be calibrated using a PWV-E_{es} relationship and/or using intermittent echocardiographic measurements (Chen et al., 2001), monitoring continuous VA coupling becomes much easier in clinical settings, and can be used to guide/monitor therapy.

7.4.2.3 Mechanical Efficiency and Ratios C_V/Z_{ao}

The results from Figure 7.8 show linear relationships between ME and the ratio C_V/Z_{ao}. However, in Pigs 3 and 5, there were regions where ME was unchanged while there were variations in C_V/Z_{ao}. This plateauing of ME might be due to reaching the maximum absolute mechanical efficiency of the heart for a specific pig. Theoretically, an increase in the ratio, C_V/Z_{ao}, increases the ME of the heart, as shown in Figure 7.5. However, such conditions can only be achieved if there is no limit for the end-diastolic volume, V_{ed}. In reality, this volume restriction of the heart limits the increase in ME even when the ratio, C_V/Z_{ao}, continues to increase. For this reason, the relationship between these parameters is only valid up to certain level of ME.

The correlation coefficients for Pig 6 were very low, showing no relationship between ME and C_V/Z_{ao}. The calculation of ME involves assuming $V_d=0$, as explained in Section 7.2.2. This assumption can alter the absolute value of ME, especially when V_{es} is close to V_d. If the real value of V_d for Pig 6 was higher than the other pigs, it can be seen that Pig 6 could have already reached the maximum ME of the heart. In addition, Pig 6 had an extremely low blood pressure with a normal level of contractility, as can be seen in Table 3.1 and Table 7.1, which would suggest that Pig 6 had a high ME to begin with. With maximum ME throughout the experiment, the linear part of the relationship between ME and C_V/Z_{ao} was thus not observed in Pig 6.

The gradient for Pigs 2, 3, and 5 were relatively close to each other suggesting a general ability to estimate an increase in ME from C_V/Z_{ao} across the population. To confirm the validity of this result, further investigation is necessary, including larger sample size. It can be approximated that for a unit increase in C_V/Z_{ao}, 2 ~ 5% increase in ME is expected, as shown in Figure 7.8.

7.4.4 Limitations

One limitation of this analysis is similar to those described in Section 3.4.3.2, that measurement error/noise involved in PWV estimation and PV-loop data could alter the relationships identified in this chapter. However, high correlation coefficients identified from each relationship suggest that only regression coefficients would be affected from minor measurement inaccuracy. Thus, the identified linear relationship between PWV-E_{es}, VAC-Z_{ao}, and ME- C_V / Z_{ao} in this chapter is still valid.

Another limitation of this analysis is that all experiments were performed on otherwise healthy pigs and the hemodynamic response from dobutamine in heart failure may involve additional physiological influences/responses that were not considered in this analysis. The relationship identified and its accuracy described in this chapter requires further validation covering lager number of subjects with wider range of physiological conditions.

7.5 Summary

The relationships analysed in this chapter showed promising results for identifying the changes in contractility, VA coupling, and ME from the parameters that can be determined from central pressure measurements. PWV and Z_{ao} were highly correlated with contractility and VA coupling, respectively, demonstrating clinical capability for monitoring effectiveness of inotropic treatment. The relationship between the ratio, C_V /Z_{ao}, and ME showed a linear relationship can only be drawn before reaching maximum ME of the heart, but these two parameters were highly correlated before reaching maximum ME. In the linear region, the relationship showed 2 ~ 5% increase in ME from a unit increase in C_V /Z_{ao}.

The regression coefficients of the relationships for contractility and VA coupling showed different absolute effects are expected from changes in PWV and Z_{ao}, respectively. However, PWV and Z_{ao} were reliable in detecting the trends of contractility and VA coupling, showing its ability to separate affected/unaffected case for hemodynamic modification made from inotrope. The relationships identified in this chapter have great potential for estimating contractility, VA coupling, and ME in a minimally invasive fashion, and thus, could improve management of heart failure by guiding/titrating inotropic therapy to optimal level.

Chapter 8: Estimation of Pulse Wave Velocity using Single Aortic Pressure and Electrocardiogram Measurements

This chapter investigates the clinical applicability of estimating PWV using ECG and a single aortic pressure measurement to reduce the need for specialised devices and/or additional invasive pressure measurements for estimating PWV. Beat-to-beat transit time is calculated using the time from the ECG R-peak to the foot of abdominal aortic pressure waveform. A method of estimating distance between the heart and the aortic pressure catheter site is also presented. The accuracy of SV estimation in Chapter 5 and relationship between contractility and PWV identified in Chapter 7 are re-analysed using PWV estimated from ECG and aortic pressure measurements to assess clinical and practical implications. Limitations and possible errors introduced using this approach are discussed.

8.1 Introduction

The clinical application of PWV measurement was expanded in Chapter 5 by improving the pressure contour method for estimating SV and in Chapter 7 by relating PWV to contractility. Despite its usefulness, the method of estimating PWV in these analyses uses pressure measurements at two separate locations within the aorta, which is not currently common in the ICU, but can be achieved with a dual-lumen catheter. For this reason, the clinical applicability

of the aortic pressure model in Chapter 5 and relationships identified in Chapter 7 are limited by the availability of PWV measurements, where their quality will also impact these estimates.

PWV can be estimated non-invasively using specialised devices (Rajzer et al., 2008). However, PWV measurements from non-invasive methods produce regional average PWV values including stiffer peripheral arteries, and may not accurately reflect the changes in aortic PWV (Pereira et al., 2015). Another limitation of estimating PWV is that the estimated distance between two measurement sites can be inaccurate due to curvature of the vasculature (van der Meer et al., 2007). The straight-line distance between two points differ from the distance travelled by the pressure wave. Thus, these errors need to be minimized for accurate monitoring.

ECG measurements are non-invasive and commonly available in the ICU for patients suffering from cardiovascular disease and its waveform could potentially be used to limit the invasiveness required for PWV measurement. The ECG signal shows the electrical activity due to depolarization/repolarization of the heart. The signal from a single heartbeat can be separated into three main characteristic waveforms, P-wave, QRS complex, and T-wave as shown in Figure 8.1.

The P-wave represents atrial depolarization, the QRS complex represents ventricular depolarization, and the T wave represents repolarization of ventricular muscle (Becker, 2006). Within the QRS complex, the R-wave reflects depolarization of the main mass of the ventricle and indicates the starting time of heart contraction (Ashley and Niebauer, 2004). The timing of heart contraction can be used to approximate starting time of the travelling pressure wave, and thus, the ECG R-wave can be used instead of the foot of the pressure measurement closer to the heart. This approach would remove the necessity of additional pressure measurements

within the aorta, and nearby vasculature, and provides a method of estimating transit time using commonly available measurements in the ICU.

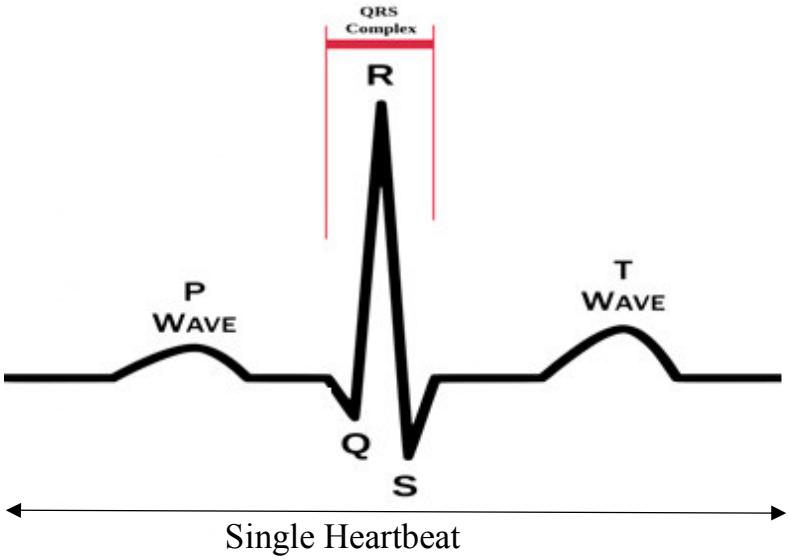

Figure 8.1 – Typical ECG waveform for a single heart beat consisting P-wave, QRS complex, and T-wave.

The limitation of estimating distance between the heart and the pressure catheter site can be overcome using an accurate value of PWV. This accurate value of PWV can be obtained by moving the pressure catheter a known distance within the aorta and recording transit time using foot of the pressure waveform at two locations. Using this PWV value combined with transit time estimated from ECG to the pressure catheter site, the distance between the heart and the catheter site can be estimated. With this estimated distance, beat-to-beat PWV can be calculated from the measured transit time.

This chapter investigates the accuracy and clinical applicability of PWV measurements using the ECG waveform and a single pressure measurement instead of the two pressure measurements in the method described in Chapter 3 Section 3.2.3. The value of PWV estimated

from the ECG R-wave and the two pressure method are compared. In addition, the accuracy of estimating SV, and the relationship between PWV and contractility are re-analysed using the PWV estimated from the ECG measurement, to assess its practical and clinical impact.

8.2 Method

ECG measurements were not taken in the endotoxin pig experiments as these were conducted with open chest to facilitate aortic flow measurement, and consequently, only the dobutamine experimental data are analysed for the estimation of PWV using the ECG measurement. A method of detecting ECG R-wave and estimation of transit time are described. Beat-to-beat PWV are then calculated from ECG and abdominal pressure waveforms without using the information from the aortic arch pressure waveform.

The distance calibration procedure of moving the pressure catheter a known distance within aorta was only performed in Pig 7, and thus is presented here as another possible method that could be combined and implemented to estimate PWV using ECG measurement. Consequently, the distances used to calculate PWV for the dobutamine pigs were calibrated by matching the mean PWV values for the first 10 heartbeat of the experiment. This calibration method results in an optimal case for identifying absolute value of PWV. However, the error involved in using the ECG measurement could still be investigated as relative change in transit time may still differ from the two pressure measurements method. In normal clinical settings, distance calibration can be performed at any time, but, for a retrospective analysis using limited data, the distance calibration method was applied using different pigs in this chapter.

8.2.1 Transit Time Estimation from ECG and Single Pressure Waveforms

To determine transit time using ECG and abdominal pressure measurements, the ECG R-wave and foot of the abdominal pressure waveform need to be identified. The foot of the abdominal pressure waveform was identified using the method described in Section 3.2.3. For detecting the R-wave, the minimum magnitude of the ECG signal was used to identify its position. The minimum magnitude of ECG signal per heartbeat was identified using the Matlab function 'findpeaks'. From the identified minimum location, seven previous sampled data were selected, and the maximum value within the selected region was identified as the ECG R-wave. The equations for R-wave detection are defined:

$$v = [\upsilon_{n-7}\ \upsilon_{n-6}\ \upsilon_{n-5}\ \upsilon_{n-4}\ \upsilon_{n-3}\ \upsilon_{n-2}\ \upsilon_{n-1}\ \upsilon_{n}]$$

$$R\ wave = max(v) \tag{8.1}$$

Where υ_n = detected location of minimum magnitude within single beat. An example of a detected R-wave on a single beat ECG waveform is shown in Figure 8.2.

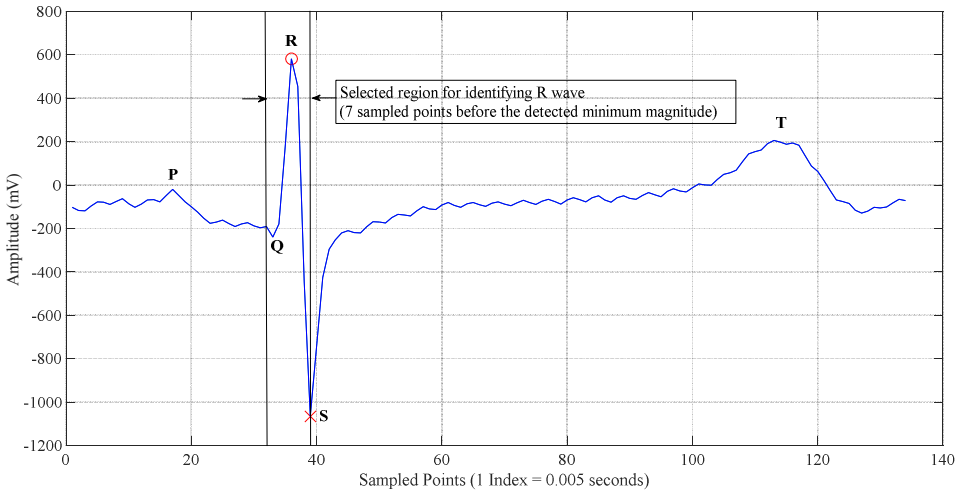

Figure 8.2 – Example of detected R wave on a measured single beat ECG waveform. P wave, QRS complex, and T wave are shown on the ECG measurement (blue line). Detected location of minimum magnitude within a single beat ECG waveform is shown with red cross. The region selected for identifying the R wave are shown by black vertical lines, and detected R wave within the region are shown with red circle.

The uniqueness of peaks within QRS complex varies depending on the location of ECG leads. Patterns, signs and shapes of the ECG signal can be different if positions of the ECG leads are changed (Biel et al., 2001). Thus, the algorithms for detecting R-waves may need to be adjusted accordingly. In this analysis, the algorithm presented in Equation (8.1) was applied as the most unique points seen on the overall ECG measurements were the minimum magnitude or the S wave. The identified ECG R-wave was then used to determine transit time. Figure 8.3 shows an example of estimated transit time using the time between the foot of the abdominal pressure waveform and ECG R-wave identified.

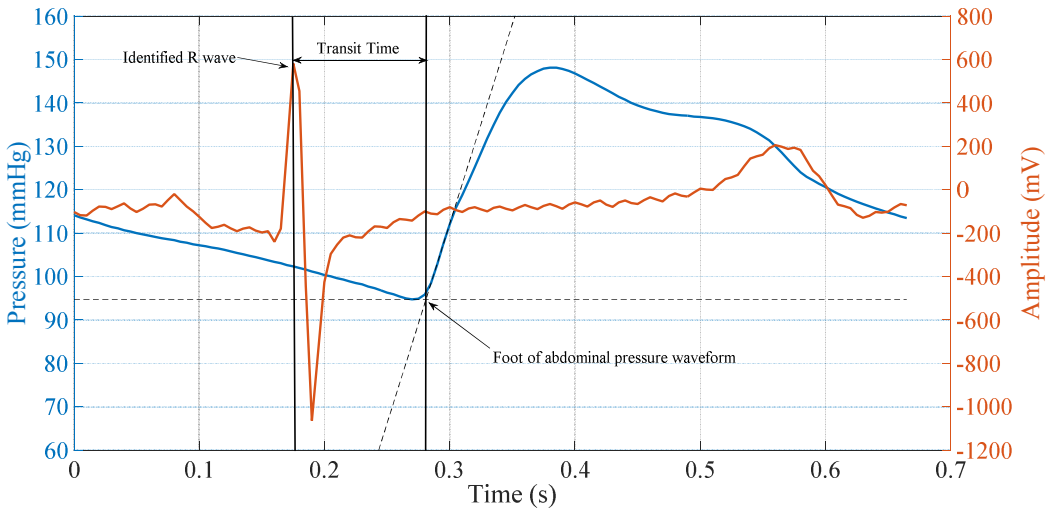

Figure 8.3 – Typical ECG (orange line) and abdominal pressure (blue line) measurements for a single heartbeat. Identified R wave and foot of abdominal pressure waveform are shown by black vertical lines. Transit time estimated from these two points are indicated by the width of black lines and represents the time pressure wave took to travel from the heart to the catheter site.

8.2.2 Distance Calibration

The distance travelled by the pressure wave between the heart and the abdominal pressure measurement site can be determined if the value of PWV is known. Using the value of PWV with the value of transit time from ECG R-wave to the abdominal pressure catheter, Equation

3.5 can be rearranged to calculate the distance. To determine the value of PWV, the abdominal pressure catheter can be moved a known distance to obtain accurate information of both the transit time and the distance.

During an endotoxin experiment (Pig 7), the abdominal pressure catheter was shifted towards the heart in increments of 7, 12, 17, and 22cm. The distance inserted was measured using a ruler on catheter cord. Transit times between aortic arch and abdominal pressure measurements were captured at each increment. In this analysis, aortic arch pressure was used for the value of transit time as ECG measurements were not recorded. However, the calibration process would be identical using the transit time determined using ECG R-wave. Approximately 5-10 heartbeats worth of data were obtained at each catheter position within the aorta. Figure 8.4 shows the mean value of recorded transit time at each location and calculated PWV on a distance-time diagram.

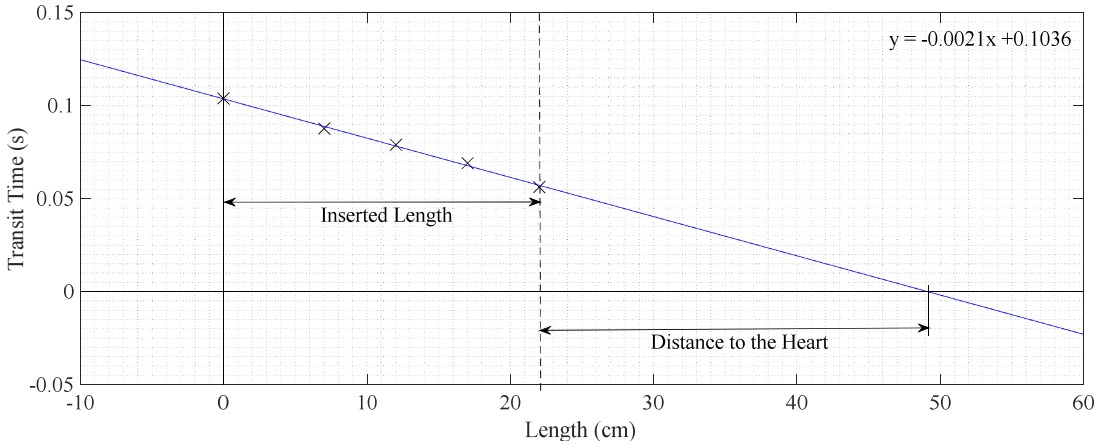

Figure 8.4 – Scatter plot showing recorded mean transit time (black cross) at inserted length of 0, 7, 12, 17, and 22 cm. The regression line represents negative inverse value of PWV in centimetres per second. Estimated distance between the heart and the pressure catheter site is shown as x-interception of the regression line.

As seen in Figure 8.4, the distance-time relationship can be obtained from the difference in transit time recorded between locations. The gradient of regression line represents negative inverse value of PWV along aorta, and the distance between two measurement points can be calculated using the identified linear coefficients. PWV is assumed to be constant during the calibration period (20-30 heartbeats), and thus, required to be performed when patient circulatory conditions are relatively stable. Once calibrated, this distance can be used to estimate beat-to-beat PWV for the entire duration of ICU stay. In addition, if the catheter is replaced or moved from the original position, the calibration method can be repeated without requiring additional devices.

8.2.3 Data Analysis

The data from dobutamine Pigs 2, 3, 5, and 6 were used to estimate transit time between the ECG R-wave and foot of abdominal pressure catheter. As the distance calibration method was developed after these experiments were conducted, the distance between the heart and the pressure catheter site were calculated using initial 10 beats of measured PWV from two pressure measurements method (Chapter 3 Section 3.2.3). The PWV calibration process using ECG data is defined:

$$Distance_{heart-catheter} = 40cm \,.\, \frac{\overline{TT_{ECG,initial\ 10\ beats}}}{\overline{TT_{pressure,initial\ 10\ beats}}} \tag{8.2}$$

$$PWV_{ECG} = \frac{Distance_{heart-catheter}}{TT_{ECG}} \tag{8.3}$$

Where *TT* is transit time and subscript *ECG* and *pressure* represents transit time estimated using the ECG R-wave and aortic arch pressure measurement, respectively. The 40cm in Equation (8.2) is the approximate distance used to calculate PWV with the two pressure measurements method (Chapter 3 Section 3.2.3).

To test its effectiveness, the beat-to-beat PWV_{ECG} using Equation (8.3) is used to re-analyse the accuracy of SV estimation described in Chapter 5 and the relationship identified between contractility and PWV in Chapter 7. Measured abdominal pressure waveforms with PWV_{ECG} were used to estimate beat-to-beat SV. Reservoir-excess pressure separation was performed using Equation (5.2) with the value of PWV replaced with PWV_{ECG}. The values of aortic length and area used are the same as those in Table 5.1, as the first 10 PWV_{ECG} values were calibrated to match $PWV_{pressure}$. After the pressure separation, aortic characteristic impedance was calculated using Equation (5.5) with PWV_{ECG}, and SV was calculated using Equation (5.6). For the relationship between contractility and PWV_{ECG}, correlation and regression coefficients are analysed.

8.3 Results

8.3.1 Comparison of PWV Estimated from ECG and Two Pressure Measurements

The correlation plots between PWV estimated from Equation (8.3), PWV_{ECG}, and two pressure method, $PWV_{pressure}$, for each pig are presented in Figure 8.5. It is evident that identified PWV_{ECG} and $PWV_{pressure}$ were dissimilar except in Pig 6. In Pig 2, PWV_{ECG} and $PWV_{pressure}$ were linearly related, but the gradient was steeper than 1. Pig 3 showed underestimation of PWV_{ECG} in the pre-dobutamine period and overestimation in the post-dobutamine section. For Pig 5, PWV_{ECG} values were underestimated for duration of the experiment.

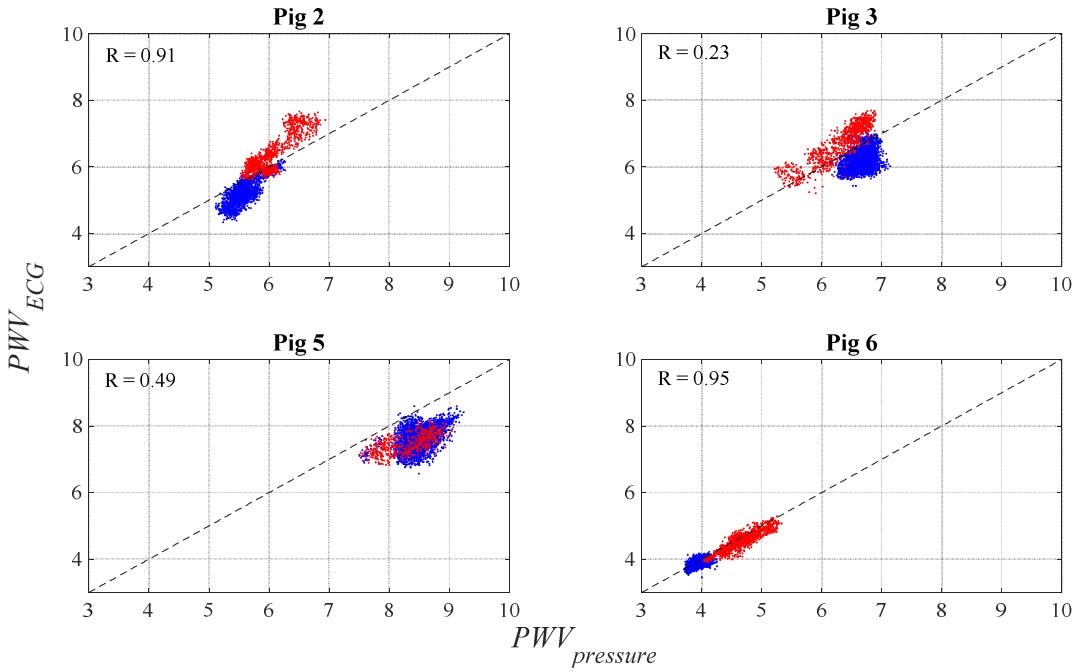

Figure 8.5 – Correlation plots comparing PWV estimated from ECG measurement, PWV_{ECG}, and two pressure measurements, $PWV_{pressure}$. The identity line is also drawn on the plot to show any deviation in PWV_{ECG} from $PWV_{pressure}$. Pre-dobutamine period is shown with blue dots and post-dobutamine period are shown with red dots. Correlation coefficients are shown on the top left corner in each plot.

8.3.2 Accuracy of SV Estimation using PWV_{ECG}

Figure 8.6 shows Bland-Altman plots between estimated SV from PWV_{ECG} and measured SV from the admittance catheter. The summary of bias, 95% interval, and precision accuracy calculated as the 95% range divided by mean SV for each pig are shown in Table 8.1. To compare the accuracy of estimated SV between PWV_{ECG} and $PWV_{pressure}$, Table 8.1 also includes Bland-Altman results for estimated SV using $PWV_{pressure}$.

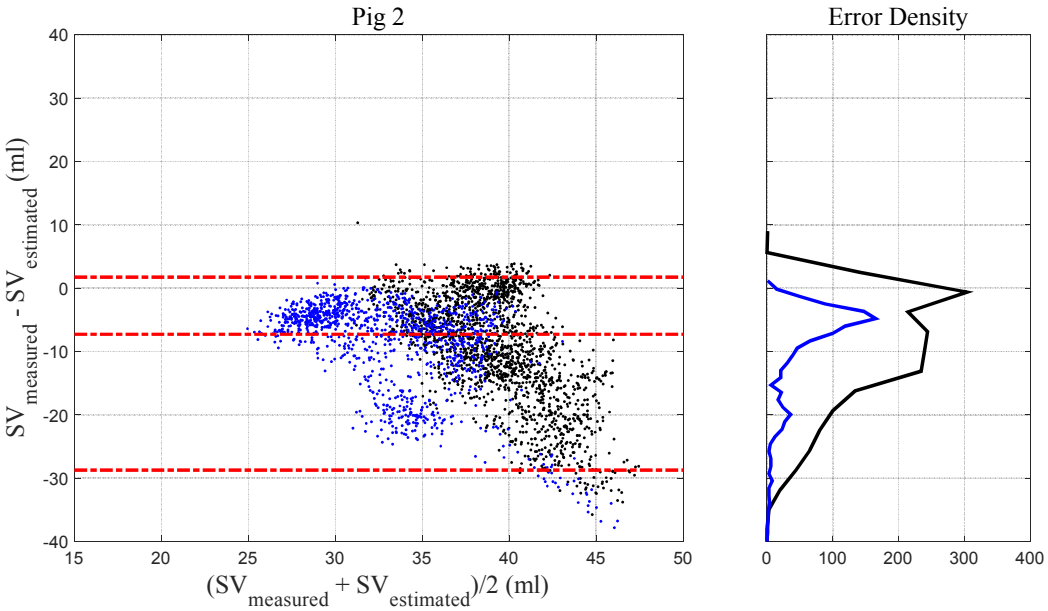
Pig 2
Error Density
SV measured - SV estimated (ml)
(SV measured + SV estimated)/2 (ml)
40
30
20
10
0
-10
-20
-30
-40
15
20
25
30
35
40
45
50
0
100
200
300
400

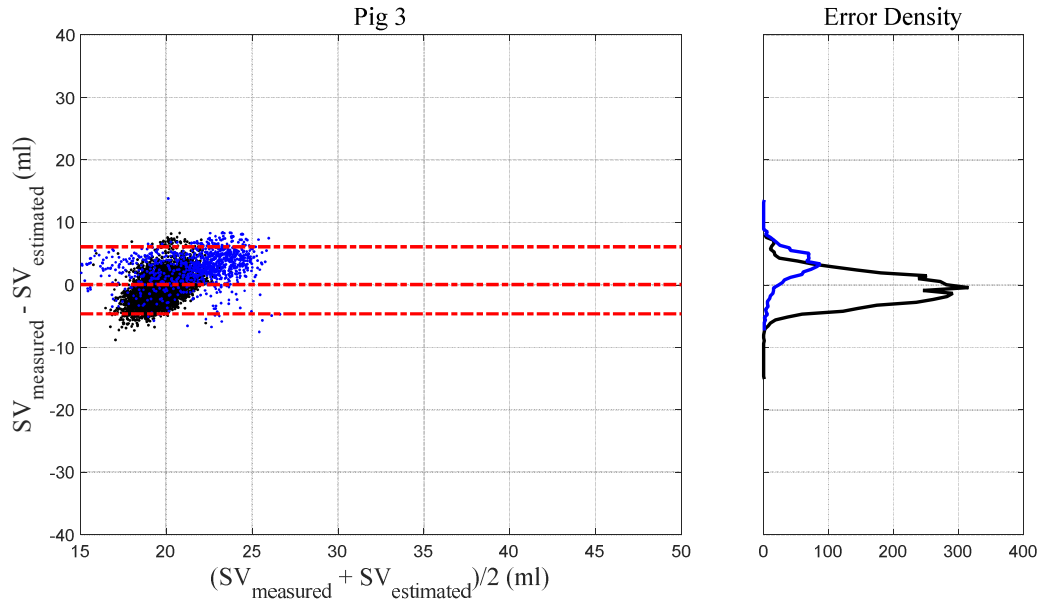
Pig 3
Error Density
SV measured - SV estimated (ml)
(SV measured + SV estimated)/2 (ml)
40
30
20
10
0
-10
-20
-30
-40
15
20
25
30
35
40
45
50
0
100
200
300
400

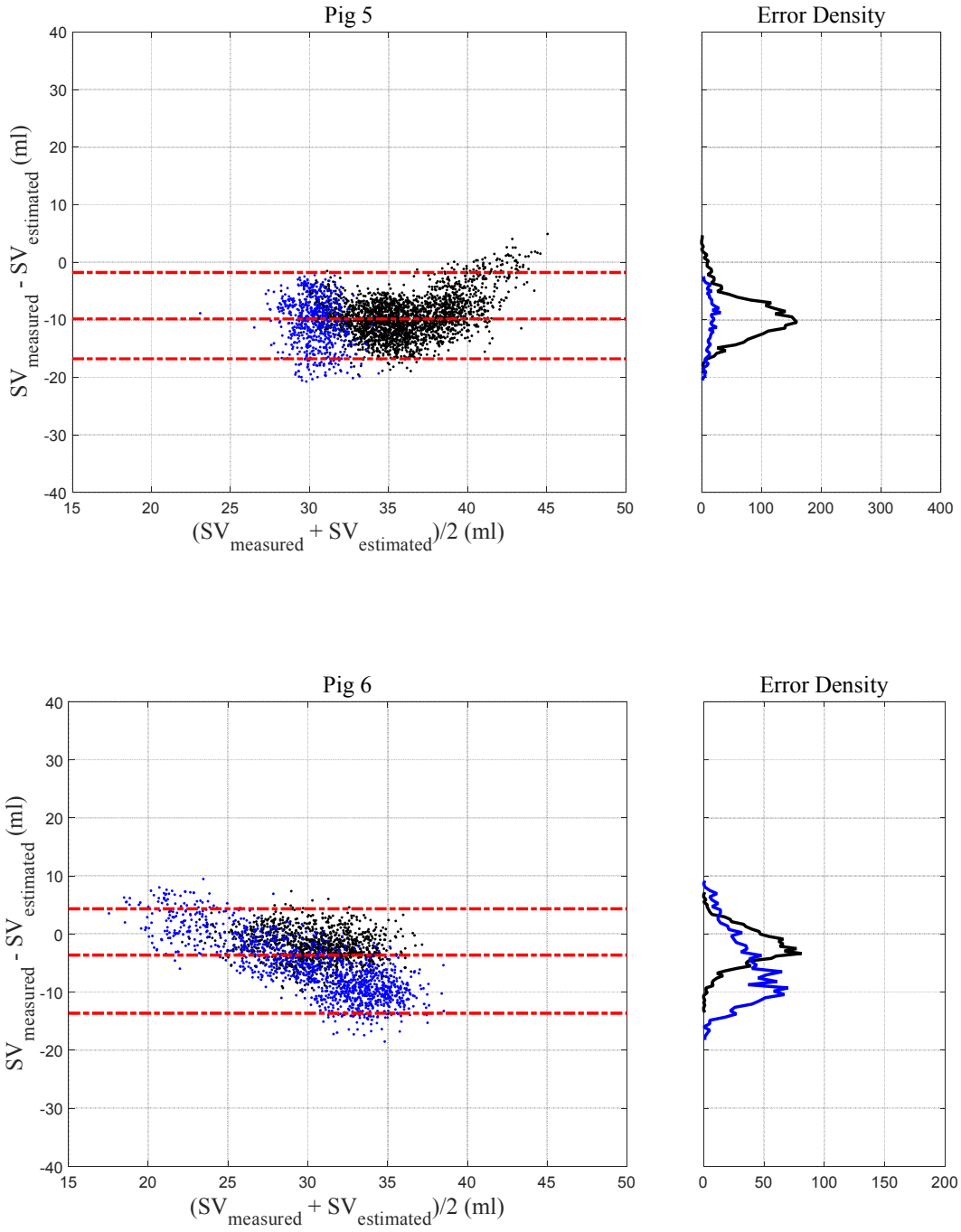

Figure 8.6 - Bland Altman plots showing agreements between measured and estimated SV for each pig. Pre-dobutamine periods are shown with black dots, and post-dobutamine periods are shown with blue dots. The red dashed line shows the bias and 95% interval. Right panel shows the error distribution between measured and estimated SV values.

Table 8.1 – Summary of Bland-Altman analysis for SV estimated using PWV_{ECG} and $PWV_{pressure}$. Data are presented as bias [2.5th – 97.5th percentiles] and precision as 95% range divided by mean SV value.

	***PWV*$_{ECG}$**		***PWV*$_{pressure}$**	
Pig No	***Bland-Altman results** (ml)*	***Precision** (%)*	***Bland-Altman results** (ml)*	***Precision** (%)*
Pig 2	-7.2 [-28.7 – 1.7]	+28, -66	-6.8 [-17.7 – 2.2]	+27, -34
Pig 3	0.0 [-4.3 – 6.1]	+30, -23	1.7 [-1.3 – 4.9]	+21, -18
Pig 5	-9.8 [-16.8 – -1.8]	+27, -23	-3.3 [-9.2 – 2.2]	+22, -23
Pig 6	-3.7 [-13.7 – 4.3]	+28, -35	-2.7 [-11.4 – 3.9]	+22, -31

8.3.3 Correlation between Contractility and PWV_{ECG}

The relationships identified in Section 7.3.2 are re-analysed using PWV_{ECG}. Figure 8.7 shows correlation plots between beat-to-beat contractility estimated using the ventricular pressure-volume loop and PWV_{ECG}. The correlation and regression coefficients calculated for each pig are summarised in Table 8.2.

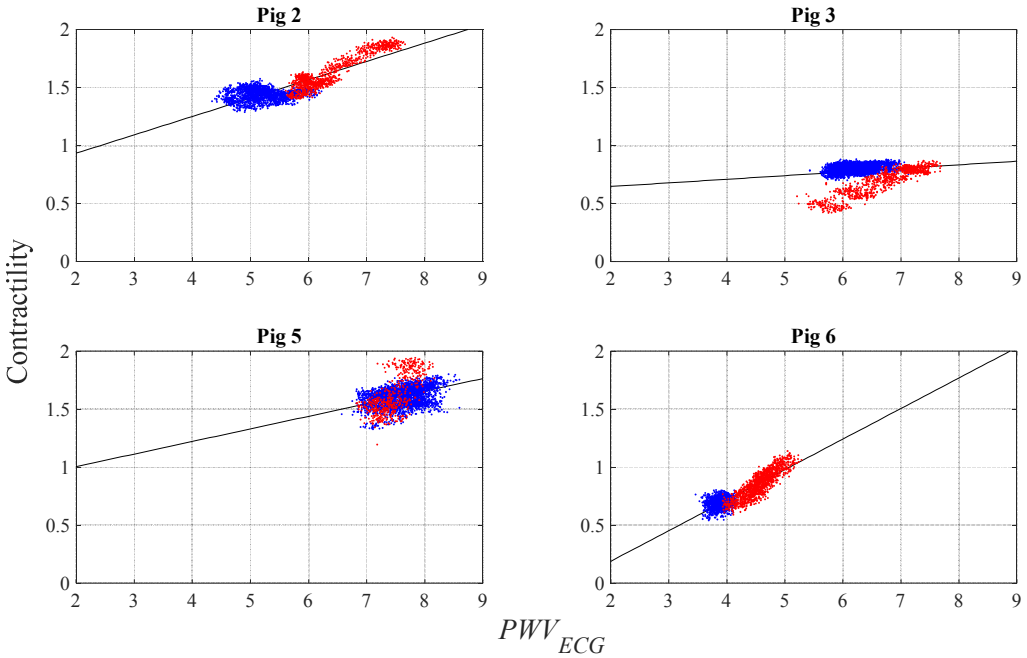

Figure 8.7 – Correlation plots showing relationship between contractility and PWV_{ECG}. Pre-dobutamine period are shown with blue dots and post-dobutamine period are shown with red dots.

Table 8.2 – Summary of correlation and regression coefficients for the relationships identified between PWV_{ECG}, $PWV_{pressure}$, and contractility estimated from ventricular PV-loop. Regression coefficients are presented as *m* and *c*, where *Contractility = mPWV+c*.

	PWV_{ECG}		$PWV_{pressure}$	
Pig No.	***Correlation Coefficient (r)***	***Regression Coefficients (m, c)***	***Correlation Coefficient (r)***	***Regression Coefficients (m, c)***
Pig 2	0.84	0.16, 0.61	0.84	0.32, -0.32
Pig 3	0.17	0.27, 0.58	0.94	0.27, -0.97
Pig 5	0.37	0.13, 0.79	0.76	0.13, -0.35
Pig 6	0.87	0.62, -0.34	0.93	0.62, -1.09

8.4 Discussion

8.4.1 Clinical feasibility of PWV_{ECG}

The correlation plots in Figure 8.5 show PWV estimated using the transit time from the ECG R-wave to the foot of the abdominal pressure waveform can be different from PWV estimated using the two pressure measurements method. The relationship between PWV_{ECG} and $PWV_{pressure}$ in Pig 6 were on the identity line showing PWV_{ECG} can be used to accurately capture $PWV_{pressure}$. However, the relationship diverged from the identity line for Pigs 2, 3, and 5 revealing the error associated using the ECG measurements and the inter-subject variability in applying this method. There were positive linear relationships in all pigs suggesting that relative/trend changes in $PWV_{pressure}$ are captured by PWV_{ECG}, but with low linear correlation coefficients in Pig 3 and Pig 5, particularly the overall accuracy is decreased.

The correlation coefficients between PWV_{ECG} and contractility showed lower values than the relationship between $PWV_{pressure}$ and contractility. Despite lower coefficient values, Pig 2 and Pig 6 showed good linear correlation, indicating the potential clinical usefulness of the relationship. The result in Pig 3 shows dobutamine producing large errors in estimated PWV from ECG measurement. There were small increase in the measured $PWV_{pressure}$ from dobutamine administration (Table 7.1), but PWV_{ECG} were significantly increased during this

period as it can be seen in Figure 8.5. This error in PWV_{ECG} produced low correlation coefficients for Pig 3 seen in Figure 8.7 and Table 8.2. There are evidence that PWV_{ECG} could predict change in contractility, however, the potential error associated with use of inotrope needs to be further investigated.

Table 8.1 shows the accuracy of SV estimated using PWV_{ECG} resulted in similar precision to SV estimated using $PWV_{pressure}$, except for Pig 2. In Pigs 3 and 5, $PWV_{pressure}$ variation was small compared with $PWV_{pressure}$ variation in Pig 2 by approximately half as seen in Figure 8.5. Therefore, the SV error produced using PWV_{ECG} in these pigs were not as significant as for Pig 2. In addition, variation of PWV_{ECG} for Pig 3 in the post-dobutamine period followed the identity line closely producing minimal difference in the estimated SV. Overall, the accuracy of estimating SV using PWV_{ECG} was within approximately ±30% for 3 out of 4 pigs, demonstrating good initial outcomes for clinical feasibility of PWV_{ECG}. However, taking into account the potential error which can be seen in Pig2, the accuracy of PWV_{ECG} for estimating aortic PWV needs to be improved.

8.4.2 Transit Time Estimated from ECG R-wave

8.4.2.1 Phases of Systole

The time interval between the ECG R-wave and the dicrotic notch on the aortic pressure waveform is known as the total mechanical systolic interval (Lewis et al., 1977). The total mechanical systolic interval consists of two phases of ventricular contraction which are: 1) Isovolumetric Contraction Time (ICT); and 2) Ventricular Ejection Time (VET) (Weissler et al., 1968). The VET can be further divided into two sections on the pressure waveform: 1) transit time from aortic valve to pressure catheter site; and 2) the time from the foot of the pressure waveform to the dicrotic notch.

The transit time recorded using two pressure measurements contains only the time taken for the pressure wave to travel between two points, and thus, the 'true' value of aortic PWV can be estimated. In contrast, the transit time recorded using ECG measurement contains the ICT, which introduces error in calculating aortic PWV. Disagreement between PWV_{ECG} and $PWV_{pressure}$ seen in Figure 8.5 can be explained by variability of ICT due to changes in cardiovascular parameters (Payne et al., 2006). The accuracy of PWV_{ECG} would be improved if the ICT could be subtracted from the transit time measured from ECG R wave to foot of abdominal pressure waveform.

8.4.2.1 Factors Affecting ICT

ICT can be influenced by contractility (Harris et al., 1967). Contractility of the heart is related to the velocity of myocardium fibre shortening (Glick et al., 1965), and ICT will be reduced if contractility is increased and vice versa (Talley et al., 1971). This effect can likely be seen in Pig 2 from Figure 8.5. The relationship between PWV_{ECG} and $PWV_{pressure}$ produced a higher gradient than the identity line indicating a shortening of ICT at higher contractility or higher $PWV_{pressure}$. Another example of this phenomena can likely be seen in Pig 3, as there were significant increase in PWV_{ECG} due to reduced ICT in the post-dobutamine period.

Other factors determining the duration of ICT are preload and afterload. Preload changes contractility of the heart by the Frank-Starling mechanism, and thus, increased preload decreases ICT and vice versa. Afterload changes the ICT by changing the load on the aortic valve resisting opening (Wallace et al., 1963). Increased afterload prolongs ICT as longer time would be taken for ventricular pressure to rise above increased aortic pressure. However, some studies suggest that ICT variability due to change in afterload are minimal or insignificant (Obrist et al., 1979, Cousineau et al., 1978).

In Pig 6, contractility was increased by dobutamine (Table 7.1), while ICT remained relatively constant. A combination of changes in cardiovascular parameters could have produced this outcome. Further investigations are required to quantify the effect of each of the cardiovascular parameters with the time of ICT. In addition, if a model could be developed for identifying ICT, it could be combined to give an accurate value of aortic PWV from ECG and a single pressure measurement.

8.4.3 Potential Error Related to Detecting R-Wave

The ECG waveform recorded during the experiment showed clear R-waves within the QRS complex for approximately 90 percent of the data. The rest of the data showed clear S-waves without a uniquely located R-wave and/or T-wave amplitude higher than R-wave. This type of ECG waveform was often recorded in the post-dobutamine period. The adrenergic stimulation from dobutamine may have introduced changes in the characteristics of the ECG waveforms (Yates and F Manini, 2012). An example of such an ECG waveform is shown in Figure 8.8.

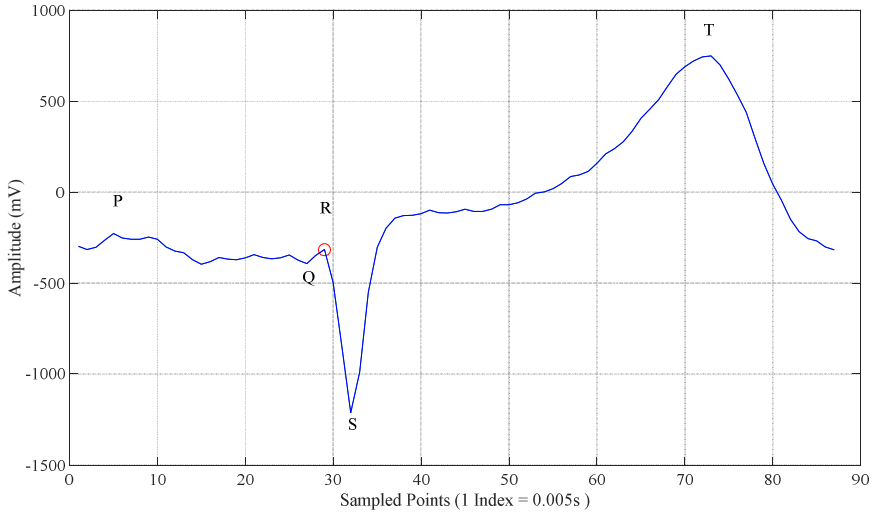

Figure 8.8 – Example of ECG waveform having non-distinctive R wave. Location of R wave detected using algorithm in section 8.2.1 are shown with red circle. Estimated regions of P wave, QRS complex, and T wave are also shown on the plot.

Figure 8.8 shows that the width of QRS complex can be uncertain, as there were no distinctive Q-wave and R-wave in the ECG waveform. The algorithm in Section 8.2.1 estimated the location of the R-wave peaks, while the 'true' location of R wave could have been closer to the P-wave with the R-wave hidden/covered by the Q-wave. The calculated PWV_{ECG} includes errors due to R-wave detection. However, unique R-waves were present in approximately 90 percent of the data, and thus, the result from this chapter is still valid.

The problem of identifying the R-wave peak could be solved in the ICU environment, if ECG leads could be relocated to a position where a clear R-wave can be seen within the QRS complex. If patients have 6 or 12 leads ECG measurement, signal with the greatest R-wave magnitude could be used to ensure accurate detection. With a clear R-wave present on the ECG signal, the error associated with incorrect estimation of transit time can thus be minimised.

8.4.4 Distance Calibration limitation

The distance calibration method presented in section 8.2.2 assumes constant PWV through the aorta. In reality, PWV in the lower abdominal region will be higher than PWV near the aortic valve (Westerhof et al., 2015a). This space variation of PWV through the aorta produces a small error in the calculated distance. The accuracy of distance calibration can be improved with increased catheter movement distance. However, this approach may increase the risk of catheter related problems (Scheer et al., 2002). Further investigation are required to identify optimal catheter movement distance and related error produced from this method.

8.5 Summary

Estimation of PWV using transit time between the ECG R-wave and a single aortic pressure measurement were investigated in this chapter to improve clinical applicability of the aortic

model presented in Chapter 5 and the relationship identified in Chapter 7. Transit time estimated using ECG R-wave consists duration of ICT, and thus, did not accurately reflect values of aortic PWV when contractility, preload, and afterload are significantly altered. Dobutamine induced changes in these cardiovascular parameters showed the potential error associated with this approach.

The accuracy of estimating SV using PWV_{ECG} was within the clinically acceptable range (±30%) if changes in aortic PWV were relatively small, however, when aortic PWV was significantly changed, SV estimation using PWV_{ECG} was unreliable as it was seen in Pig 2. The relationship between PWV_{ECG} and contractility had lower correlation coefficients than those identified in Chapter 7. It was observed that when changes in ICT are positively proportional to changes in aortic PWV, PWV_{ECG} is still clinically useful in predicting the changes in contractility.

The use of the ECG R-wave for determining transit time can be improved if variability in ICT can be identified from changes in factors affecting ICT. Subtracting the value of ICT from transit time between ECG R-wave to a pressure measurement within aorta would provide an accurate value of aortic transit time. This method combined with the distance calibration technique presented would remove the necessity of additional pressure measurements or specialised devices for measuring aortic PWV. The methods presented have the potential to enhance efficiency of available data in the ICU, and increase clinical practicality of the aortic model presented in Chapter 5 and the relationship between PWV and contractility.

Chapter 9: Conclusions

Diagnosis and treatment of patients suffering from cardiovascular dysfunctions is very difficult due to regularly changing physiological state and complex interactions between the physiological responses to both dysfunction and treatment. These patients require hemodynamic monitoring that provides a full and clear picture of their cardiovascular state, where current approaches do not allow clear differentiation of dysfunction and thus make proper treatment selection difficult. This approach would enable optimal and patient-specific treatment, leading to better patient outcomes.

The key hemodynamic parameters to monitor are SV and the circulatory factors influencing SV, such as vascular resistance and compliance. This information allows clinicians to differentiate dysfunction types, which in turn can guide them to correct diagnosis of evolving patient condition. Moreover, cardiovascular treatment involves modification of these parameters, and thus, providing quantifiable 'direct' response enables patient-specific titration of fluid and drug therapies in a way not currently possible.

Currently, several methods are available for estimating SV. However, these methods are either accurate, but highly invasive, or less invasive, but only provide intermittent SV and/or are less accurate during hemodynamic instability, which is the point at which they are most needed. Because hemodynamic monitors are typically used for patients suffering from dysfunctions and requiring modification of hemodynamic parameters via treatment, hemodynamic instability in this cohort is inevitable. The more accurate, highly invasive methods may not be clinically or ethically feasible considering benefit-to-risk ratio.

Thus, the main aim of this research was to investigate, develop, and validate methods for continuous, accurate beat-to-beat estimation of SV using non-additionally invasive and/or typical ICU measurements. This goal was achieved by incorporating PWV measurements, traditionally used as a measure of vascular stiffness, into pressure contour analysis using a reservoir-excess pressure method. The developed method was validated using dobutamine/endotoxin porcine experimental data, and showed good accuracy compared with the direct, invasive measurements of SV.

9.1 Novel SV Estimation Method

In Chapter 3, the relationship between PWV and SV was investigated. The analysis revealed a linear relationship between these two parameters, but only when preload is the dominant influence for changes in SV. The relationship was much weaker when effects from dobutamine and endotoxin were involved. This new knowledge can be useful for monitoring fluid treatment, where the main hemodynamic changes arise from preload changes. However, continuous SV estimation from PWV measurements alone are unreliable, as both preload and afterload changes are not only expected from patients with cardiovascular dysfunction, but can define and differentiate these dysfunctions.

Chapter 4 investigated a pressure contour method combining the three element Windkessel model and reservoir-excess method proposed by Wang et al. (2003). The aortic model developed utilizing these two methods provided relationships between the shapes of the aortic pressure waveform, Windkessel model parameters, and aortic blood flow. However, the model was structurally non-identifiable with the information from pressure measurements alone. Consequently, the model had to be calibrated with reference SV measurement, and assuming constant Windkessel model parameter for continuous estimation of SV. This choice was clearly

not ideal as hemodynamic instability indicates changes in Windkessel model parameters. The result showed larger errors in the estimated SV due to modification in Windkessel model parameters made by dobutamine and endotoxin.

In Chapter 5, the aortic model developed in Chapter 4 was extended by combining the information from PWV and aortic pressure waveform, to overcome the limitations of fixing Windkessel model parameters for continuous SV estimation. This goal was achieved utilizing the water-hammer equation to identify aortic characteristic impedance from excess pressure and PWV, both of which were measured beat-to-beat. Thus, all the Windkessel model parameters were dynamically captured, enabling accurate SV estimation during significant hemodynamic changes. The result from the extended model showed significant improvement in estimated SV over previous methods. In particular, the estimation error caused by dobutamine/endotoxin changes was significantly reduced. Estimated SV accuracy from the extended model compared to direct measurement of SV was within approximately ±30%, demonstrating clinically acceptable accuracy according to clinical criteria from Critchely and Critchely (1999).

Chapter 6 compared the accuracy of the novel SV estimation method developed in Chapter 5 with the PiCCO system from PULSION and a nonlinear three-element model developed by Wesseling et al. (1993), both of which are widely known, but very different, pressure contour methods. The PiCCO system was calibrated before and after the administration of dobutamine and endotoxin to minimize error from hemodynamic changes, representing a best case scenario. The Wesseling model was optimized to the direct SV measurement, retrospectively. These calibrations and optimizations gave the best possible accuracy for these two methods. However, a method requiring multiple calibrations, particularly to minimizing error in unpredictable instability, suggests that patient SV trends between the calibration times could be unreliable,

thus minimizing the clinical utility. In addition, optimization of a model using SV data is thus clinically impossible. However, these issues do not affect the proposed method, highlighting its clinical advantages.

The comparison between the aortic model, the PiCCO system, and the Wesseling model showed similar SV accuracy. This result demonstrates the ability of the proposed aortic model to capture relative changes in SV without calibration. Thus, estimated SV trends are reliable and patient progression from treatment can be correctly assessed, again, without requiring calibration or foreknowledge of when instability might occur.

In summary, combined information from PWV and pressure contours enabled improved SV estimation from pressure measurements, even when significant homonymic instabilities are present. Furthermore, continuous arterial pressure measurements are often available in the ICU. Thus, the developed method is continuous, accurate, and potentially non-additionally invasive.

9.2 Extending Clinical Functionality

In Chapter 7, the relationship between contractility of the heart, ME, VAC, and outputs of the aortic model in Chapter 5 were investigated. Specifically, the strength of relationships between contractility and PWV, VAC and aortic characteristic impedance, and ME and the ratio of aortic compliance to impedance (C_V/Z_{ao}) were analysed. This analysis was performed as knowledge of ME and contractility of the heart in addition to SV provides greater insight into the mechanics of the heart, as well as delineating the effects from the inotropes dosing to enhance contractility. Relationships identified can be used in a non-additionally invasive fashion, as required measurements are already obtained for estimation of SV.

The analysis revealed strong linear correlation between contractility and PWV, VAC and aortic characteristic impedance. These results add to the value of obtaining PWV and aortic characteristic impedance, as contractility and VAC trends can be monitored utilizing the identified relationships. However, inter-subject variability in the identified linearity limited identification of absolute changes. The relationship between ME and the ratio C_V/Z_{ao} was weaker, but showed less inter-subject variability with 2 ~ 5% expected increase in ME from a unit increase to C_V/Z_{ao} in s^{-1}.

In Chapter 8, accuracy of estimating aortic PWV using ECG R-wave and a single pressure measurement was investigated. Currently, two spatially separated pressure measurements within the aorta is uncommon in the ICU, thus the accuracy of PWV values obtained utilizing ECG signal was analysed as a way to obtain PWV with no additional equipment. The result revealed potential errors associated with this approach as transit time estimated includes isovolumetric contraction time and did not represent true wave transit time. It was found that variability of ICT must be identified to accurately capture PWV using the ECG R-wave.

9.3 Overall Outcome

A final major conclusion of this work is that a model-based approach can elucidate existing clinical data, turning them into physiologically relevant metrics. The output values from physiological models can then be used to assess patient-specific "direct" response from treatments. Such an approach is essential for developing effective patient-specific treatment protocols without adding new devices, sensors, or cost. The overall results thus provides an avenue to improve the quality and productivity of care, which is under significant economic pressure.

Specifically and more broadly, patient condition in cardiac or circulatory failure may appear essentially the same despite having different underlying physiological conditions. In such cases, a "standard" management is sub-optimal and can potentially be harmful. The model developed in this work allow clinicians to identify the exact cause of modulation in the blood pressure measurement, which is crucial for patient-specific diagnosis and treatment, and has not previously been possible. A treatment protocol based on unambiguous clinical measurement will significantly improve quality of patient care in the ICU.

Chapter 10: Future Work

This chapter outlines the possible future avenues to expand, improve, and further validate the models/concepts presented in this thesis.

10.1 Relationship between Ejection Time and Aortic Area

The aortic model developed in Chapter 5 uses linear relationship identified between ejection time and aortic area calculated using direct SV measurement, as shown in Figure 5.3. The population relationship obtained between these two variables were employed to minimize the error in the estimation of aortic characteristic impedance using water-hammer equation. However, true aortic area was not measured in the porcine experiment, and thus, further investigation is required to confirm the validity of this relationship.

Parameters identified based on population data could introduce additional error in the estimated SV, depending on the strength of the relationship. The identified relationship between ejection time and aortic area presented may weaken as future data including wider cardiovascular states are added. Therefore, the exact rationale behind this relationship needs to be clarified with measured aortic area.

A possible explanation of this relationship could be the viscoelastic behaviour of aorta. The energy loss due to hysteresis of the aorta may change according to the speed of expansion, which is related to ejection time. The water-hammer equation does not take these variabilities into account, and when the amount of energy absorbed by the aorta is altered, calculated aortic

characteristic impedance deviates from the true value, where this effect is corrected by 'dynamic aortic area' in this study. In such cases, changes in aortic area can be assumed negligible and relationship between energy loss and ejection time must be investigated.

Continuous measurement of aortic cross sectional area is possible using sonomicrometry or using echo devices. With measured cross sectional area and aortic pressure value, beat-to-beat stress-strain loops can be produced revealing the time-dependent mechanisms of the aortic wall. Such data would clarify the relationship identified in Figure 5.3, potentially making the model entirely data-driven and the accuracy can be further improved.

10.2 Validation with Human Data

The aortic model presented in Chapter 5 has only been validated using porcine experimental data. Although human and porcine cardiovascular systems are very similar, human SV is approximately 3-4 times larger than pig and the total circulatory length is much longer. These physiological/anatomical differences may introduce new errors and limitations, which are not seen with the porcine data. In addition, the dobutamine experiment was performed on healthy pigs without any cardiovascular dysfunction. In reality, more complex cardiovascular interactions from various diseases and treatments are expected. Thus, further analysis and validation must be done with human data covering wider range of dysfunction states and inotropes/vasoactive drugs to confirm the clinical utility of these results.

At the Christchurch Hospital ICU, PAC is used to monitor SV and pulmonary circulation, after mitral valve replacement or repair surgery. The data set for these patients would include intermittent SV from thermodilution, ECG, and continuous pulmonary arterial pressure waveform. These measurements would enable right ventricular SV to be estimated using the

model in Chapter 5. Furthermore, estimated SV can be validated against intermittent SV obtained from the PAC.

The reservoir-excess separation can be performed on the pulmonary arterial pressure waveform as the pressure contour is similar to aortic pressure waveform. PWV can be estimated using the method presented in Chapter 8. The error introduced from ICT is thought to be reduced in the pulmonary circulation as PWV is much slower, taking up more time of the transit time estimated from the ECG R-peak to the foot of pulmonary arterial pressure. Using the determined excess pulmonary arterial pressure with PWV, pulmonary arterial impedance can be calculated. The continuous right ventricular SV can then be estimated from the excess pressure and the arterial impedance.

All of the hemodynamic measurements required are taken as part of normal care for patients recovering from post mitral valve surgery. Hence, no additional interventions/measurements are required for this analysis, and thus, they provide the perfect starting point for human validation. In addition, past patient data can be retrospectively collected from the ICU data base, making larger data set.

10.3 Integrating Aortic Model with Treatment Protocols

Hemodynamic monitoring can only provide benefit to the patient when coupled with a defined and effective treatment protocol. For the aortic model developed in Chapter 5 to be clinically useful, the estimated hemodynamic parameters must influence treatment decisions, forming a feedback loop between the cause and the effect. Thus, allowing patient-specific titration of fluid/dosage in an attempt to achieve desired outcomes.

The aortic model is capable of continuously estimating SV as well as aortic characteristic impedance, aortic compliance, and systemic resistance. Utilizing these physiological parameters, an example of a treatment protocol in sepsis can be: administer/increase vasopressors until systemic resistance reaches a desired level, and once reached, titrate vasopressors, so that systemic resistance is maintained within a certain band. Similar approach can be applied for SV with fluid and inotropes. In addition, aortic characteristic impedance and compliance could be used for level of maldistribution, which are often present with hyper-dynamic state of septic shock.

Bibliography

Abel, F. L. (1981). Maximal negative dP/dt as an indicator of end of systole. *American Journal of Physiology - Heart and Circulatory Physiology,* volume 240**,** H676-H679.

Ackermann, U. (2004). Regulation of arterial blood pressure. *Surgery (Oxford),* volume 22**,** 120a-120f.

Alberts, B. (2012). Table 22-1 Blood cells. *Molecular Biology of the cell. NCBI Bookshelf,* volume 1.

Alhashemi, J. A., Cecconi, M. and Hofer, C. K. (2011). Cardiac output monitoring: an integrative perspective. *Critical Care,* volume 15.

Anavekar, N. S. and Oh, J. K. (2009). Doppler echocardiography: A contemporary review. *Journal of cardiology,* volume 54**,** 347-358.

Antonelli, M., Levy, M., Andrews, P. J., Chastre, J., Hudson, L. D., Manthous, C., Meduri, G. U., Moreno, R. P., Putensen, C. and Stewart, T. (2007). Hemodynamic monitoring in shock and implications for management. *Intensive care medicine,* volume 33**,** 575-590.

Anzics (2015). Centre for outcome and resource evaluation annual report 2014–2015. *Australian and New Zealand Intensive Care Society, Melbourne,* volume 1.

Asanoi, H., Sasayama, S. and Kameyama, T. (1989). Ventriculoarterial coupling in normal and failing heart in humans. *Circulation Research,* volume 65**,** 483-493.

Asfar, P., Meziani, F., Hamel, J.-F., Grelon, F., Megarbane, B., Anguel, N., Mira, J.-P., Dequin, P.-F., Gergaud, S. and Weiss, N. (2014). High versus low blood-pressure target in patients with septic shock. *New England Journal of Medicine,* volume 370**,** 1583-1593.

Ashley, E. A. and Niebauer, J. (2004). *Cardiology explained*, Remedica.

Awad, H. H., Anderson, F. A., Gore, J. M., Goodman, S. G. and Goldberg, R. J. (2012). Cardiogenic shock complicating acute coronary syndromes: insights from the Global Registry of Acute Coronary Events. *American heart journal,* volume 163**,** 963-971.

Bajorat, J., Hofmockel, R., Vagts, D., Janda, M., Pohl, B., Beck, C. and Noeldge-Schomburg, G. (2006). Comparison of invasive and less-invasive techniques of cardiac output measurement under different haemodynamic conditions in a pig model. *European journal of anaesthesiology,* volume 23**,** 23-30.

Bangash, M. N., Kong, M. L. and Pearse, R. M. (2012). Use of inotropes and vasopressor agents in critically ill patients. *British Journal of Pharmacology,* volume 165**,** 2015-2033.

Bauernschmitt, R., Mehmanesh, H., Schulz, S., Vahl, C., Lange, R., Hanfler, M., Müller, A. and Hagl, S. (1999). Aortic Input impedance and ventriculoarterial coupling following cardioversion/defibrillation. *Pacing and clinical electrophysiology,* volume 22**,** 1047-1053.

Becker, D. E. (2006). Fundamentals of electrocardiography interpretation. *Anesthesia progress,* volume 53**,** 53-64.

Bein, B., Meybohm, P., Cavus, E., Renner, J., Tonner, P. H., Steinfath, M., Scholz, J. and Doerges, V. (2007). The reliability of pulse contour-derived cardiac output during hemorrhage and after vasopressor administration. *The Journal of the American Society of Anesthesiologists,* volume 107**,** 107-113.

Bein, B., Worthmann, F., Tonner, P. H., Paris, A., Steinfath, M., Hedderich, J. and Scholz, J. (2004). Comparison of esophageal Doppler, pulse contour analysis, and real-time pulmonary artery thermodilution for the continuous measurement of cardiac output. *Journal of cardiothoracic and vascular anesthesia,* volume 18**,** 185-189.

Bellomo, R. and Uchino, S. (2003). Cardiovascular monitoring tools: use and misuse. *Current opinion in critical care,* volume 9**,** 225-229.

Ben-Shlomo, Y., Spears, M., Boustred, C., May, M., Anderson, S. G., Benjamin, E. J., Boutouyrie, P., Cameron, J., Chen, C.-H. and Cruickshank, J. K. (2014). Aortic pulse wave velocity improves cardiovascular event prediction: an individual participant meta-analysis of prospective observational data from 17,635 subjects. *Journal of the American College of Cardiology,* volume 63**,** 636-646.

Bendjelid, K. (2009). When to recalibrate the PiCCO™? From a physiological point of view, the answer is simple. *Acta Anaesthesiologica Scandinavica,* volume 53**,** 689-690.

Biel, L., Pettersson, O., Philipson, L. and Wide, P. (2001). ECG analysis: a new approach in human identification. *IEEE Transactions on Instrumentation and Measurement,* volume 50**,** 808-812.

Blacher, J., Asmar, R., Djane, S., London, G. M. and Safar, M. E. (1999). Aortic pulse wave velocity as a marker of cardiovascular risk in hypertensive patients. *Hypertension,* volume 33**,** 1111-1117.

Bonate, P. L. and Steimer, J.-L. (2006). *Pharmacokinetic-pharmacodynamic modeling and simulation*, Springer.

Boyd, J. H., Forbes, J., Nakada, T.-A., Walley, K. R. and Russell, J. A. (2011). Fluid resuscitation in septic shock: A positive fluid balance and elevated central venous

pressure are associated with increased mortality*. *Critical care medicine,* volume 39**,** 259-265.

Boyle, M., Lawrence, J., Belessis, A., Murgo, M. and Shehabi, Y. (2007). Comparison of dynamic measurements of pulse contour with pulsed heat continuous cardiac output in postoperative cardiac surgical patients. *Australian Critical Care,* volume 20**,** 27-32.

Brace, R. A. (1977). Fitting straight lines to experimental data. *American Journal of Physiology-Regulatory, Integrative and Comparative Physiology,* volume 233**,** R94-R99.

Bramwell, J. C. and Hill, A. V. (1922). The velocity of the pulse wave in man. *Proceedings of the Royal Society of London. Series B, Containing Papers of a Biological Character,* volume 93**,** 298-306.

Brun-Buisson, C. (2000). The epidemiology of the systemic inflammatory response. *Intensive Care Medicine,* volume 26**,** S64-S74.

Burkoff, D. (2002). Mechanical properties of the heart and its interaction with the vascular system. *Cardiac Physiology,* volume**,** 1-23.

Butlin, M. (2008). Structural and functional effects on large artery stiffness: an in-vivo experimental investigation. volume.

Button, D., Weibel, L., Reuthebuch, O., Genoni, M., Zollinger, A. and Hofer, C. (2007). Clinical evaluation of the FloTrac/VigileoTM system and two established continuous cardiac output monitoring devices in patients undergoing cardiac surgery†‡. *British journal of anaesthesia,* volume 99**,** 329-336.

Camporota, L. and Beale, R. (2010). Pitfalls in haemodynamic monitoring based on the arterial pressure waveform. *Crit Care,* volume 14**,** 124.

Cappello, A., Gnudi, G. and Lamberti, C. (1995). Identification of the three-element windkessel model incorporating a pressure-dependent compliance. *Ann Biomed Eng,* volume 23**,** 164 - 177.

Cavazzoni, S. L. Z. and Dellinger, R. P. (2006). Hemodynamic optimization of sepsis-induced tissue hypoperfusion. *Critical Care,* volume 10**,** 1.

Cecconi, M., De Backer, D., Antonelli, M., Beale, R., Bakker, J., Hofer, C., Jaeschke, R., Mebazaa, A., Pinsky, M. R. and Teboul, J. L. (2014). Consensus on circulatory shock and hemodynamic monitoring. Task force of the European Society of Intensive Care Medicine. *Intensive care medicine,* volume 40**,** 1795-1815.

Cecconi, M. and Rhodes, A. (2010). Pulse pressure analysis: to make a long story short. *Critical Care,* volume 14**,** 1.

Cecelja, M. and Chowienczyk, P. (2012). Role of arterial stiffness in cardiovascular disease. *JRSM cardiovascular disease,* volume 1**,** 11.

Chantler, P. D. and Lakatta, E. (2012). Arterial–ventricular coupling with aging and disease. *Frontiers in physiology,* volume 3**,** 90.

Cheatham, M. L., Block, E. F., Promes, J., Smith, H., Dent, D. and Mueller, D. (2008). Shock: an overview. *Irwin RS si Rippe JM (editori)"Intensive care medicine". Lippincott Williams & Wilkins, Philadelphia,* volume**,** 1831-1842.

Chen, C.-H., Fetics, B., Nevo, E., Rochitte, C. E., Chiou, K.-R., Ding, P.-A., Kawaguchi, M. and Kass, D. A. (2001). Noninvasive single-beat determination of left ventricular end-systolic elastance in humans. *Journal of the American College of Cardiology,* volume 38**,** 2028-2034.

Cheryl, H. (1999). Reflexes that control cardiovascular function. volume.

Chirinos, J. A. (2013). Ventricular–arterial coupling: invasive and non-invasive assessment. *Artery research,* volume 7**,** 2-14.

Collaboration, R. V. F. a. S. (2010). Determinants of pulse wave velocity in healthy people and in the presence of cardiovascular risk factors:'establishing normal and reference values'. *European heart journal,* volume 31**,** 2338-2350.

Cousineau, D., Lapointe, L. and De Champlain, J. (1978). Circulating catecholamines and systolic time intervals in normotensive and hypertensive patients with and without left ventricular hypertrophy. *American heart journal,* volume 96**,** 227-234.

Cousins, T. R. and O'donnell, J. M. (2004). Arterial cannulation: a critical review. *AANA journal,* volume 72.

Critchley, L. A. and Critchley, J. A. (1999). A meta-analysis of studies using bias and precision statistics to compare cardiac output measurement techniques. *Journal of clinical monitoring and computing,* volume 15**,** 85-91.

Dart, A. M. and Kingwell, B. A. (2001). Pulse pressure—a review of mechanisms and clinical relevance. *Journal of the American College of Cardiology,* volume 37**,** 975-984.

De Wilde, R., Schreuder, J., Van Den Berg, P. and Jansen, J. (2007). An evaluation of cardiac output by five arterial pulse contour techniques during cardiac surgery. *Anaesthesia,* volume 62**,** 760-768.

De Wilde, R., Van Den Berg, P. and Jansen, J. (2008). Review of the PiCCO device; our experience in the ICU. *Netherlands J Crit Care,* volume 12**,** 177-179.

De Wildt, D. J. and Sangster, B. (1983). An evaluation of derived aortic flow parameters as indices of myocardial contractility in rats. *Journal of pharmacological methods,* volume 10**,** 55-64.

Dean, D. A., Jia, C.-X., Cabreriza, S. E., D'Alessandro, D. A., Dickstein, M. L., Sardo, M. J., Chalik, N. and Spotnitz, H. M. (1996). Validation study of a new transit time ultrasonic flow probe for continuous great vessel measurements. *ASAIO Journal,* volume 42**,** M671-676.

Della Rocca, G., Costa, M. G., Coccia, C., Pompei, L., Di Marco, P., Vilardi, V. and Pietropaoli, P. (2003). Cardiac output monitoring: aortic transpulmonary thermodilution and pulse contour analysis agree with standard thermodilution methods in patients undergoing lung transplantation. *Canadian journal of anaesthesia,* volume 50**,** 707-711.

Dellinger, R. P. (2003). Cardiovascular management of septic shock. *Critical care medicine,* volume 31**,** 946-955.

Dubin, A., Pozo, M. O., Casabella, C. A., Pálizas, F., Murias, G., Moseinco, M. C., Edul, V. S. K., Estenssoro, E. and Ince, C. (2009). Increasing arterial blood pressure with norepinephrine does not improve microcirculatory blood flow: a prospective study. *Critical Care,* volume 13**,** 1.

Eaton, G. M., Cody, R. J. and Binkley, P. (1993). Increased aortic impedance precedes peripheral vasoconstriction at the early stage of ventricular failure in the paced canine model. *Circulation,* volume 88**,** 2714-2721.

Eisenberg, P. R., Jaffe, A. S. and Schuster, D. P. (1984). Clinical evaluation compared to pulmonary artery catheterization in the hemodynamic assessment of critically ill patients. *Critical care medicine,* volume 12**,** 549-553.

Elbers, P. W. and Ince, C. (2006). Bench-to-bedside review: Mechanisms of critical illness–classifying microcirculatory flow abnormalities in distributive shock. *Critical care,* volume 10**,** 1.

Ellender, T. J. and Skinner, J. C. (2008). The use of vasopressors and inotropes in the emergency medical treatment of shock. *Emergency Medicine Clinics of North America,* volume 26**,** 759-86.

Eren, H. Year. Accuracy in real time ultrasonic applications and transit-time flow meters. *In:* Instrumentation and Measurement Technology Conference, 1998. IMTC/98. Conference Proceedings. IEEE, 1998. IEEE, 568-572.

Esper, S. A. and Pinsky, M. R. (2014). Arterial waveform analysis. *Best Practice & Research Clinical Anaesthesiology,* volume 28**,** 363-380.

Evans, D., Doraiswamy, V., Prosciak, M., Silviera, M., Seamon, M., Funes, V. R., Cipolla, J., Wang, C., Kavuturu, S. and Torigian, D. (2009). Complications associated with

pulmonary artery catheters: a comprehensive clinical review. *Scandinavian Journal of Surgery,* volume 98**,** 199-208.

Felker, G. M. and O'connor, C. (2001). Rational use of inotropic therapy in heart failure. *Current Cardiology Reports,* volume 3**,** 108-113.

Francis, G. S., Bartos, J. A. and Adatya, S. (2014). Inotropes. *Journal of the American College of Cardiology,* volume 63**,** 2069-2078.

Frank, O. (1895). *Zur Dynamik des Herzmuskels*, Druck v. R. Oldenbourg.

Franklin, C. and Mathew, J. (1994). Developing Strategies to Prevent Inhospital Cardiac-Arrest - Analyzing Responses of Physicians and Nurses in the Hours before the Event. *Critical Care Medicine,* volume 22**,** 244-247.

Fukuda, N., Terui, T., Ohtsuki, I., Ishiwata, S. I. and Kurihara, S. (2009). Titin and troponin: central players in the Frank-Starling mechanism of the heart. *Current cardiology reviews,* volume 5**,** 119-124.

Ganz, W., Donoso, R., Marcus, H. S., Forrester, J. S. and Swan, H. J. (1971). A new technique for measurement of cardiac output by thermodilution in man. *The American journal of cardiology,* volume 27**,** 392-396.

Garg, S., Singhal, S., Sharma, P. and Jha, A. (2012). Inotropes and vasopressors review of physiology and clinical use. *J Pulmon Resp Med,* volume 2**,** 128.

Glick, G., Sonnenblick, E. H. and Braunwald, E. (1965). Myocardial force-velocity relations studied in intact unanesthetized man. *Journal of Clinical Investigation,* volume 44**,** 978.

Gödje, O., Höke, K., Goetz, A. E., Felbinger, T. W., Reuter, D. A., Reichart, B., Friedl, R., Hannekum, A. and Pfeiffer, U. J. (2002). Reliability of a new algorithm for continuous cardiac output determination by pulse-contour analysis during hemodynamic instability. *Critical care medicine,* volume 30**,** 52-58.

Goldhaber, S. Z. and Elliott, C. G. (2003a). Acute pulmonary embolism: Part I Epidemiology, pathophysiology, and diagnosis. *Circulation,* volume 108**,** 2726-2729.

Goldhaber, S. Z. and Elliott, C. G. (2003b). Acute Pulmonary Embolism: Part II Risk Stratification, Treatment, and Prevention. *Circulation,* volume 108**,** 2834-2838.

Gomez, C. and Palazzo, M. (1998). Pulmonary artery catheterization in anaesthesia and intensive care. *British journal of anaesthesia,* volume 81**,** 945-956.

Gondos, T., Marjanek, Z., Kisvarga, Z. and Halász, G. (2009). Precision of transpulmonary thermodilution: how many measurements are necessary? *European Journal of Anaesthesiology (EJA),* volume 26**,** 508-512.

Gowda, R. M., Fox, J. T. and Khan, I. A. (2008). Cardiogenic shock: basics and clinical considerations. *International journal of cardiology,* volume 123**,** 221-228.

Graham, C. and Parke, T. (2005). Critical care in the emergency department: shock and circulatory support. *Emergency Medicine Journal,* volume 22**,** 17-21.

Grodins, F. S. (1962). Basic concepts in the determination of vascular volumes by indicator-dilution methods. *Circulation research,* volume 10**,** 429-446.

Gruenewald, M., Meybohm, P., Renner, J., Broch, O., Caliebe, A., Weiler, N., Steinfath, M., Scholz, J. and Bein, B. (2011). Effect of norepinephrine dosage and calibration frequency on accuracy of pulse contour-derived cardiac output. *Critical Care,* volume 15**,** 1.

Guarracino, F., Baldassarri, R. and Pinsky, M. R. (2013). Ventriculo-arterial decoupling in acutely altered hemodynamic states. *Critical Care,* volume 17**,** 1.

Guarracino, F., Ferro, B., Morelli, A., Bertini, P., Baldassarri, R. and Pinsky, M. R. (2014). Ventriculoarterial decoupling in human septic shock. *Critical Care,* volume 18**,** 1.

Hadian, M., Kim, H. K., Severyn, D. A. and Pinsky, M. R. (2010). Cross-comparison of cardiac output trending accuracy of LiDCO, PiCCO, FloTrac and pulmonary artery catheters. *Critical Care,* volume 14**,** 1.

Hall, J. E. (2011). Guyton and Hall textbook of medical physiology. *Philadelphia, PA: Saunders/Elsevier,* volume.

Halvorsen, P., Espinoza, A., Lundblad, R., Cvancarova, M., Hol, P., Fosse, E. and Tønnessen, T. (2006). Agreement between PiCCO pulse‐contour analysis, pulmonal artery thermodilution and transthoracic thermodilution during off‐pump coronary artery by‐pass surgery. *Acta anaesthesiologica scandinavica,* volume 50**,** 1050-1057.

Hametner, B., Wassertheurer, S., Hughes, A. D., Parker, K. H., Weber, T. and Eber, B. (2014). Reservoir and excess pressures predict cardiovascular events in high-risk patients. *International journal of cardiology,* volume 171**,** 31-36.

Harley, A., Starmer, C. F. and Greenfield Jr, J. C. (1969). Pressure-flow studies in man. An evaluation of the duration of the phases of systole. *Journal of Clinical Investigation,* volume 48**,** 895.

Harms, M. P., Wesseling, K. H., Frank, P., Jenstrup, M., Van Goudoever, J., Secher, N. H. and Van Lieshout, J. J. (1999). Continuous stroke volume monitoring by modelling flow from non-invasive measurement of arterial pressure in humans under orthostatic stress. *Clinical Science,* volume 97**,** 291-301.

Harris, W. S., Schoenfeld, C. D. and Weissler, A. M. (1967). Effects of adrenergic receptor activation and blockade on the systolic preejection period, heart rate, and arterial pressure in man. *Journal of Clinical Investigation,* volume 46**,** 1704.

Hayes, M. A., Timmins, A. C., Yau, E., Palazzo, M., Hinds, C. J. and Watson, D. (1994). Elevation of systemic oxygen delivery in the treatment of critically ill patients. *New England Journal of Medicine,* volume 330**,** 1717-1722.

Hirata, K., Kawakami, M. and O'rourke, M. F. (2006). Pulse wave analysis and pulse wave velocity: a review of blood pressure interpretation 100 years after Korotkov. *Circulation journal: official journal of the Japanese Circulation Society,* volume 70**,** 1231-1239.

Hofer, C. K., Senn, A., Weibel, L. and Zollinger, A. (2008). Assessment of stroke volume variation for prediction of fluid responsiveness using the modified FloTrac™ and PiCCOplus™ system. *Critical Care,* volume 12**,** 1.

Hollenberg, S. M., Kavinsky, C. J. and Parrillo, J. E. (1999). Cardiogenic shock. *Annals of internal medicine,* volume 131**,** 47-59.

Hori, M. and Okamoto, H. (2012). Heart rate as a target of treatment of chronic heart failure. *Journal of cardiology,* volume 60**,** 86-90.

Horvath, I. G., Nemeth, A., Lenkey, Z., Alessandri, N., Tufano, F., Kis, P., Gaszner, B. and Cziraki, A. (2010). Invasive validation of a new oscillometric device (Arteriograph) for measuring augmentation index, central blood pressure and aortic pulse wave velocity. *Journal of hypertension,* volume 28**,** 2068-2075.

Hughes, A., Wang, J.-J., Bouwmeester, C., Davies, J., Shrive, N., Tyberg, J. and Parker, K. (2012). The reservoir-wave paradigm. *Journal of hypertension,* volume 30**,** 1880-1881.

Hughes, A. D. and Parker, K. H. (2009). Forward and backward waves in the arterial system: impedance or wave intensity analysis? *Medical & biological engineering & computing,* volume 47**,** 207-210.

Ince, C. (2005). The microcirculation is the motor of sepsis. *Critical care,* volume 9**,** 1.

Jansen, J., Schreuder, J., Mulier, J. P., Smith, N., Settels, J. and Wesseling, K. (2001). A comparison of cardiac output derived from the arterial pressure wave against thermodilution in cardiac surgery patients. *British journal of anaesthesia,* volume 87**,** 212-222.

Jansen, J., Wesseling, K., Settels, J. and Schreuder, J. (1990). Continuous cardiac output monitoring by pulse contour during cardiac surgery. *European heart journal,* volume 11**,** 26-32.

Jawad, I., Lukšić, I. and Rafnsson, S. B. (2012). Assessing available information on the burden of sepsis: global estimates of incidence, prevalence and mortality. *population,* volume 2**,** 4.

Jellema, W. T., Wesseling, K. H., Groeneveld, J. A., Stoutenbeek, C. P., Thijs, L. G. and Van Lieshout, J. J. (1999). Continuous Cardiac Output in Septic Shock by Simulating a Model of the Aortic Input Impedance A Comparison with Bolus Injection Thermodilution. *The Journal of the American Society of Anesthesiologists,* volume 90**,** 1317-1328.

Kamoi, S., Pretty, C., Docherty, P., Squire, D., Revie, J., Chiew, Y. S., Desaive, T., Shaw, G. M. and Chase, J. G. (2014). Continuous stroke volume estimation from aortic pressure using zero dimensional cardiovascular model: proof of concept study from porcine experiments. *PloS one,* volume 9**,** e102476.

Kass, D. (1992). Clinical evaluation of left heart function by conductance catheter technique. *European heart journal,* volume 13**,** 57-64.

Kelley, D. M. (2005). Hypovolemic shock: an overview. *Critical care nursing quarterly,* volume 28**,** 2-19.

Khir, A., O'brien, A., Gibbs, J. and Parker, K. (2001). Determination of wave speed and wave separation in the arteries. *Journal of biomechanics,* volume 34**,** 1145-1155.

Kinsman, J. M., Moore, J. W. and Hamilton, W. (1929). Studies on the circulation. *American Journal of Physiology--Legacy Content,* volume 89**,** 322-330.

Knaapen, P., Germans, T., Knuuti, J., Paulus, W. J., Dijkmans, P. A., Allaart, C. P., Lammertsma, A. A. and Visser, F. C. (2007). Myocardial energetics and efficiency current status of the noninvasive approach. *Circulation,* volume 115**,** 918-927.

Kougias, P., Weakley, S. M., Yao, Q., Lin, P. H. and Chen, C. (2010). Arterial baroreceptors in the management of systemic hypertension. *Medical science monitor: international medical journal of experimental and clinical research,* volume 16**,** RA1.

Kutty, S., Kottam, A. T., Padiyath, A., Bidasee, K. R., Li, L., Gao, S., Wu, J., Lof, J., Danford, D. A. and Kuehne, T. (2013). Validation of admittance computed left ventricular volumes against real‐time three‐dimensional echocardiography in the porcine heart. *Experimental physiology,* volume 98**,** 1092-1101.

Ky, B., French, B., Khan, A. M., Plappert, T., Wang, A., Chirinos, J. A., Fang, J. C., Sweitzer, N. K., Borlaug, B. A. and Kass, D. A. (2013). Ventricular-arterial coupling, remodeling, and prognosis in chronic heart failure. *Journal of the American College of Cardiology,* volume 62**,** 1165-1172.

La Rovere, M. T., Pinna, G. D. and Raczak, G. (2008). Baroreflex sensitivity: measurement and clinical implications. *Annals of Noninvasive Electrocardiology,* volume 13**,** 191-207.

Lamia, B., Chemla, D., Richard, C. and Teboul, J.-L. (2005). Clinical review: interpretation of arterial pressure wave in shock states. *Critical Care,* volume 9**,** 1.

Landgarten, M. J., Kumar, A. and Parrillo, J. E. (2000). Cardiovascular dysfunction in sepsis and septic shock. *Current treatment options in cardiovascular medicine,* volume 2**,** 451-459.

Langewouters, G., Wesseling, K. and Goedhard, W. (1984). The static elastic properties of 45 human thoracic and 20 abdominal aortas in vitro and the parameters of a new model. *Journal of biomechanics,* volume 17**,** 425-435.

Lantelme, P., Mestre, C., Lievre, M., Gressard, A. and Milon, H. (2002). Heart rate an important confounder of pulse wave velocity assessment. *Hypertension,* volume 39**,** 1083-1087.

Laurent, S., Cockcroft, J., Van Bortel, L., Boutouyrie, P., Giannattasio, C., Hayoz, D., Pannier, B., Vlachopoulos, C., Wilkinson, I. and Struijker-Boudier, H. (2006). Expert consensus document on arterial stiffness: methodological issues and clinical applications. *European heart journal,* volume 27**,** 2588-2605.

Lavdaniti, M. (2008). Invasive and non-invasive methods for cardiac output measurement. *International Journal of Caring Sciences,* volume 1**,** 112.

Ledoux, D., Astiz, M. E., Carpati, C. M. and Rackow, E. C. (2000). Effects of perfusion pressure on tissue perfusion in septic shock. *CRITICAL CARE MEDICINE-BALTIMORE-,* volume 28**,** 2729-2732.

Lefrant, J., Bruelle, P., Aya, A., Saissi, G., Dauzat, M., De La Coussaye, J. and Eledjam, J. (1998). Training is required to improve the reliability of esophageal Doppler to measure cardiac output in critically ill patients. *Intensive care medicine,* volume 24**,** 347-352.

Lehtonen, L. A., Antila, S. and Pentikäinen, P. J. (2004). Pharmacokinetics and pharmacodynamics of intravenous inotropic agents. *Clinical pharmacokinetics,* volume 43**,** 187-203.

Lewis, R. P., Rittogers, S., Froester, W. and Boudoulas, H. (1977). A critical review of the systolic time intervals. *Circulation,* volume 56**,** 146-158.

Li, W. C., Yu, M. H., Zhang, H. M., Wang, H. Q., Xi, G. M., Yao, B. C., Deng, Z. H. and Zeng, Y. J. (2008). Biomechanical properties of ascending aorta and pulmonary trunk in pigs and humans. *Xenotransplantation,* volume 15**,** 384-389.

Lobo, S. M., Lobo, F. R., Polachini, C. A., Patini, D. S., Yamamoto, A. E., De Oliveira, N. E., Serrano, P., Sanches, H. S., Spegiorin, M. A. and Queiroz, M. M. (2006). Prospective, randomized trial comparing fluids and dobutamine optimization of oxygen delivery in high-risk surgical patients [ISRCTN42445141]. *Critical care,* volume 10**,** 1.

Loukogeorgakis, S., Dawson, R., Phillips, N., Martyn, C. N. and Greenwald, S. E. (2002). Validation of a device to measure arterial pulse wave velocity by a photoplethysmographic method. *Physiological measurement,* volume 23**,** 581.

Luecke, T. and Pelosi, P. (2005). Clinical review: Positive end-expiratory pressure and cardiac output. *Critical Care,* volume 9**,** 607-21.

Mackenzie, I., Wilkinson, I. and Cockcroft, J. (2002). Assessment of arterial stiffness in clinical practice. *Qjm,* volume 95**,** 67-74.

Marik, P. E. (2013). Noninvasive cardiac output monitors: a state-of the-art review. *J Cardiothorac Vasc Anesth,* volume 27**,** 121-34.

Marik, P. E., Cavallazzi, R., Vasu, T. and Hirani, A. (2009). Dynamic changes in arterial waveform derived variables and fluid responsiveness in mechanically ventilated patients: a systematic review of the literature*. *Critical care medicine,* volume 37**,** 2642-2647.

Marik, P. E., Monnet, X. and Teboul, J.-L. (2010). Hemodynamic parameters to guide fluid therapy. *Transfusion Alternatives in Transfusion Medicine,* volume 11**,** 102-112.

Mayer, J., Boldt, J., Poland, R., Peterson, A. and Manecke, G. R. (2009). Continuous arterial pressure waveform–based cardiac output using the FloTrac/Vigileo: a review and meta-analysis. *Journal of cardiothoracic and vascular anesthesia,* volume 23**,** 401-406.

Mckinley, M. and O'loughlin, V. 2007. Human Anatomy. McGraw-Hill

Mehta, Y. and Arora, D. (2014). Newer methods of cardiac output monitoring. *World journal of cardiology,* volume 6**,** 1022.

Merx, M. and Weber, C. (2007). Cardiovascular Involvement in General Medical Conditions. *infection,* volume 793**,** 802.

Metafratzi, Z. M., Efremidis, S. C., Skopelitou, A. S. and De Roos, A. (2002). The clinical significance of aortic compliance and its assessment with magnetic resonance imaging. *Journal of Cardiovascular Magnetic Resonance,* volume 4**,** 481-491.

Metra, M., Bettari, L., Carubelli, V., Bugatti, S., Dei Cas, A., Del Magro, F., Lazzarini, V., Lombardi, C. and Dei Cas, L. (2011). Use of inotropic agents in patients with advanced heart failure. *Drugs,* volume 71**,** 515-525.

Michard, F. and Teboul, J. L. (2002). Predicting fluid responsiveness in ICU patients - A critical analysis of the evidence. *Chest,* volume 121**,** 2000-2008.

Millasseau, S. C., Stewart, A. D., Patel, S. J., Redwood, S. R. and Chowienczyk, P. J. (2005). Evaluation of carotid-femoral pulse wave velocity influence of timing algorithm and heart rate. *Hypertension,* volume 45**,** 222-226.

Milnor, W. R. (1975). Arterial impedance as ventricular afterload. *Circulation research,* volume 36**,** 565-570.

Modine, T., Decoene, C., Al-Ruzzeh, S., Athanasiou, T., Poivre, P., Pol, A. and Fayad, G. (2005). Dobutamine improves thoracic aortic blood flow during off-pump coronary artery bypass surgery: results of a prospective randomised controlled trial. *European journal of cardio-thoracic surgery,* volume 27**,** 289-295.

Mohsenin, V. (2015). Assessment of preload and fluid responsiveness in intensive care unit. How good are we? *Journal of critical care,* volume 30**,** 567-573.

Monnet, X., Anguel, N., Naudin, B., Jabot, J., Richard, C. and Teboul, J.-L. (2010). Arterial pressure-based cardiac output in septic patients: different accuracy of pulse contour and uncalibrated pressure waveform devices. *Critical Care,* volume 14**,** 1.

Monnet, X. and Teboul, J.-L. (2013). Assessment of volume responsiveness during mechanical ventilation: recent advances. *Crit Care,* volume 17**,** 217.

Montenij, L. J., De Waal, E. E. C. and Buhre, W. F. (2011). Arterial waveform analysis in anesthesia and critical care. *Current Opinion in Anesthesiology,* volume 24**,** 651-656.

Morgan, C. and Wheeler, D. S. (2013). Obstructive Shock. *Open Pediatric Medicine Journal,* volume 7**,** 35-37.

Mozaffarian, D., Benjamin, E. J., Go, A. S., Arnett, D. K., Blaha, M. J., Cushman, M., De Ferranti, S., Després, J.-P., Fullerton, H. J., Howard, V. J., Huffman, M. D., Judd, S. E., Kissela, B. M., Lackland, D. T., Lichtman, J. H., Lisabeth, L. D., Liu, S., Mackey, R. H., Matchar, D. B., Mcguire, D. K., Mohler, E. R., Moy, C. S., Muntner, P., Mussolino, M. E., Nasir, K., Neumar, R. W., Nichol, G., Palaniappan, L., Pandey, D. K., Reeves, M. J., Rodriguez, C. J., Sorlie, P. D., Stein, J., Towfighi, A., Turan, T. N., Virani, S. S., Willey, J. Z., Woo, D., Yeh, R. W. and Turner, M. B. (2015). Heart Disease and Stroke Statistics—2015 Update. *A Report From the American Heart Association,* volume 131**,** e29-e322.

Murgo, J. P., Westerhof, N., Giolma, J. P. and Altobelli, S. A. (1980). Aortic input impedance in normal man: relationship to pressure wave forms. *Circulation,* volume 62**,** 105-116.

Nahouraii, R. A. and Rowell, S. E. (2010). Static measures of preload assessment. *Critical care clinics,* volume 26**,** 295-305.

Nieminen, M. S. and Harjola, V.-P. (2005). Definition and epidemiology of acute heart failure syndromes. *The American journal of cardiology,* volume 96**,** 5-10.

Norton, J. M. (2001). Toward consistent definitions for preload and afterload. *Advances in Physiology Education,* volume 25**,** 53-61.

Obrist, P. A., Light, K. C., Mccubbin, J. A., Hutcheson, J. and Hoffer, J. L. (1979). Pulse transit time: Relationship to blood pressure and myocardial performance. *Psychophysiology,* volume 16**,** 292-301.

Oommen, B., Karamanoglu, M. and Kovács, S. J. (2003). Modeling time varying elastance: the meaning of "load-independence". *Cardiovascular Engineering: An International Journal,* volume 3**,** 123-130.

Oren-Grinberg, A. (2010). The PiCCO monitor. *International anesthesiology clinics,* volume 48**,** 57-85.

Oren-Grinberg, A., Talmor, D. and Brown, S. M. (2013). Concise definitive review: focused critical care echocardiography in the ICU. *Critical care medicine,* volume 41**,** 2618.

Østergaard, M., Nielsen, J., Rasmussen, J. and Berthelsen, P. (2006). Cardiac output–pulse contour analysis vs. pulmonary artery thermodilution. *Acta anaesthesiologica scandinavica,* volume 50**,** 1044-1049.

Overgaard, C. B. and Dzavik, V. (2008). Inotropes and vasopressors - Review of physiology and clinical use in cardiovascular disease. *Circulation,* volume 118**,** 1047-1056.

Parker, K., Alastruey, J. and Stan, G.-B. (2012). Arterial reservoir-excess pressure and ventricular work. *Medical & Biological Engineering & Computing,* volume 50**,** 419-424.

Payne, R., Symeonides, C., Webb, D. and Maxwell, S. (2006). Pulse transit time measured from the ECG: an unreliable marker of beat-to-beat blood pressure. *Journal of Applied Physiology,* volume 100**,** 136-141.

Pearse, R. M. and Rhodes, A. (2004). Haemodynamic monitoring and management of the circulation in intensive care. *Surgery (Oxford),* volume 22**,** 88-93.

Pereira, T., Correia, C. and Cardoso, J. (2015). Novel methods for pulse wave velocity measurement. *Journal of medical and biological engineering,* volume 35**,** 555-565.

Perkins, G. D., Mcauley, D. F., Davies, S. and Gao, F. (2003). Discrepancies between clinical and postmortem diagnoses in critically ill patients: an observational study. *Critical Care,* volume 7**,** R129-R132.

Peyton, P. J. and Chong, S. W. (2010). Minimally Invasive Measurement of Cardiac Output during Surgery and Critical CareA Meta-analysis of Accuracy and Precision. *The Journal of the American Society of Anesthesiologists,* volume 113**,** 1220-1235.

Phillips, R. and Brierley, J. (2015). Fluid responsiveness is about stroke volume, and not pulse pressure Yogi: the power of Doppler fluid management and cardiovascular monitoring. *Journal of clinical monitoring and computing,* volume 29**,** 197-200.

Phillips, R. A., Hood, S. G., Jacobson, B. M., West, M. J., Wan, L. and May, C. N. (2012). Pulmonary artery catheter (PAC) accuracy and efficacy compared with flow probe and transcutaneous Doppler (USCOM): an ovine cardiac output validation. *Critical care research and practice,* volume 2012.

Pinsky, M. R. (1984). Determinants of pulmonary arterial flow variation during respiration. *Journal of Applied Physiology,* volume 56**,** 1237-1245.

Pironet, A., Dauby, P. C., Chase, J. G., Docherty, P. D., Revie, J. A. and Desaive, T. (2016). Structural identifiability analysis of a cardiovascular system model. *Medical engineering & physics,* volume 38**,** 433-441.

Pittarello, D., Bonato, R., Marcassa, A., Pasini, L., Falasco, G. and Giron, G. (2004). Ventriculo‐arterial coupling and mechanical efficiency with remifentanil in patients with coronary artery disease. *Acta anaesthesiologica scandinavica,* volume 48**,** 61-68.

Porhomayon, J., El-Solh, A., Papadakos, P. and Nader, N. D. (2012a). Cardiac output monitoring devices: an analytic review. *Internal and emergency medicine,* volume 7**,** 163-171.

Porhomayon, J., Zadeii, G., Congello, S. and Nader, N. D. (2012b). Applications of minimally invasive cardiac output monitors. *International journal of emergency medicine,* volume 5**,** 1.

Porterfield, J. E., Kottam, A. T., Raghavan, K., Escobedo, D., Jenkins, J. T., Larson, E. R., Treviño, R. J., Valvano, J. W., Pearce, J. A. and Feldman, M. D. (2009). Dynamic correction for parallel conductance, GP, and gain factor, α, in invasive murine left ventricular volume measurements. *Journal of Applied Physiology,* volume 107**,** 1693-1703.

Pugsley, J. and Lerner, A. B. Year. Cardiac output monitoring: is there a gold standard and how do the newer technologies compare? *In:* Seminars in cardiothoracic and vascular anesthesia, 2010. SAGE Publications, 1089253210386386.

Rajzer, M. W., Wojciechowska, W., Klocek, M., Palka, I., Brzozowska-Kiszka, M. and Kawecka-Jaszcz, K. (2008). Comparison of aortic pulse wave velocity measured by three techniques: Complior, SphygmoCor and Arteriograph. *Journal of hypertension,* volume 26**,** 2001-2007.

Revie, J. a. M. (2013). Model-based cardiovascular monitoring in critical care for improved diagnosis of cardiac dysfunction. volume.

Reynolds, H. R. and Hochman, J. S. (2008). Cardiogenic shock current concepts and improving outcomes. *Circulation,* volume 117**,** 686-697.

Rhodes, A. and Sunderland, R. 2005. Arterial Pulse Power Analysis: The LiDCO$\mathcal{M}$ plus System. *Functional hemodynamic monitoring.* Springer.

Rivers, E., Nguyen, B., Havstad, S., Ressler, J., Muzzin, A., Knoblich, B., Peterson, E. and Tomlanovich, M. (2001). Early goal-directed therapy in the treatment of severe sepsis and septic shock. *New England Journal of Medicine,* volume 345**,** 1368-1377.

Robson, S., Murray, A., Peart, I., Heads, A. and Hunter, S. (1988). Reproducibility of cardiac output measurement by cross sectional and Doppler echocardiography. *British heart journal,* volume 59**,** 680-684.

Roch, A., Guervilly, C. and Papazian, L. (2011). Fluid management in acute lung injury and ards. *Ann Intensive Care,* volume 1**,** 16.

Rödig, G., Prasser, C., Keyl, C., Liebold, A. and Hobbhahn, J. (1999). Continuous cardiac output measurement: pulse contour analysis vs thermodilution technique in cardiac surgical patients. *British Journal of Anaesthesia,* volume 82**,** 525-530.

Romano, S. M. and Pistolesi, M. (2002). Assessment of cardiac output from systemic arterial pressure in humans. *Critical care medicine,* volume 30**,** 1834-1841.

Ruffolo Jr, R. R. (1987). The pharmacology of dobutamine. *The American journal of the medical sciences,* volume 294**,** 244-248.

Sagawa, K. (1978). The ventricular pressure-volume diagram revisited. *Circulation Research,* volume 43**,** 677-687.

Sagawa, K. (1981). Editorial: the end-systolic pressure-volume relation of the ventricle: definition, modifications and clinical use. *Circulation,* volume 63.

Sakka, S., Reinhart, K. and Meier-Hellmann, A. (1999). Comparison of pulmonary artery and arterial thermodilution cardiac output in critically ill patients. *Intensive Care Med,* volume 25**,** 843 - 846.

Sakka, S. G., Reuter, D. A. and Perel, A. (2012). The transpulmonary thermodilution technique. *Journal of clinical monitoring and computing,* volume 26**,** 347-353.

Sakr, Y., Reinhart, K., Vincent, J.-L., Sprung, C. L., Moreno, R., Ranieri, V. M., De Backer, D. and Payen, D. (2006). Does dopamine administration in shock influence outcome?

Results of the Sepsis Occurrence in Acutely Ill Patients (SOAP) Study. *Critical care medicine,* volume 34**,** 589-597.

Salvi, P., Palombo, C., Salvi, G. M., Labat, C., Parati, G. and Benetos, A. (2013). Left ventricular ejection time, not heart rate, is an independent correlate of aortic pulse wave velocity. *Journal of Applied Physiology,* volume 115**,** 1610-1617.

Scheer, B. V., Perel, A. and Pfeiffer, U. J. (2002). Clinical review: complications and risk factors of peripheral arterial catheters used for haemodynamic monitoring in anaesthesia and intensive care medicine. *Critical Care,* volume 6**,** 1.

Schmid, E., Schmidlin, D., Tornic, M. and Seifert, B. (1999). Continuous thermodilution cardiac output: clinical validation against a reference technique of known accuracy. *Intensive care medicine,* volume 25**,** 166-172.

Scholz, H. (1984). Inotropic drugs and their mechanisms of action. *Journal of the American College of Cardiology,* volume 4**,** 389-397.

Senzaki, H., Chen, C.-H. and Kass, D. A. (1996). Single-beat estimation of end-systolic pressure-volume relation in humans a new method with the potential for noninvasive application. *Circulation,* volume 94**,** 2497-2506.

Shekerdemian, L. and Bohn, D. (1999). Cardiovascular effects of mechanical ventilation. *Archives of Disease in Childhood,* volume 80**,** 475-480.

Shi, Y., Lawford, P. and Hose, R. (2011). Review of Zero-D and 1-D Models of Blood Flow in the Cardiovascular System. *BioMedical Engineering OnLine,* volume 10**,** 33.

Singer, M., Allen, M. J., Webb, A. R. and Bennett, E. D. (1991). Effects of alterations in left ventricular filling, contractility, and systemic vascular resistance on the ascending aortic blood velocity waveform of normal subjects. *Critical care medicine,* volume 19**,** 1138-1145.

Slifka, M. K. and Whitton, J. L. (2000). Clinical implications of dysregulated cytokine production. *Journal of molecular medicine,* volume 78**,** 74-80.

Smartt, S. (2005). The pulmonary artery catheter: gold standard or redundant relic. *Journal of PeriAnesthesia Nursing,* volume 20**,** 373-379.

Steinman, D. (2002). Image-based computational fluid dynamics modeling in realistic arterial geometries. *Ann Biomed Eng,* volume 30**,** 483 - 497.

Stevenson, D. (2013). Estimation of the time-varying elastance of the left and right ventricles. volume.

Stevenson, L. W. (2003). Clinical use of inotropic therapy for heart failure: looking backward or forward? Part I: inotropic infusions during hospitalization. *Circulation,* volume 108**,** 367-372.

Suga, H., Hayashi, T., Shirahata, M., Suehiro, S. and Hisano, R. (1981). Regression of cardiac oxygen consumption on ventricular pressure-volume area in dog. *American Journal of Physiology-Heart and Circulatory Physiology,* volume 240**,** H320-H325.

Suga, H. and Sagawa, K. (1972). Mathematical interrelationship between instantaneous ventricular pressure-volume ratio and myocardial force-velocity relation. *Annals of biomedical engineering,* volume 1**,** 160-181.

Sunagawa, K., Maughan, W. L. and Sagawa, K. (1985). Optimal arterial resistance for the maximal stroke work studied in isolated canine left ventricle. *Circulation research,* volume 56**,** 586-595.

Sundar, S. and Panzica, P. (2010). LiDCO systems. *International anesthesiology clinics,* volume 48**,** 87-100.

Talley, R. C., Meyer, J. F. and Mcnay, J. L. (1971). Evaluation of the pre-ejection period as an estimate of myocardial contractility in dogs. *The American journal of cardiology,* volume 27**,** 384-391.

Taylor, S. (1966). Measurement of the cardiac output in man. *Proceedings of the Royal Society of Medicine,* volume 59**,** 35.

Thames, M. D., Kinugawa, T., Smith, M. L. and Dibner-Dunlap, M. E. (1993). Abnormalities of baroreflex control in heart failure. *Journal of the American College of Cardiology,* volume 22**,** A56-A60.

Thiele, R. H. and Durieux, M. E. (2011). Arterial Waveform Analysis for the Anesthesiologist: Past, Present, and Future Concepts. *Anesthesia and Analgesia,* volume 113**,** 766-776.

Tibby, S. M. and Murdoch, I. A. (2003). Monitoring cardiac function in intensive care. *Archives of Disease in Childhood,* volume 88**,** 46-52.

Tijsseling, A. and Anderson, A. (2012). CASA-Report 12-42 December 2012. volume.

Tortora, G. J. and Derrickson, B. H. (2008). *Principles of anatomy and physiology*, Wiley. com.

Transonic Science Inc. 2013. *Theory of Operation* [Online]. Available: http://www.transonic.com/resources/research/pressure-volume-theory-of-operation/ [Accessed 20th October 2016].

Transonic Science Inc. 2015. *Flow Matters News letters* [Online]. Available: http://www.transonic.com/about-us/flowmatters-newsletters/spring-2015/ [Accessed 20th October 2016].

Trudnowski, R. J. and Rico, R. C. (1974). Specific gravity of blood and plasma at 4 and 37 C. *Clinical chemistry,* volume 20**,** 615-616.

Truijen, J., Van Lieshout, J. J., Wesselink, W. A. and Westerhof, B. E. (2012). Noninvasive continuous hemodynamic monitoring. *Journal of clinical monitoring and computing,* volume 26**,** 267-278.

Tyberg, J. V., Bouwmeester, J. C., Parker, K. H., Shrive, N. G. and Wang, J.-J. (2014). The case for the reservoir-wave approach. *International journal of cardiology,* volume 172**,** 299-306.

Vadakel, H. and Rizzolo, D. (2013). Shock: Early recognition and resuscitation are key: Review common types of this life-threatening condition and how to respond appropriately. *Journal of the American Academy of Physician Assistants,* volume 26**,** 21-24.

Valentinuzzi, M., Geddes, L. and Baker, L. (1969). A simple mathematical derivation of the Stewart-Hamilton formula for the determination of cardiac output. *Medical and biological engineering,* volume 7**,** 277-282.

Valtier, B., Cholley, B. P., Belot, J.-P., De La Coussaye, J.-E., Mateo, J. and Payen, D. M. (1998). Noninvasive monitoring of cardiac output in critically ill patients using transesophageal Doppler. *American journal of respiratory and critical care medicine,* volume 158**,** 77-83.

Van Der Meer, R. W., Diamant, M., Westenberg, J. J., Doornbos, J., Bax, J. J., De Roos, A. and Lamb, H. J. (2007). Magnetic resonance assessment of aortic pulse wave velocity, aortic distensibility, and cardiac function in uncomplicated type 2 diabetes mellitus. *Journal of Cardiovascular Magnetic Resonance,* volume 9**,** 645-651.

Vincent, J.-L. and De Backer, D. (2013). Circulatory shock. *New England Journal of Medicine,* volume 369**,** 1726-1734.

Vincent, J.-L., Rhodes, A., Perel, A., Martin, G., Rocca, G., Vallet, B., Pinsky, M., Hofer, C., Teboul, J.-L., De Boode, W.-P., Scolletta, S., Vieillard-Baron, A., De Backer, D., Walley, K., Maggiorini, M. and Singer, M. (2011). Clinical review: Update on hemodynamic monitoring - a consensus of 16. *Critical Care,* volume 15**,** 229.

Vincent, J., Sakr, Y., Sprung, C. L., Ranieri, V. M., Reinhart, K., Gerlach, H., Moreno, R., Carlet, J., Le Gall, J. and Payen, D. (2006). Sepsis in European intensive care units: results of the SOAP study. *CRITICAL CARE MEDICINE-BALTIMORE-,* volume 34**,** 344.

Wallace, A. G., Mitchell, J. H., Skinner, N. S. and Sarnoff, S. J. (1963). Duration of the phases of left ventricular systole. *Circulation Research,* volume 12**,** 611-619.

Wang, J.-J., O'brien, A. B., Shrive, N. G., Parker, K. H. and Tyberg, J. V. (2003). Time-domain representation of ventricular-arterial coupling as a windkessel and wave system. *American Journal of Physiology - Heart and Circulatory Physiology,* volume 284**,** H1358-H1368.

Wei, A. E., Maslov, M. Y., Pezone, M. J., Edelman, E. R. and Lovich, M. A. (2014). Use of Pressure-volume Conductance Catheters in Real-time Cardiovascular Experimentation. *Heart, Lung and Circulation,* volume 23**,** 1059-1069.

Wei, C.-L., Valvano, J. W., Feldman, M. D. and Pearce, J. A. (2005). Nonlinear conductance-volume relationship for murine conductance catheter measurement system. *IEEE Transactions on Biomedical Engineering,* volume 52**,** 1654-1661.

Weil, M. H. and Henning, R. J. (1979). New Concepts in the Diagnosis and Fluid Treatment of Circulatory Shock: Thirteenth Annual Becton, Dickinson and Company Oscar Schwidetsky Memorial Lecture. *Anesthesia & Analgesia,* volume 58**,** 124-132.

Weissler, A. M., Harris, W. S. and Schoenfeld, C. D. (1968). Systolic time intervals in heart failure in man. *Circulation,* volume 37**,** 149-159.

Weissler, A. M., Peeler, R. G. and Roehll, W. H. (1961). Relationships between left ventricular ejection time, stroke volume, and heart rate in normal individuals and patients with cardiovascular disease. *American heart journal,* volume 62**,** 367-378.

Werdan, K. (2001). Pathophysiology of septic shock and multiple organ dysfunction syndrome and various therapeutic approaches with special emphasis on immunoglobulins. *Therapeutic Apheresis,* volume 5**,** 115-122.

Wesseling, K., Jansen, J., Settels, J. and Schreuder, J. (1993). Computation of aortic flow from pressure in humans using a nonlinear, three-element model. *J Appl Physiol,* volume 74**,** 2566 - 2573.

Westerhof, N. (2000). Cardiac work and efficiency. *Cardiovascular research,* volume 48**,** 4-7.

Westerhof, N., Lankhaar, J. and Westerhof, B. (2009). The arterial Windkessel. *Medical & Biological Engineering & Computing,* volume 47**,** 131 - 141.

Westerhof, N., Segers, P. and Westerhof, B. E. (2015a). Wave Separation, Wave Intensity, the Reservoir-Wave Concept, and the Instantaneous Wave-Free Ratio Presumptions and Principles. *Hypertension,* volume 66**,** 93-98.

Westerhof, N., Segers, P. and Westerhof, B. E. (2015b). Wave Separation, Wave Intensity, the Reservoir-Wave Concept, and the Instantaneous Wave-Free RatioNovelty and Significance. *Hypertension,* volume 66**,** 93-98.

Wetterslev, M., Møller-Sørensen, H., Johansen, R. R. and Perner, A. (2016). Systematic review of cardiac output measurements by echocardiography vs. thermodilution: the techniques are not interchangeable. *Intensive care medicine,* volume**,** 1-11.

Yamashina, A., Tomiyama, H., Takeda, K., Tsuda, H., Arai, T., Hirose, K., Koji, Y., Hori, S. and Yamamoto, Y. (2002). Validity, reproducibility, and clinical significance of noninvasive brachial-ankle pulse wave velocity measurement. *Hypertension Research,* volume 25**,** 359-364.

Yamashita, K., Nishiyama, T., Yokoyama, T., Abe, H. and Manabe, M. (2007). Effects of vasodilation on cardiac output measured by PulseCO™. *Journal of clinical monitoring and computing,* volume 21**,** 335-339.

Yamashita, K., Nishiyama, T., Yokoyama, T., Abe, H. and Manabe, M. (2008). The effects of vasodilation on cardiac output measured by PiCCO. *Journal of cardiothoracic and vascular anesthesia,* volume 22**,** 688-692.

Yang, X. X., Critchley, L. A., Rowlands, D. K., Fang, Z. and Huang, L. (2013). Systematic error of cardiac output measured by bolus thermodilution with a pulmonary artery catheter compared with that measured by an aortic flow probe in a pig model. *Journal of cardiothoracic and vascular anesthesia,* volume 27**,** 1133-1139.

Yates, C. and F Manini, A. (2012). Utility of the electrocardiogram in drug overdose and poisoning: theoretical considerations and clinical implications. *Current cardiology reviews,* volume 8**,** 137-151.

Zierler, K. L. (1962). Theoretical basis of indicator-dilution methods for measuring flow and volume. *Circulation Research,* volume 10**,** 393-407.